Master's thesis

NTNU
Norwegian University of Science and Technology
Faculty of Engineering
Department of Mechanical and Industrial Engineering

Eirik Lødemel

Fatigue loads in a Francis turbine runner

Master's thesis in Department of Mechanical Engineering and Industrial Design
Supervisor: Roy Johnsen
Academic Supervisor: Ole Gunnar Dahlhaug

January 2019

NTNU
Norwegian University of Science and Technology

Eirik Lødemel

Fatigue loads in a Francis turbine runner

Master's thesis in Department of Mechanical Engineering and Industrial Design
Supervisor: Roy Johnsen
Academic Supervisor: Ole Gunnar Dahlhaug
January 2019

Norwegian University of Science and Technology
Faculty of Engineering
Department of Mechanical and Industrial Engineering

NTNU
Norwegian University of
Science and Technology

NTNU
Norwegian University of Science and Technology
Department of Energy and Process Engineering

EPT-M-2018-

MASTER THESIS

for
Eirik Lødemel

Autumn 2018

Fatigue loads in a Francis turbine runner
Utmattingslaster i et høytrykks Francis løpehjul

Background

The average age of Norwegian hydropower plants is 45 years, and many show sign of fatigue and needs to be constantly maintained or refurbished. Additionally, some power plants in Norway has experienced failures on new Francis runners. The main problem is the formation of cracks in the turbine runner.
A classic problem in the start-up phase of a Francis turbine is the synchronization with the grid: The turbine is sped up to synchronous speed, and spins at spin-no-load for a while until it is in stable phase with the grid. Due to the large pressure pulsations at this operating regime, the turbine will not in fact be rotating at a fixed RPM, making the synchronization time longer, further exposing the runner to the stresses of the operating regime. This causes reduced lifetime of the runner. With a variable-speed turbine, there is no need for this synchronization, and speed-control can be employed at lower-than-synchronous speeds, where the pressure pulsations are less aggressive. The challenges in this work is to investigate the fatigue loads of the turbine runner and estimate crack growth in extreme flexible operating conditions.

Objective

Evaluate how variable speed operation of Francis turbines be utilized to minimize dynamic loads at start-stop scenarios.

The following tasks are to be considered:

1. Literature study
   a. Pressure pulsations of a Francis turbine
   b. Fatigue loads on a Francis turbine
2. Software knowledge
   a. Labview will be used for the measurements
   b. Matlab will be used for the evaluation of the measurements
3. Laboratory preparations
   a. Dynamic and static calibration of the instruments used in the test rig.
4. Measurements in the Waterpower laboratory:
   a. Complete hill diagram for a Francis-99 turbine.
   b. Stress measurements in the runner at runaway speed, start-up and shut down

-- ” --

Within 14 days of receiving the written text on the master thesis, the candidate shall submit a research plan for his project to the department.

When the thesis is evaluated, emphasis is put on processing of the results, and that they are presented in tabular and/or graphic form in a clear manner, and that they are analyzed carefully.

The thesis should be formulated as a research report with summary both in English and Norwegian, conclusion, literature references, table of contents etc. During the preparation of the text, the candidate should make an effort to produce a well-structured and easily readable report. In order to ease the evaluation of the thesis, it is important that the cross-references are correct. In the making of the report, strong emphasis should be placed on both a thorough discussion of the results and an orderly presentation.

The candidate is requested to initiate and keep close contact with his/her academic supervisor(s) throughout the working period. The candidate must follow the rules and regulations of NTNU as well as passive directions given by the Department of Energy and Process Engineering.

Risk assessment of the candidate's work shall be carried out according to the department's procedures. The risk assessment must be documented and included as part of the final report. Events related to the candidate's work adversely affecting the health, safety or security, must be documented and included as part of the final report. If the documentation on risk assessment represents a large number of pages, the full version is to be submitted electronically to the supervisor and an excerpt is included in the report.

Pursuant to “Regulations concerning the supplementary provisions to the technology study program/Master of Science” at NTNU §20, the Department reserves the permission to utilize all the results and data for teaching and research purposes as well as in future publications.

The final report is to be submitted digitally in DAIM. An executive summary of the thesis including title, student’s name, supervisor's name, year, department name, and NTNU's logo and name, shall be submitted to the department as a separate pdf file. Based on an agreement with the supervisor, the final report and other material and documents may be given to the supervisor in digital format.

☒ Work to be done in the Waterpower laboratory
☐ Field work

Department of Energy and Process Engineering, 13. August 2018

Ole G. Dahlhaug

Ole Gunnar Dahlhaug
Academic Supervisor

Roy Johnsen
Supervisor

Co-Supervisors:

- Chirag Trivedi
- Igor Iliev
- Einar Agnalt

Preface

This master's thesis was conducted, and written, at the Waterpower Laboratory, Department of Energy and Process Engineering at Norwegian University of Science and Technology during the autumn of 2018. My background as a student of Product Development and Material Engineering, so that is why this thesis is under the department of Mechanical Engineering and Industrial Design. Which is why I have two professors as supervisors, as well as three co-supervisors. It should be noted that Ole Gunnar Dahlhaug is the supervisor I have worked with and who has provided guidance during this thesis.

The work has been demanding, challenging and overall- fun. The work consisted of a large amount of practical laboratory measurements. I would like to thank Joar Grimstad and PhD candidate Einar Agnalt for helping me both understand and conduct the practical experiments.

As a student with no background in hydropower, there was quite a lot to learn about turbines during this semester. Professor Ole Gunnar Dahlhaug and PhD candidate Igor Iliev for helping me understand the dynamics of the Francis turbines.

I would also like to thank my last co-supervisor PhD candidate Chiraq Trivedi, as well as all the students and employees at the Waterpower Laboratory for creating a welcoming and supportive atmosphere during my time there.

Eirik Lødemel
Trondheim, January 7, 2019

Abstract

The expansion of intermittent renewable energy sources in the European energy market is leading to an increasing demand of regulatory energy sources to stabilize the energy grid. Hydropower can act as a regulatory energy supply, but that is requiring a more flexible day-to-day operation of turbines. This leads to turbines having to operate to a larger degree in unfavorable operating conditions when it comes to efficiency and fatigue, and an increase in start-stop cycles.

Variable speed turbines do not have to operate at a synchronous speed, and therefore has greater flexibility when it comes to operation. This thesis aims to investigate the effect variable speed operation can have on the fatigue life of the runner. To accomplish this, pressure measurements for a scaled model of a low-specific-speed Francis turbine has been conducted.

These pressure measurements are used to map the pressure pulsations and calculate stresses and fatigue over the operating range for start-stop cycles and for steady-state operation.
The frequencies of the pressure pulsations were also analyzed. But couldn't be used for the fatigue analyzes since they were not measured for the runner blade.
The results show that the fatigue loads can be significantly reduced by reducing the runner speed with a variable speed turbine. The most significant reductions in fatigue loads are from start-stop cycles, where a slight reduction in runner speed at part load gave above 80 percent reduction in fatigue loads.

Because the fatigue results were based solely on pressure measurements, several assumptions had to be made in order to produce results. The uncertainty these assumptions bring are large enough that the results should not be used directly, but rather as indications on the relative differences on the operating range.

Sammendrag

Utvidelsen av fornybare energikilder i det europeiske energimarkedet fører til en økende etterspørsel etter regulerbare energikilder som kan stabilisere nettfrekvensen. Vannkraft kan fungere som en regulerbar energikilde, men det stiller krav om en mer fleksibel daglig drift av turbinene. Dette fører til at turbinene i større grad å operere under ugunstige driftsforhold når det gjelder effektivitet og utmattelse, i tillegg til en økning i antall start-stop sykluser.

Turbiner med som kan operere med variabel turtallskjøring har større fleksibilitet når det gjelder hva slags operasjonsparametere de kan driftes med. Dette oppgaven tar til sikte å undersøke hvordan operasjon med variabelt turtallskjøring kan redusere utmattelsen i løpehjulet til Francis turbiner. For å oppnå dette har det blitt utført trykkmålinger på en skalert modellturbin med lav spesifikk hastighet.

Trykkmålingene har blitt brukt til å kartlegge trykkpulsasjoner og beregne spenninger og utmattelse i løpeskovlen for hele driftsområdet. Frekvensene til trykkpulsasjonene har også blitt undersøkt, men har ikke blitt brukt videre siden spenningene som oppstår på løpehjulsskovlen har andre frekvenser.

Resultatene viser at utmattelsesbelastningen kan reduseres kraftig ved å bruke en turbin med variable hastighet. De største reduseringene i utmattelsesbelastninger finner man for start-stop sykluser, hvor en liten reduksjon i løpehjulshastighet førte til over 80 prosent mindre utmattelsesbelastninger.

Siden utmattelsesberegningene kun var basert på trykkmålinger måtte en rekke antagelser tas for å produsere resultater. Usikkerhetene disse beregningene skaper gjør at resultatene ikke kan bruker som absoluttverdier, men heller som indikatorer på de relative forskjellene innenfor driftsområdet.

Symbols and abbreviations

Symbol	Description	Unit
ϵ	Strain	-
σ	Stress	Pa
v	Poisson's ratio	-
n	Runner Speed	RPM
S	Constant amplitude stress range	Pa
P	Pressure	Pa
N	Cycles to failure	-
C	Fraction of lifetime consumed	-
T	Torque	Nm
Q_{ED}	Dimensionless Discharge Factor	-
Q	Charge	V
Q	Minimum change in value	-
N_{ED}	Dimensionless Rotational Speed Factor	-
M	Number of bits	-
m	Constant for inverse slope of S-N curve	-
K_t	Stress concentration factor	-
K_1	Constant for S-N curve.	-
g	Gravity	m/s^2
E	Modulus of Elasticity	Pa
σ_m	Mean stress	Pa
σ_{eff}	Effective stress	Pa
σ_a	Stress amplitude	Pa
σ_{VM}	Von Mises stress	Pa
n_h	Cycles per hour	-
Z_{sb}	Number of Splitter Blades	-
Z_r	Number of Runner Blades	-
Z_{gv}	Number of Guide Vanes	-
P_σ	Stress to pressure factor	-
N_O	Cycles to failure for operating point	-
F_{rsb}	Splitter Blade Passing Frequency	Hz
F_{rb}	Runner Blade Frequency	Hz
F_r	Rheingans Frequency	Hz
F_n	Runner Frequency	Hz
F_{gv}	Guide Vane Frequency	Hz
E_{FSR}	Range of analog signal	-

Abbreviation	Description
BEP	Best Efficiency Point
CAL	Constant Amplitude Loads
VAL	Variable Amplitude Loads
cDAQ	Compact Data Acquisition System
CFD	Computer Fluid Dynamics
FEM	Finite Element Method
FFT	Fast Fourier Transform
H	Head
HCF	High Cycle Fatigue
Hz	Frequency
LCF	Low Cycle Fatigue
RPM	Revolves Pr. Minute
RSI	Rotor-Stator Interaction
S-N	Stress-Cycles to failure
VAL	Variable Amplitude Loads
NTNU	Norwegian University of Science and Technology
LSB	Least Significant Bit
FE	Finite Element
DAQ	Data Acquisition
cDAQ	Compact Data Acquisition
NI	National Instruments
FSI	Fluid Structure Interaction
UTS	Ultimate Tensile Strength
SNL	Speed-No-Load

Contents

1.Theory

1.1. Pressure pulsations

One of the most common operational difficulties for Francis turbines is pressure pulsations. Pressure pulsations creates vibrations which can cause fatigue and material defects. Because of the design of Francis turbines and the nature of flow, pressure pulsations will occur in all operational regimes.
Due to the expansion in intermittent renewable energy in Europe the European energy market to an increasing degree is in need of regulatory energy supplies. Hydropower has the ability to meet these demands, but that requires the turbines to operate at a higher number of start-stop cycles and to a larger degree operate on part-load. [11]
Operating on part load can be severely damaging to Francis turbines as a vortex rope will appear in the draft tube at some operation points, usually between 50% and 85% load. [8]

Pressure pulsations with particularly high amplitudes are mainly cause by four different frequencies. Guide vane frequency, Runner blade frequency, Rheingans frequency, Runner frequency. [6]

Runner frequency:
The runner frequency will usually not have large enough amplitudes to cause significant problems if the runner is undamaged and balanced. The frequency is determined by the runner speed. [5]

$$F_n = \frac{n}{60} \qquad \text{(Hz)} \qquad [1]$$

Where n is the runner speed denoted in rpm.

Two different frequencies occur between the runner blades and the guide vanes. One for every time a particular runner blade passes a guide vane and one for every time a particular guide vane is passed by one of the runner blades. This is known as Rotor-Stator Interaction. [7]

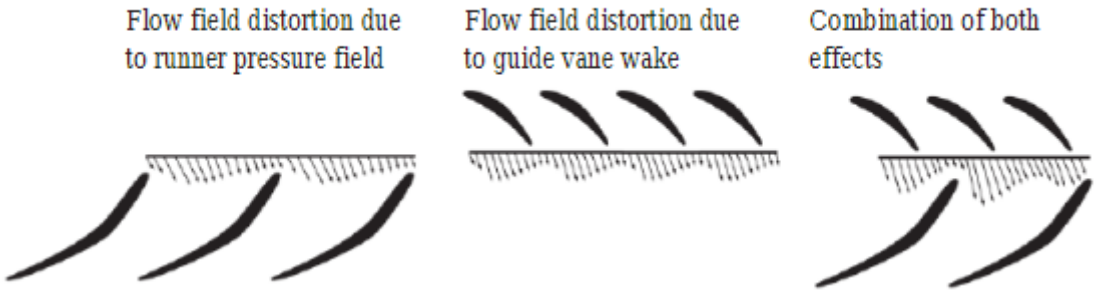

Figure 1.1: Flow field distortion between guide vanes and runner blades. Figure from One-dimensional modeling of rotor stator interaction in Francis pump-turbine. [9]

Runner blade frequency:

$$F_{rb} = Z_r * F_n \qquad \text{(Hz)} \qquad [2]$$

Where Z_r is the number of runner blades on the runner.

Every time a runner blade approaches a guide vane there will be an increase in local pressure, creating a pressure pulsation. Because this pressure pulsation is created every time a runner blade passes the same guide vane its frequency is determined by the number of runner blades and the runner frequency. The amplitude is greatly affected by the distance between the runner blades and the guide vanes, where an increase in the distance causes a formidable reduction. [7]

Guide vane frequency:

$$F_{gv} = Z_{gv} * F_n \qquad \text{(Hz)} \qquad [3]$$

Z_{gv} is the number of guide vanes.
The pressure difference between the pressure-and suction side between two guide vanes creates a non-uniform pressure and velocity field that the runner blades passes every time they move past a guide vane. There are created one such non-uniform pressure and velocity field for each guide vane, which means that the frequency is decided by the number of guide vanes and the runner frequency. [5,7]

Rheingans frequency:

Due to the rotating component of the absolute velocity at the outlet from the runner, a cavitated vortex rope appears in the draft tube. This creates low frequency pressure amplitudes. The direction of the vortex is decided by the operating regime of the turbine. At full load, the rotating component of the absolute velocity will move in the opposite direction of the runner and at part load the same direction as the runner. This is because there is a rotational component of the absolute velocity when the water exits the runner when it is operating outside of the Best Efficiency Point. The rotational velocity of the water exiting the runner will be larger the further away from BEP the runner is operating.

$$\frac{F_n}{3{,}6} < F_r < \frac{F_n}{3} \qquad \text{(Hz)} \qquad [4]$$

1.2. Material science

$$\text{Stress } \sigma = \frac{Force}{Cross\text{-}sectional\ Area} = \frac{F}{A} \qquad \text{(Pa)} \qquad [5]$$

$$\text{Strain } \epsilon = \frac{Elongation}{Original\ length} = \frac{\Delta L}{L} \qquad \text{(-)} \qquad [6]$$

Strain can be separated into nominal tensile strain and nominal lateral strain. Where tensile strain is the strain that occurs parallel to the stress applied and lateral strain is the strain that occurs normal to the stress applied.

The relationship between the nominal lateral strain and the nominal tensile strain is called Poisson's ratio and is defined by

$$\nu = \frac{\varepsilon_l}{\varepsilon_t} \qquad \text{(-)} \qquad [7]$$

For elastic deformation, the relationship between stress and strain is described by Hooks law.

$$\sigma = E * \varepsilon \qquad \text{(Pa)} \qquad [8]$$

Where σ is the stress applied, ε is the strain and E is Young's modulus. Which is the stiffness value of the material. This relationship only applies when the stress is relatively small, after a certain threshold, the yield limit σ_Y, plastic deformation will occur. If the stress keeps increasing this will eventually lead to fracture. Fracture can also occur as a fatigue or fast fracture. Fast fracture is the result of a flaw in the material, often a crack, expands quickly due to applied stress so that the material fractures.

1.2.1. Fatigue

During the lifetime of most materials they are subjugated to both constant amplitude fatigue loads and variable amplitude loads. The runner blades in a Francis turbine are exposed to both. These low level stress cycles will at some point form cracks in the material which will grow until the material fractures.
To give a lifetime assessment of the runner blades, measuring the impact of both amplitude loads are performed and then the number of cycles the given material can withstand is plotted in an S-N curve. The S-N curve describes the relationship between amplitude size of cyclic loads and the number cycles to failure. Both in a logarithmic scale. An S-N curve can usually be divided into three regions. The plastic region, elastic region and the infinite life region. Stress amplitudes that leads to plastic deformation leads to a low number of cycles before failure, this region describes what is called low cycle fatigue. While stress amplitudes that

leads to elastic deformation either leads to a medium number of cycles or if they are low enough over large number of cycles, often referred to as infinite life. These are called high cycle fatigue. [33]

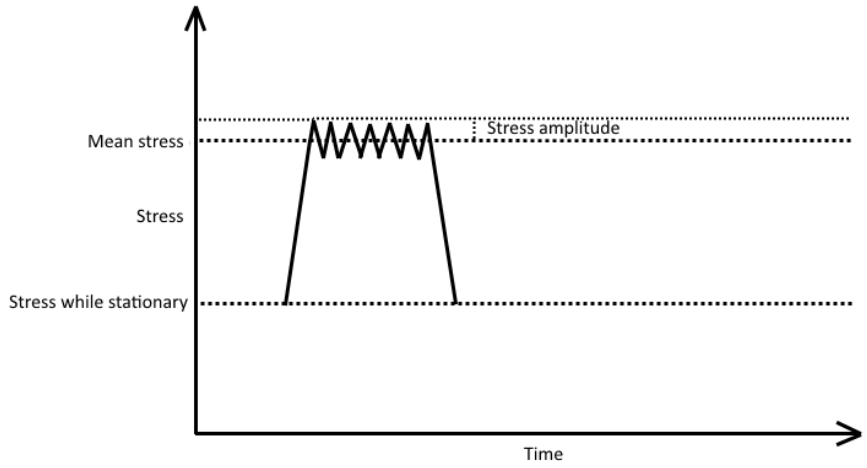

Figure 1.2: Stresses. Showing a cycle of a one mean stress and several stress amplitudes occurring on top of it.

For Francis turbine runners, high cycle fatigue is the result of fluctuating stresses during operation at a specific operating point, noted as stress amplitude in the picture above. Because of the high rotational speed of the turbine these amplitudes occur thousands of times per minute. The larger stress amplitudes that creates low cycle fatigue occur when changing operating conditions, the largest being a change from stationary condition to operating condition, which occurs during start-stop cycles.

When the stress amplitudes are low enough they will reach the endurance limit, and one can assume that they will never lead to failure. Since infinite number of cycles can't be tested on a material this is commonly assumed at over 10^7 cycles. However, for Francis turbines infinite life cannot be assumed at 10^7 cycles, as there are pressure fluctuations occurring at very high frequencies during operation. RSI from the guide vane passing frequency for a turbine with 20 guide vanes occurs 12000 times every minute if operating at 600 RPM, which would result in over 10^7 cycles in under 14 operating hours.

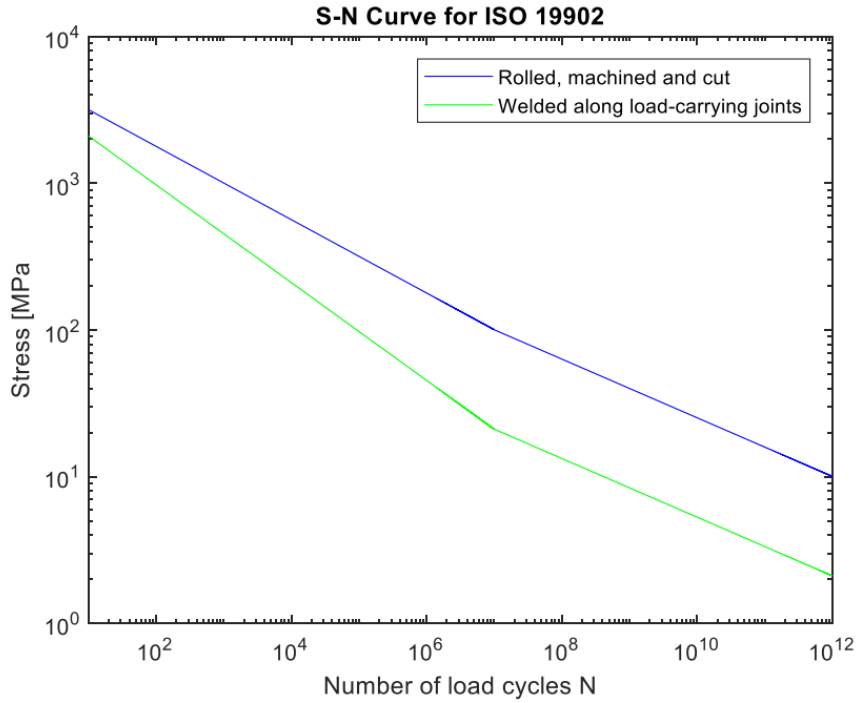

Figure 1.3: S-N curve from ISO 19902[16]. Showing two different S-N curves based on structure parameters.

In this thesis an S-N Curve model from ISO 19902 is used. [16]
ISO 19902 describes the relationship between the number of cycles to failure N and the constant amplitude stress range S with the following equation.

$$log_{10}N = log_{10}K_1 - m \cdot log_{10}S \qquad \text{(Cycles)} \qquad [9]$$

Where K_1 is a constant and m is the inverse slope for the S-N curve. Their values are values are determined by the size of N and the construction details of the material at the spot which are being considered. Important to notice that the constant amplitude stress range is measured in MPa in this equation.

1.2.2. Goodman's Method

It's not only the stress amplitude that contributes to the fatigue of a material. A stress amplitude during already high levels of stress contributes more than a stress amplitude in a lower state of stress. To account for the mean stress an effective stress parameter is calculated. A commonly used method to account for this is Goodman's method. [32] [14]

$$\sigma_{eff} = \sigma_a * (\frac{UTS}{UTS - \sigma_m}) \qquad \text{(Pa)} \qquad [10]$$

Where σ_a is the stress amplitude: $\sigma_a = \frac{\sigma_{max} - \sigma_{min}}{2}$ (Pa) [11]
UTS is the ultimate tensile strength of the material and σ_m is the mean stress

$$\sigma_m = \frac{\sigma_{max} + \sigma_{min}}{2} \qquad \text{(Pa)} \qquad [12]$$

1.2.3. Cumulative Damage

When there is variable amplitude loads the lifetime of the structure is described by Miner's rule.

$$C = \sum_{i=1}^{k} \frac{n_i}{N_i} \qquad (-) \qquad [13]$$

Where k is the number of different levels of stress, n is the number of cycles for stress level i and N is the number of cycles before failure for stress level i. The result, C, is the fraction of lifetime consumed by the stresses. [8]

1.3. Recent studies done on Francis turbines

In the recent years there have been done a lot of different studies on fatigue on Francis runners. Both by doing experiments and simulations, often a combination.

1.3.1. Pressure pulsations and fatigue

Fatigue analysis of the Prototype Francis runner based on site measurements and simulation. [3]

In Fatigue analysis of the Prototype Francis runner based on site measurements and simulation, Huang, Chamberland-Lauzon, Oram, Klopfer and Ruchonnet presents fatigue analysis on prototype Francis runners based strain gauge site measurements and numerical simulations. The paper also discusses the damage factors at different operating points, arguing that due to the increasing energy production from intermittent renewable energy sources hydropower plants will have to operate more outside of BEP.

Strain gauges were installed on the blades of several Francis runners. They used stress calculations for different operating conditions to place the strain gauges at stress hot spots. The results from the strain gauge measurements provided them with the static and dynamic stresses at the different operating conditions.
They obtained the corresponding numerical static stress with CFD simulation and FEM calculation. X Huang et al validated the static stress calculation using strain gauge measurements on several turbines.

Fast Fourier transform analysis were used to evaluate the dynamic stresses caused by rotor-stator interaction. CFD calculation for dynamic pressure and the harmonic response of the

runner is standard analysis in the industry. They created a finite element model of a runner with boundary conditions for dynamic stress analysis.

The stochastic loads regime occurs during start-up, speed-no-load and transient events.
From a group of blade deformations procured by standard calculations, the one matching best with the strain gauge measurements was selected. Geometrical extrapolation from the strain gauges to the peak stress location was used to find the peak stress amplitude.

5 turbines were studied in regards of fatigue and life time assessment, with varying design types and power categories.
Stochastic stresses dominate from speed-no-load to 40 percent of maximum power. As the power increases above 40%, the fatigue load from the rotor-stator interaction gave the dominating fatigue component until best efficiency point was reached.
Low load operation can have a huge impact on lifetime if the runner is operated in it over extended periods of time and the runner hasn't been specifically designed for it.
Each start-stop can equal the fatigue load of extended periods of operation on speed-no-load or low part load and several years of operation on full load. Because of the high fatigue load from start-stop there is a case for running the turbine on speed-no-load instead of stopping it to prevent damage.

Static and Dynamic stress analyses of the prototype high head Francis runner based on site measurement [2]

In 2014, X Huang, together with Oram and Sick takes a closer look at static and dynamic stress in Static and Dynamic stress analyses of the prototype high head Francis runner based on site measurement
Due to the increased demand of hydropower to operate outside of BEP there is a need to analyze life time expectancy based on dynamic behavior analysis of Francis turbine runners. There have been plenty of such analysis during the past years, but most of them have not been validated by site measurement. Therefore, both site measurements and numerical analysis on a high head Francis turbine were performed. The prototype had 28 guide vanes, 17 runner blades, a head of 377 meters and the nominal rotational speed was 375 RPM. They placed both pressure transducers and strain gauges on both the suction and pressure side of the runner blades. The strain gauges were placed both in radial and tangential directions.

The sampling frequency used when recording the measurement data was 1613 Hz. They split the measurements into 12 operating points.

	OP0	OP1	OP2	OP3	OP4	OP5	OP6	OP7	OP8	OP9	OP10	OP11
P/P_{rated}	0%	21%	29%	36%	45%	53%	61%	71%	79%	88%	97%	106%

Figure 1.4: Table of selected operating points used in Static and Dynamic stress analyses of the prototype high head Francis runner based on site measurement. [2]

They found that the radially directed static stresses decreased with increasing power while the tangentially directed slightly increased. Those located close to the band "showed an opposite behavior."

For dynamic stresses, rotor-stator interaction is the main contributor. The guide vane passing frequency for this runner at 375 RPM is 175 Hz. They graphed the dynamic stresses at the various operating conditions. Being relatively low until a steep ascent from OP4 to OP5 and then a gradual decline from OP6 to overload.

Numerical simulations:
Stress analysis were conducted with the finite element method. They used computational fluid dynamics to create pressure distributions for the different load cases. Then they compared the measurement results with their simulation for static stresses on the strain gauge locations and used linear regression to validate that their model was sufficiently accurate. The R^2 values were all above 0.890.

Thereafter locations and maximum static von Mises stresses were identified and graphed versus power output.

A numerical modal analysis was carried out, finding the important natural frequencies of the runner. One natural frequency that was very close to the guide vane passing frequency was found. Because of this the dynamic stresses are very sensitive on the damping. The damping values of OP5 and OP11 were adjusted so that the calculated stresses caused by RSI matched the measured ones.

Dynamic loads in Francis runners and their impact on fatigue life [11]

In Dynamic loads in Francis runners and their impact on fatigue life, Seidel, Mende, Hubner, Weber and Otto compares the damage contributions to a medium high-head Francis turbine for two different operational modes. Base load and grid stabilization.

Operational mode	Start up [Cycles/day]	Speed no load [%]	Low part load [%]	Part load [%]	Around BEP [%]	High load [%]
Base load	1	1	0	25	49	25
Grid stabilization	10	4	24	24	24	24

Table 1.1: Assumed load universes for different operational modes of a medium high head Francis used in Dynamic loads in Francis Runners and their impact on fatigue life[11]

The paper looks at the different flow patterns that characterizes the different operational conditions. At runaway you have cavitation in the runner and draft tube as well as strong secondary flow effects.

At speed-no-load there was a large backflow both in the draft tube and the runner creating cavitation channel vortices. This results in high amplitude pressure fluctuations.

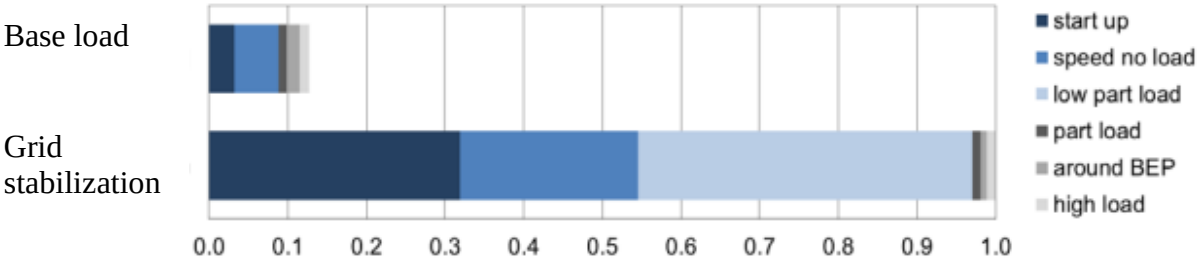

Figure 1.5: Relative damage contributions of the load universes. From Francis used in Dynamic loads in Francis Runners and their impact on fatigue life.[11]

The paper gives an insight in the difference in damage contributing factors which has to be expected for a future where hydropower to a larger degree will be used for grid stabilization.

Mechanical robustness of Francis runners, requirements to reduce the risk of cracks in blades [1]

In Mechanical robustness of Francis runners, requirements to reduce the risk of cracks in blades, Bjørndal, Reynaud and Holo measured runner stresses for both low head and high head prototype Francis runners with strain gauges as well as doing Finite Elements method (FEM) analysis on a research model runner. The objective of this research was to improve turbine contracts to "ensure the mechanical robustness of new runners".

For the low head runner, operation at part load was the major source of large stress variations. The conference paper assumes that this for the most part is related to hydraulic inter-blade vortexes in the runner. This was solved for this turbine by restricting operation at part load to only uploading and downloading.

For the high head runners, the guide vane passing frequency was the main contributor to stress variations. The amplitudes of the guide vane passing frequency were found to be the most significant between 50 and 60% opening. For fatigue loading, operating at maximum load gave high stress variations and high mean tensile stress, which is unfavorable.

Start-up scenarios was also specifically investigated. While start-up gives large variation in turbine stresses, the problem is usually negligible when evaluating runner fatigue lifetime because of the limited amount of cycles.

With strain gauge measurements they found out that the startup procedure can significantly affect the runner life expectancy. A rainflow analysis of the startup procedure gave 75 load cycles with amplitudes over 100 MPa. Which results in $1.4*10^6$ load cycles over 50 years with one start per day. Reducing the guide vane opening during the startup procedure reduced the dynamic loads on the runner.

FEM analysis found that thicker runner blade outlet will increase the runner fatigue lifetime and reduce the risk of blade cracking.

Bjørndal et al propose a temporary solution to ensure the mechanical strength of new runners. That the manufacturer should "document the expected dynamic load on the runner based on advanced studies and measurements".

1.3.2. Strain gauge measurements

[13] In 2016 Einar Agnalt did pressure measurements inside the Francis turbine runner in the waterpower laboratory at the Norwegian University for Science and Technology.

The experiments were done with a splitter blade runner design with 15+15 blades and 28 guide vanes. During the experiments semiconducturbased strain gauges were used on one runner blade as well as five pressure sensors mounted in the hub. The pressure sensors were Kulite XTE-190(m) with a range of 0-3.5 bar and the strain gauge was Kulite S/UDP-350-175. The strain gauge was set up in a quarter Wheatstone bridge configuration, which gives no temperature compensation. There was a zero point drift during the experiment, so the results from the strain gauge mostly only provided indications of correlation between strain in the blade and pressure pulsations, but not precise and reliable strain data.

1.3.3. Flexible turbines

[4] In Variable-speed Operation and Pressure Pulsations in a Francis Turbine and a Pump-Turbine(2018), Iliev, Trivedi, Agnalt and Dahlhaug experimented with variable-speed operation of the runner blades to reduce the amplitudes of pressure pulsations. They conducted the experiments with two different turbine runners. One splitter-bladed Francis turbine and one reversible-pump turbine.
The experiments were conducted with three scenarios, all assuming constant net head in the entire range of the discharge. The three scenarios were synchronous-speed operation at optimal head, +10% of the optimal head and -10% of the optimal head.
For the Francis turbine, variable-speed operation achieved 0,5% gain in maximum hydraulic efficiency compared to synchronous-speed operation at optimal head and up to 1,2% at 10% of the optimal head. Pressure pulsations were also affected by the variable-speed operation, with a reduction in the vaneless space and a none-to-slight increase in the draft tube cone.

1.4. Analysis method.

Histogram – peak to peak values

When measuring pressure pulsations, the important information is the size and frequency of the pulsations. The size is determined by the peak to peak value of each measured series. A histogram can be applied to remove statistically unlikely values by only using the data within a confidence interval, usually between 95 and 99 percent. The standard IEC60193 recommends a confidence interval of 97 percent. The pressure pulsations are measured together with the operating conditions. This makes it possible to accurately map the pressure pulsations in different operating points.

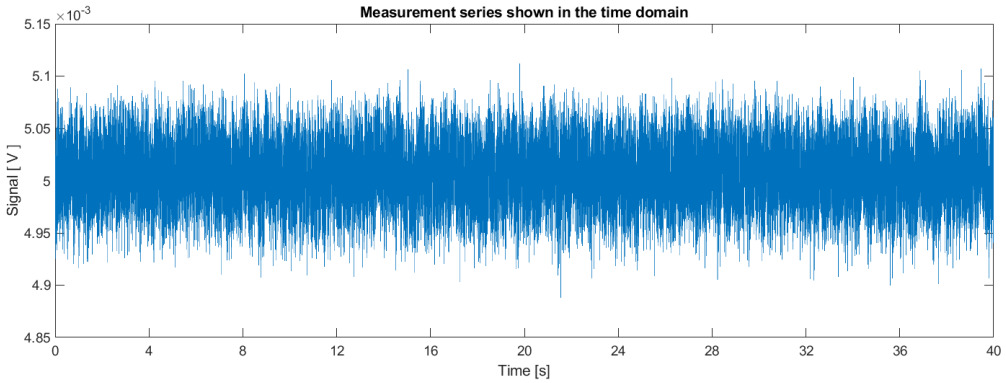

Figure 1.6: Measurement series shown in the time domain. With time in seconds along the x-axis and volts recorded along the y-axis

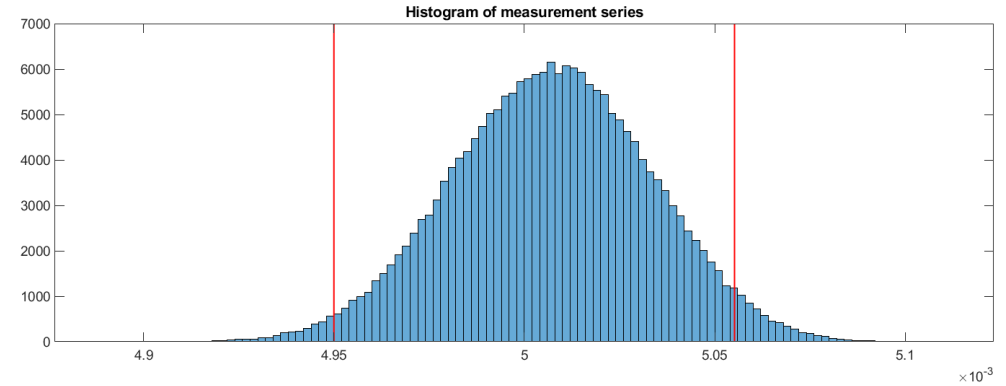

Figure 1.7: The same measurement series as shown in figure 1.6 displayed as a histogram. With volts along the x-axis and number of measured values along the y-axis. The red lines show the limits of a 97% confidence interval.

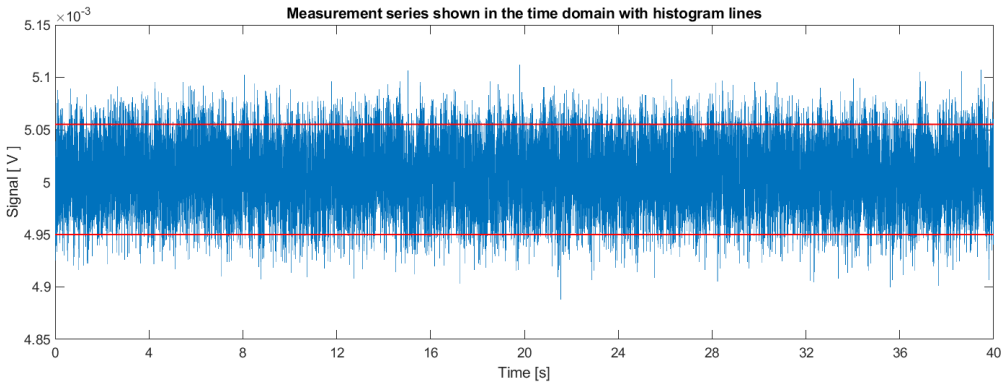

Figure 1.8: Measurement series shown in the time domain. With time in seconds along the x-axis and volts recorded along the y-axis The red lines show the limits of a 97% confidence interval.

Interpolation and number of measurements

The accuracy of hill diagrams for hydraulic efficiency and pressure pulsations is determined by the number of operating points measured, the uncertainties in measurement and the method of interpolation and extrapolation. For hill diagrams a shape-preserving interpolation method gives the most accurate results when interpolating along the guide vane angles.

Sampling rate

The data acquired during measurements is a number of analog values from an analog signal. They are then converted to a digital signal. This is beneficial because it allows for storing a vast amount of information and makes it easier to sort it and use it for practical purposes afterwards. The analog signal has infinite resolution, however, when sampling the signal, it is not possible to maintain an infinite resolution, as it would require an infinitely long number to represent an infinite resolution. The resolution of the sampled signal is determined by the number of discrete values that can be represented inside the range of the analog value. That number is determined by the number of bits used to store the digital signal. [21]

The minimum change that results in a change in the digital input is formulated by the least significant bit.

$$Q = \frac{E_{FSR}}{2^M} \qquad \text{(V)} \qquad [14]$$

Where Q is the minimum change, E_{FSR} is the range of the analog signal and M is the number of bits.

The sampling rate of the measurements is defined by the number of analog values stored per second. Since the recorded values are discrete and taken from a continuous signal, it is important to have a high enough sampling rate to imitate the continuous signal accurately.

The Nyquist-Shannon theorem [28] states that the sample rate should at least be twice the size of the highest significant frequency. If the frequency isn't high enough it can lead to aliasing. Since the signals is digitally reconstructed as sinusoids, the frequency of each cycle of sinusoids can be misrepresented if the sampling rate is too low, which is called aliasing. Which is when higher frequencies are misidentified as lower frequencies in the digitally

reconstructed signal due to too low sampling rates.

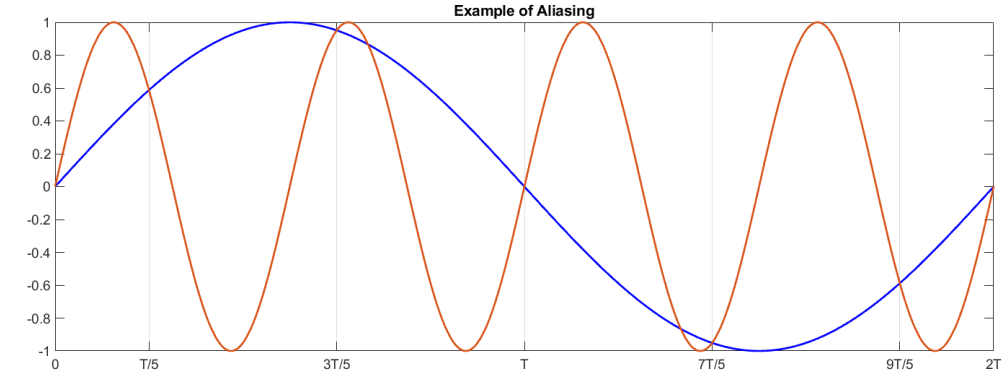

Figure 1.9: Example of how a higher frequency sinusoid can be misrepresented as lower frequency signal if the sampling rate is too low.

If the sample rate is too low, discrete values from the orange signal can be misrepresented as the blue signal, since they overlap every $\frac{2T}{5}$ periods.

The analog values can always be represented as a higher frequency section of sinusoids, there is no upper limit.

Oversampling can be used to minimize the effects of aliasing. By having a sampling rate far above what's required from the Nyquist-Shannon theorem. Oversampling can significantly increase the size of the data stored, but is common to do because it also increases the resolution and reduces the effect of noise in the measurements.

Fast Fourier transform is used to look at the impact of the different frequencies within the signal. The fast Fourier transform breaks down the sinusoids within the signal by converting it from the time domain to the frequency domain. An example of a fast Fourier transform of a signal from the time domain to the frequency domain is shown below.

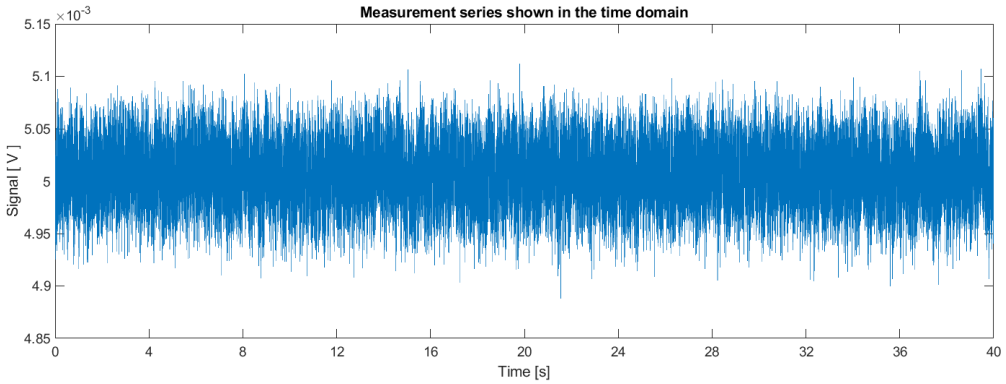

Figure 2.10:Measurement series shown in the time domain. With time in seconds along the x-axis and volts recorded along the y-axis

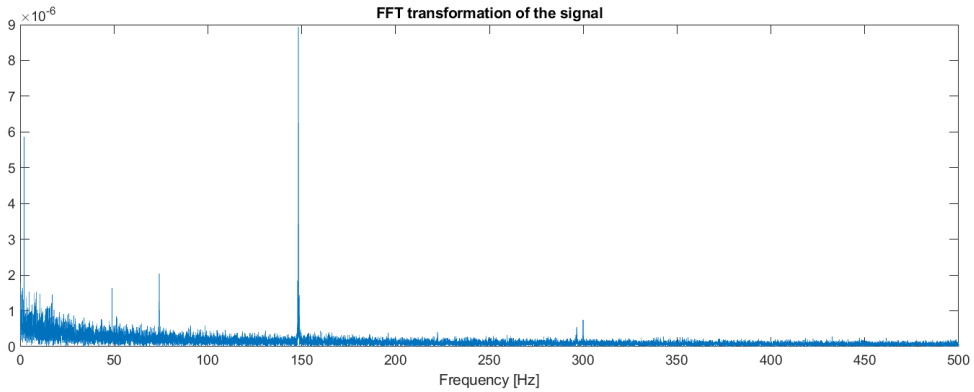

Figure 1.11: Same measurement series as shown in figure 1.10, presented in the frequency domain after a Fast Fourier Transform. Frequencies in Hz along the x-axis and signal values along the y-axis.

In this thesis the fast Fourier transform is done using Matlab R2018a. Matlab uses the following functions for FFT. Where Y is the output signal, X is the input signal and n is the length of the signal. [22]

$$Y(k) = \sum_{j=i}^{n} X(j) * W_n^{(j-1)(k-1)} \qquad (-) \qquad [15]$$

$$W_n = e^{\frac{-2\pi * i}{n}} \qquad (-) \qquad [16]$$

The frequency signal can be used to determine the sources of the pressure pulsations. It is clear in the example above that a pressure pulsation with a bit less than 150 in frequency is the main source. Because the frequency is slightly less than 150 and the runner speed is 297 RPM, we can determine that the main propagator of pressure pulsations at this operating point is the Blade Passing Frequency: $F_{rb} = Z_r * F_n = 30 * \frac{297}{60} = 148.5$

Welch method:

The Welch method separates the measurement series into several time-based segments. [30] Each of these segments are modified by a window function. This is done because the FFT assumes the signal to be periodic, and can be perfectly represented by an infinite number of sinusoids. Because this assumption does not hold true for actual measurement series, it causes errors in the transformation from time-based signal to frequency-based signal. These errors are called spectral leakage, and results in an intensity distortion of the peaks of the frequency signal.
The Welch method of time averaging over short modified periodograms aims to minimize spectral leakage by making the signal periodic in the time domain. The modification of the segmented windows does however remove information from the original signal. To counter this the windows are overlapped.

IEC60193[16] recommends using Hann window when analyzing pressure fluctuations. In this thesis a Hann window with 50 percent overlap is used. The function of the Hann window is shown below as well as the frequency specter of the same measurement series as used before. [29]

$$w(n) = \frac{1}{2}\left(1 - \cos\left(2\pi \frac{n}{N}\right)\right), \quad 0 \leq n \leq N \qquad (-) \qquad [17]$$

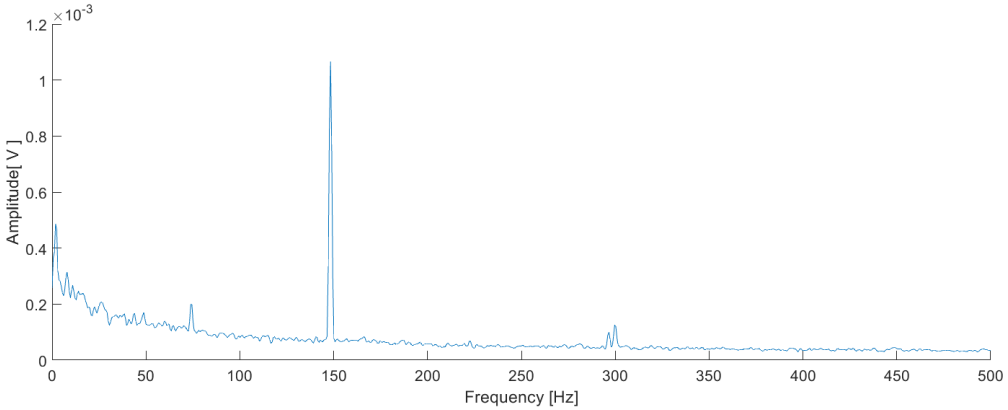

Figure 1.12: Same measurement series as shown in figure 1.10, presented in the frequency domain after a Fast Fourier Transform with the Welch method. Hann windowing used. Frequencies in Hz along the x-axis and signal values along the y-axis.

In the figure above the blade passing frequency is very easy to identify. Frequencies at around 75 Hz and 300 Hz can also be identified. The one around 75 Hz is because the runner blades are splitter blades, which means two different sets of 15 blades, resulting in a splitter blade passing frequency:

$$F_{rsb} = Z_{sb} * F_n = 15 * \frac{RPM}{60} = 74.25 \qquad (\text{Hz}) \qquad [18]$$

Where Z_{sb} is the number of splitter blades.
The frequency observed at around 300 Hz is due to harmonics. Which can be observed at every integer of each high-amplitude frequency, usually with a rapidly declining amplitude. An amplitude can also be seen closer to zero Hz. This is the Rheingans Frequency, which for 297 RPM would be between $\frac{\frac{297}{60}}{3{,}6} = 1.375$ and $\frac{\frac{297}{60}}{3} = 1.65$.

Because of the window length used is 5000 measurement values and the sample rate is 5000 Hz, a low frequency amplitude like the Rheingans Frequency will only be included once or twice per window, resulting in lower precision and a smearing of the results in the frequency spectrum.

2. Hypothesis

The objective of this thesis is to Evaluate how variable speed operation of Francis turbines can be utilized to minimize dynamic loads at start-stop scenarios.

Research has shown that start/stop cycles on Francis turbines significantly damages the runners and causes fatigue and eventually failure. [2][11] The main cause of these damages is pressure pulsations caused by RSI. To evaluate how variable speed operation can minimize dynamic loads, the amplitudes of the pressure pulsations occurring during different speed start-ups and synchronization has to be mapped.

Ideally strain gauges would be used to evaluate the strain on the runner blade. However, due to the complex surface of the runner blades, calibrating and getting absolute results from strain gauges was not possible at the time of this thesis. Strain gauges could have been used on the runner blade, but would only provide relative values and therefore would not give information that evaluating the pressure regime with pressure transducers doesn't already provide.

Since calibrated strain gauges could give valuable information about fatigue on the runner blades this thesis also attempts to calibrate strain gauges on a runner blade by comparing strain results from an FE simulation with results from a strain gauge on a runner blade.

As Illiev, Trivedi, Agnalt and Dahlhaug has shown in Variable-speed operation and pressure pulsations in a Francis turbine and a pump-turbine, it is possible to reduce pressure pulsations by operating with variable speed operation. [4]

This thesis will mostly focus on measuring pressure and pressure pulsation in the vaneless space between the guide vanes and the runner blades. Previous studies will be used to correlate these pressures with stress on the runner blade and a fatigue analysis will be conducted based on that.

2.1. Formulated Hypothesis

It is possible to significantly reduce the accumulated damage from start-stop cycles by operating with a variable speed turbine.

3. Laboratory setup

The experiments done during this thesis were conducted at The Waterpower Laboratory at NTNU. The facilities have test rigs for Francis, Pelton and pump turbines. In this thesis the Francis rig was used, which enables model test according to the IEC 60193 and IEC 60041 standards. [16] [17]

3.1. The Francis Rig

The Waterpower Laboratory at NTNU has an operational Francis turbine test rig for model testing. The system is set up so that it can be run in both an open loop and a closed loop configuration by regulating which valves are open. With an open loop configuration, which is what is used during this thesis, the Francis test rig has an available head of 16 meters. [18]

The Francis turbine is a scaled model of a 107.5 MW turbine used at Tokke power plant. It has a splitter blade runner with 15 splitter blades and 15 full length blades. It has 28 guide vanes, 14 stay vanes and 30 runner vanes. The inlet diameter is 0.63 meter and the outlet diameter is 0.349 meter.

3.1.1. Components

The Francis test rig consists of the following components.

1. Basement reservoir
2. Pumps
3. Piping
4. Upper reservoir
5. Two over-head tanks
6. A high pressure tank
7. Generator
8. Turbine
9. Draft tube
10. Draft tube tank

3.1.2. Open loop configuration

In an open loop configuration, water is pumped from the basement reservoir to the upper reservoir. From there is flows to the pressure tank and then to the turbine. After going through the turbine, the water goes through a draft tube and into a draft tube tank, which simulates a lower reservoir. After the draft tube tank, the water goes back into the basement reservoir.

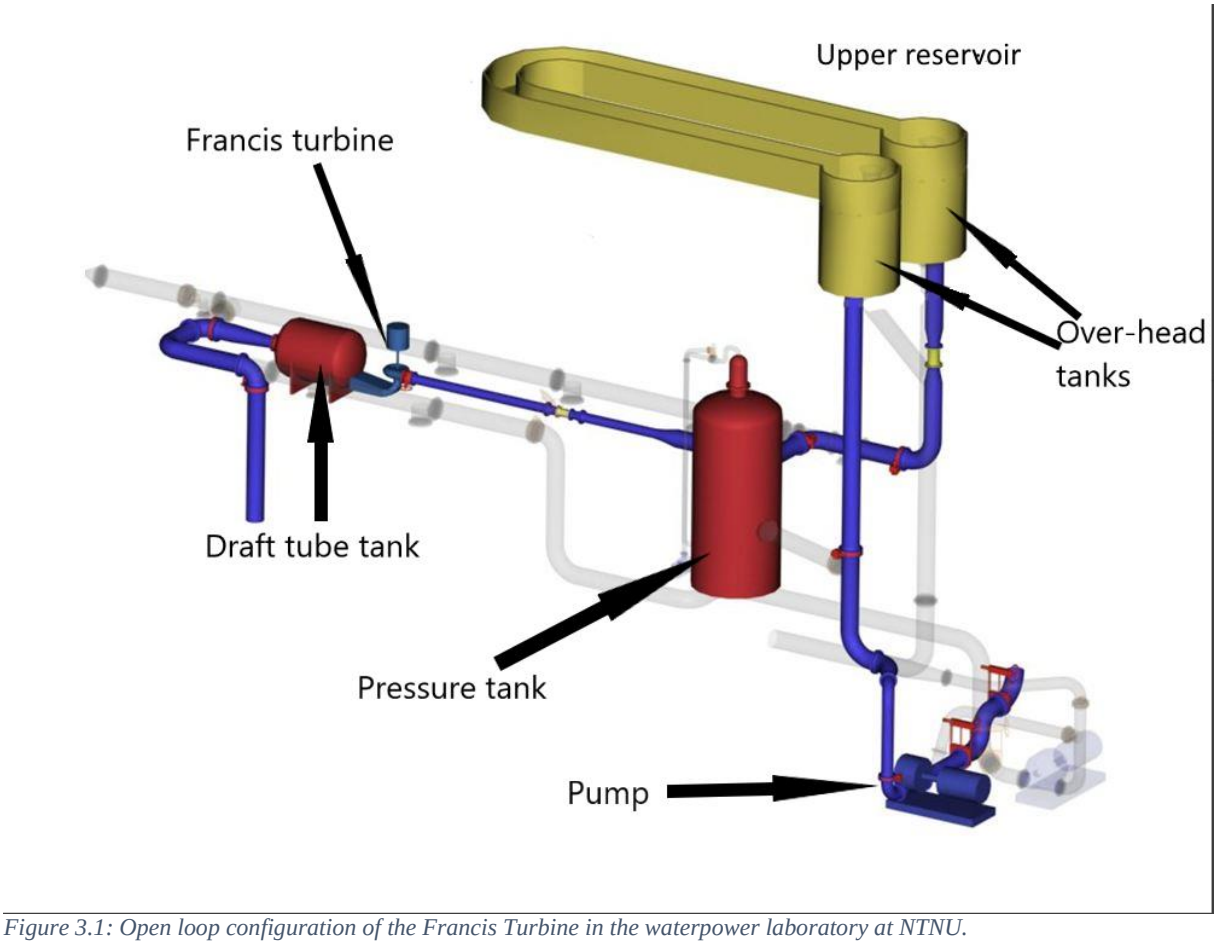

Figure 3.1: Open loop configuration of the Francis Turbine in the waterpower laboratory at NTNU.

3.2. Instrumentation

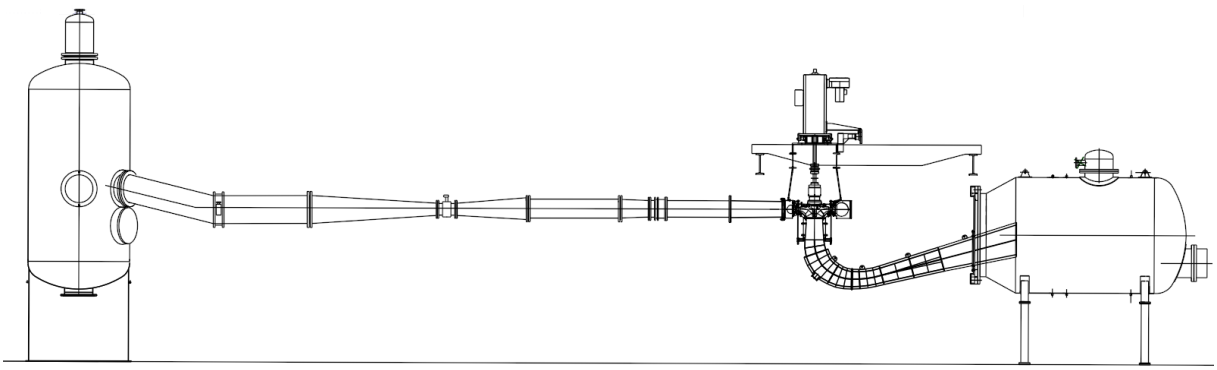

Figure 3.2: Illustration of the Francis turbine setup in the Waterpower Laboratory. Figure showing from left to right: The high pressure tank, inlet pipe to the turbine, turbine, generator, draft tube and draft tube tank.

Operating condition sensors		
Sensor placement	**Sensor name**	**Description**
Inlet pipe to turbine	FTQ1	Measuring flow rate in the inlet pipe to the turbine
Inlet pipe to turbine	PT PIN	Measuring pressure in the inlet to the turbine
Inlet pipe to turbine and draft tube	PT DP	Measuring differential pressure between inlet and outlet of turbine
Generator hydrostatic bearing	WT T1	Measuring generator torque
Thrust bearing	WT T2	Measuring friction torque
Thrust bearing	WT T3	Measuring axial load
Guide vane shaft	ZT 42	Measuring guide vane position
Inlet pipe to turbine	TT 41	Measuring temperature
Pressure transducers		
Between guide vanes and runner, position 4.	GV4	Measuring pressure in the vaneless space
Between guide vanes and runner, position 5.	GV5	Measuring pressure in the vaneless space
Between guide vanes and runner, position 6.	GV6	Measuring pressure in the vaneless space

Table 3.1: Operating condition sensors and pressure transducers. Placement, name and description.

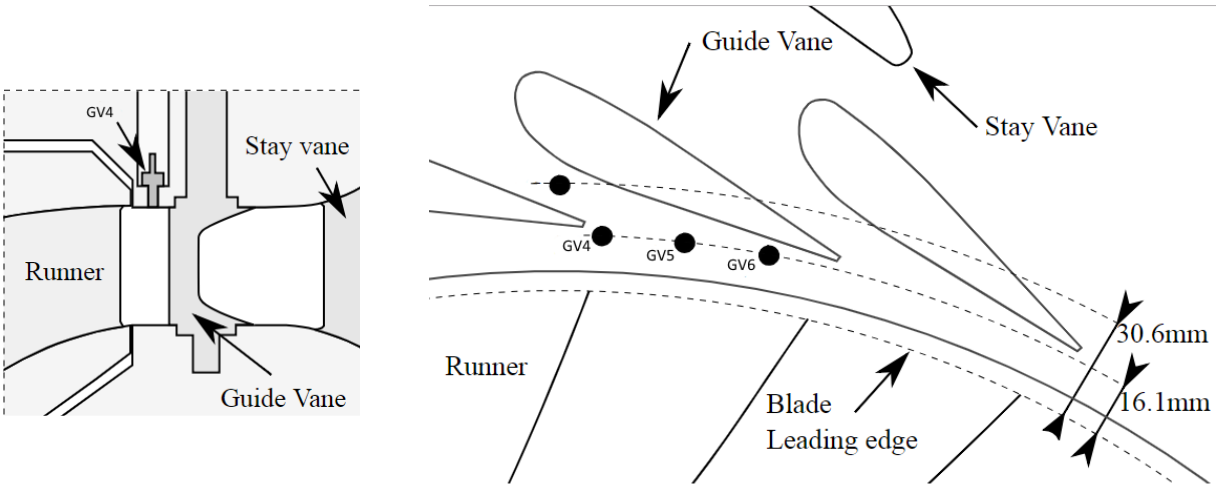

Figure 3.3: Placement of pressure transducers. Placed flush to the surface between the guide vanes and the runner blades.

3.3. Calibration and uncertainty

To ensure the validity of the results of the experiments the equipment has to be calibrated first. Both the equipment used for direct measurements and the equipment measuring the operating conditions during the experiment should be calibrated for accurate measurements. Because some of the equipment used has been calibrated recently and to decrease the scope of calibration work some of the equipment used was not calibrated right before the experiments. However, all equipment used for operating the Francis Rig have been previously calibrated to match the IEC 60193 Standard.

The uncertainty for operational sensors except for WT T1 and WT T2 are gathered from a measurement report done by Einar Agnalt in 2018. [25]
Calibration reports for friction torque and generator torque can be found in appendix C.

Sensor name	**Unit**	**Expanded calibrated uncertainty**	**Expanded long time stability**	**Expanded measurement repeatability**	**Total expanded uncertainty**	
					In units	**Percentage**
FTQ1	[m^3/s]	$0.3*10^{-3}$	$0.1*10^{-4}$	$1.1*10^{-3}$	0.001	0.56%
PT PIN	[kPa]	0.2	0.5	1.2	1.32	0.96%
PT DP	[kPa]	0.02	0.22	0.16	0.27	0.24%
ZT 42	[◦]	0.1		0.1	0.14	1.41%
AT 41	[◦C]	0.1		0.3	0.30	2.00%

Table 3.2: Uncertainties for operational sensors. Results from a measurement report done by Einar Agnalt[25].

Sensor name	**Unit**	**Expanded calibrated uncertainty**	**Total expanded uncertainty**	
			In units	**Percentage**
WT T1	[Nm]	0.6862	0.6862	0.2486%
WT T2	[Nm]	0.0910	0.0910	*

Table 3.3: Uncertainties for operational sensors.

*WT T2 was calibrated to a zero value, so the percentage is infinite.

3.3.1. Pressure transducers

The static calibration of the pressure sensors have done in accordance to the procedure by the German Calibration Service[12]. Which is a procedure designed to fulfill the requirements of IEC 17025[19], which is the main IEC standard used by calibration laboratories.
This procedure was used instead of how it has previously been done at The Waterpower Laboratory because it is designed to mitigate human errors. Unlike the previously used calibration sequences it also places a larger significance on the whole measurement range, which ensures a larger certainability that the calibration curve is linear.

The equipment used for calibration was a dead weight manometer and air as the medium. The pressure sensors were connected through a cDAQ system to a computer running a calibration program made with LabView. The cDAQ system consisted of a NI 9237 simultaneous bridge module connected to a NI cDAQ-9178 chassis. [23][24]

A minor drawback to using this procedure is that it takes longer to do the calibration, which provided some problems because the atmospheric pressure in the locale where the calibration was done was not constant. During one of the calibration processes the change in the atmospheric pressure was recorded to be over 2 millibar. To counter this the atmospheric pressure was checked before each measurement was taken in the final calibration series.

Calibration Equipment		**Model name**	**Range**	**Total expanded uncertainty**	
				In units	**Percentage**
Dead weight manometer		GE deadweight tester, P3023-6-P	30-2000 mbar	0.16 mbar	0,008 %
Pressure sensors				**Total expanded uncertainty**	
Sensor name	Model name	Unit	**Expanded calibrated uncertainty**	**In units**	**Percentage**
GV4	MEAS XP5	[kPa]	0.06630	0.06630	0.06383 %
GV5	Kulite XTE	[kPa]	0.02542	0.02542	0.02447 %
GV6	Kulite XTE	[kPa]	0.02385	0.02385	0.02296 %

Table 3.4: Uncertainties for pressure transducers.

3.3.2. Strain gauges

Due to difficulty with installing strain gauges onto the runner blades in the turbine and getting precise and accurate absolute measurement results from the strain gauges this thesis instead focuses on creating a procedure for calibration strain gauges using the finite element method.

This was done by first creating a model for measuring the strain on a runner blade with ANSYS mechanical. The model is built up by a runner blade held up by two fixed supports on at one end. The forces working on the runner blade consisting of the constant gravity as well as a remote force close to the edge of the blade.

This was recreated with a physical model. The forces were applied by gluing a nut close to the edge of the blade and then fastening weights to it.

The strain on the blade is measured with seven different sizes of remote forces. Ranging from 0.122 N to 85.0 N.

The weights added to the physical model ranged from 0.125 Kg to 8.66 Kg.

Due to the complex surface of the model, there were only two flat edges suitable for mounting the blade unto a stable surface. This put a limit on the direction of the force added to the blade.

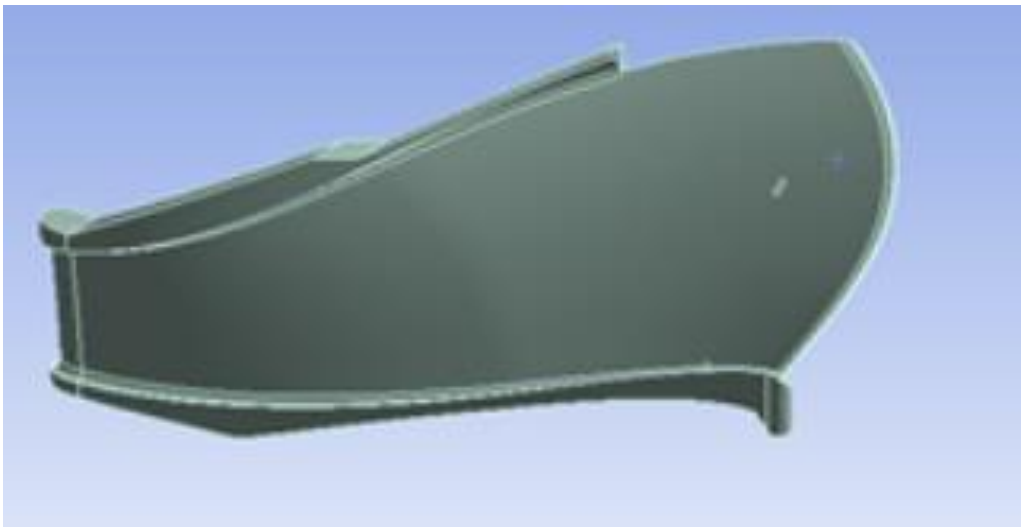

Figure 3.4:Ansys mechanical model of a runner blade.

Two strain gauges were placed on the runner blade in a half bridge configuration. The position of the strain gauge on the top side of the blade is illustrated in the picture above.

The results from the ANSYS mechanical model was used to calibrate the strain gauges. The average normal elastic strain along the direction of the strain gauges from the areas where the strain gauges were placed was graphed with the volt signals gained from the physical model.

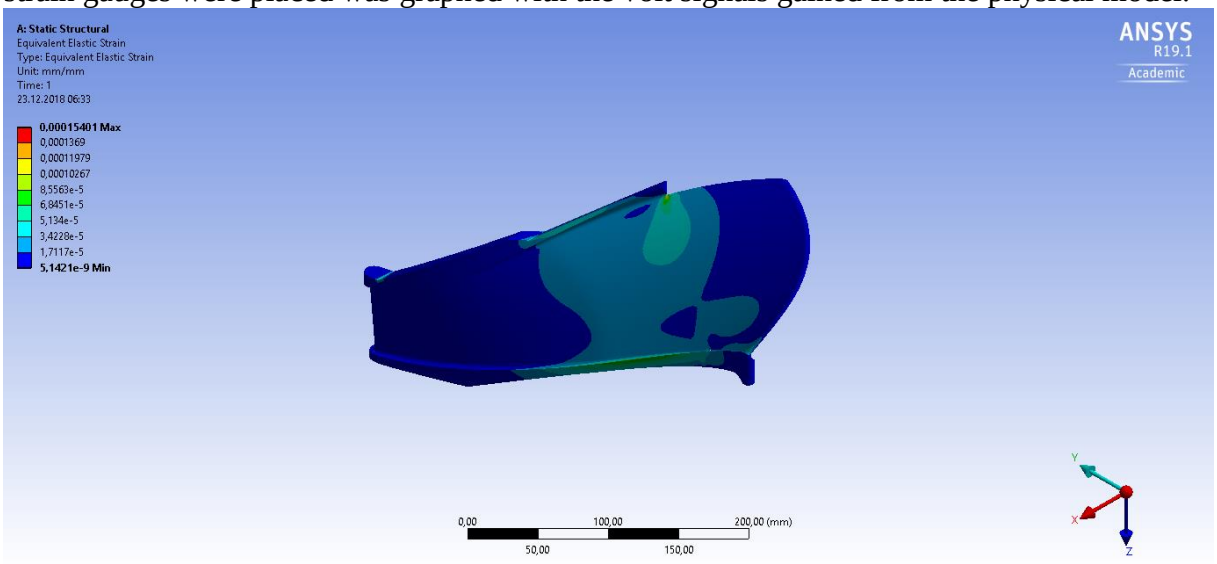

Figure 3.5: ANSYS mechanical model of the runner blade. Results for the whole blade showing equivalent elastic strain.

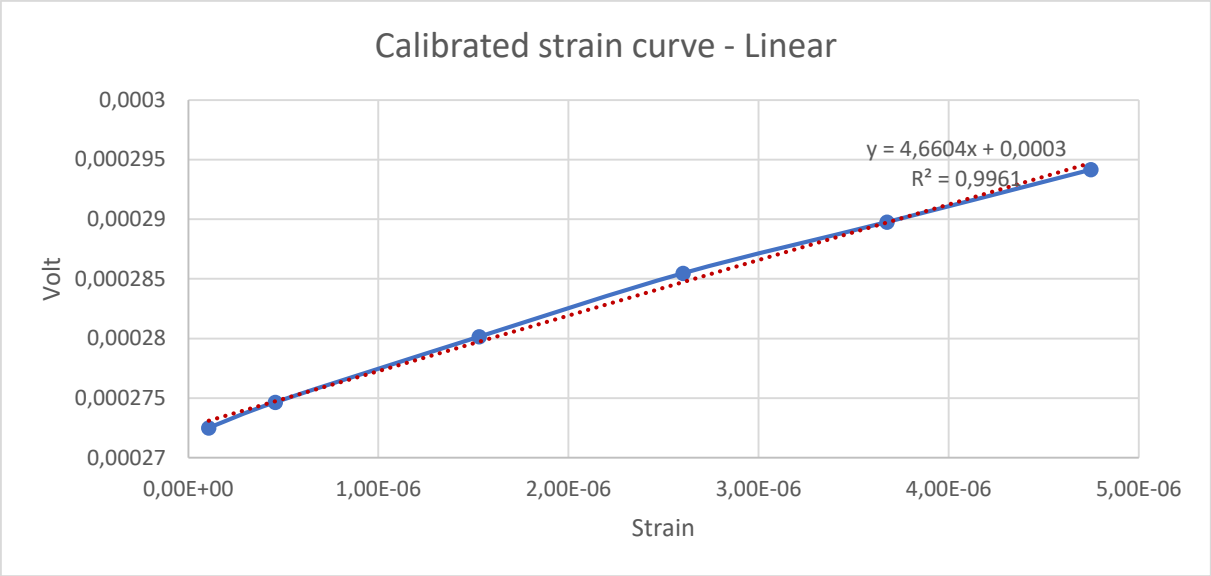

Figure 3.6: Calibrated strain curve, With Strain along the x-axis and voltage along the y-axis. Fitted with a linear regression curve.

The results show that the directional strain doesn't follow a linear curve with the volt signal from the strain gauges.

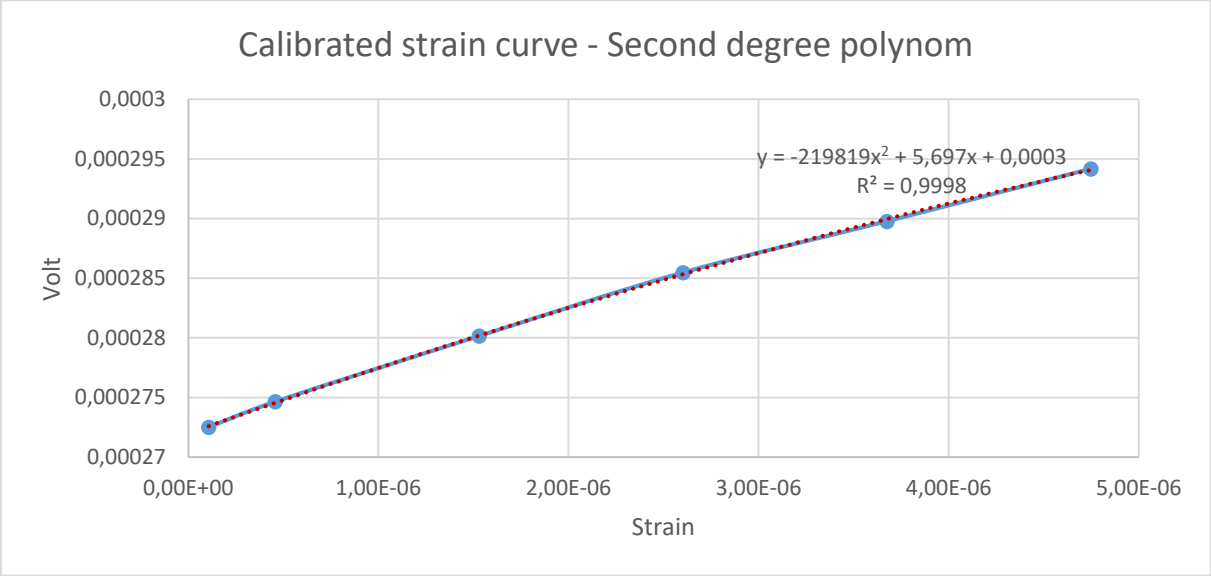

Figure 3.7: Calibrated strain curve, With Strain along the x-axis and voltage along the y-axis. Fitted with a second degree polynomial regression curve.

A second degree polynomial resulted in a much better fitting curve.

It should be noted that this procedure has several uncertainties and doesn't calibrate the strain gauges for the dynamic pressure fluctuations the runner blades experiences during operation. It also does not take into account temperature changes.

3.4. Data acquisition and processing

3.4.1. Data acquisition.

The pressure pulsations are measured with three pressure transducers connected to a cDAQ system. The cDAQ system consists of a NI 9237 simultaneous bridge module connected to a NI cDAQ-9178 chassis. The NI 9327 simultaneous bridge module has a resolution of 24 bits and a sample rate of 50 kHz/s/Ch. [23][24]

3.4.2. Sample rate and data processing

The sample rate used for the measurements was 5000Hz. With the largest expected frequency being the runner blade frequency:

$F_{rb} = Z_r * F_n$. With $F_{nmax} = \frac{n_{max}}{60} = \frac{530}{60}$ and $Z_r = 30$. $F_{rbmax} = 265$

The Nyquist-Shannon theorem requires the sample rate to be at least 530 Hz, so during the measurements oversampling with a factor of 9.43 to the Nyquist sample rate was used. [28]

The measurement series were afterwards imported to Matlab together with the operating conditions and analyzed using the histogram method to evaluate the pressure pulsations. Spectral analysis of the signals was also conducted with Matlab, using Hann-windows.

The length of most measurement series was 40 seconds. A few were also 30 or 60 seconds. The length of each window segment was 5000 measurement points and the overlap used was 50 percent.

To histogram method was used to measure the size of the pressure pulsations. A 97 percent confidence interval vas used. The values presented in the results phase of this thesis is the amplitude of the 97 percent confidence interval of the signal, which is the peak to peak value divided by 2.

4. Results

The experimental results from the pressure pulsation measurements are presented in various forms. 254 operating points were measured along 12 guide vane angles. In addition, 15 separate operation points were measured at speed no load. The results are presented below in the form of pressure pulsation diagrams, pressure pulsations along constant guide vane angles and frequency analysis of interesting operating conditions. The head of the model varied slightly during the experiments, from 12,3 to 12,6 meters.

Along the constant guide vane angles, both a reduction and increase in speed has been looked at to estimate how flexible generator operations can reduce pressure pulsations.

The Best efficiency point was found to be at 338,9 RPM, N_{ED}=0.1785 and Q_{ED}=0.1526, with a hydraulic efficiency of 93.90%. However, the flowmeter had not been calibrated prior to doing the measurements, so the hydraulic efficiency is probably lower than what is found, which would be more consistent with earlier efficiency testing done on the Francis turbine in the Waterpower Laboratory.

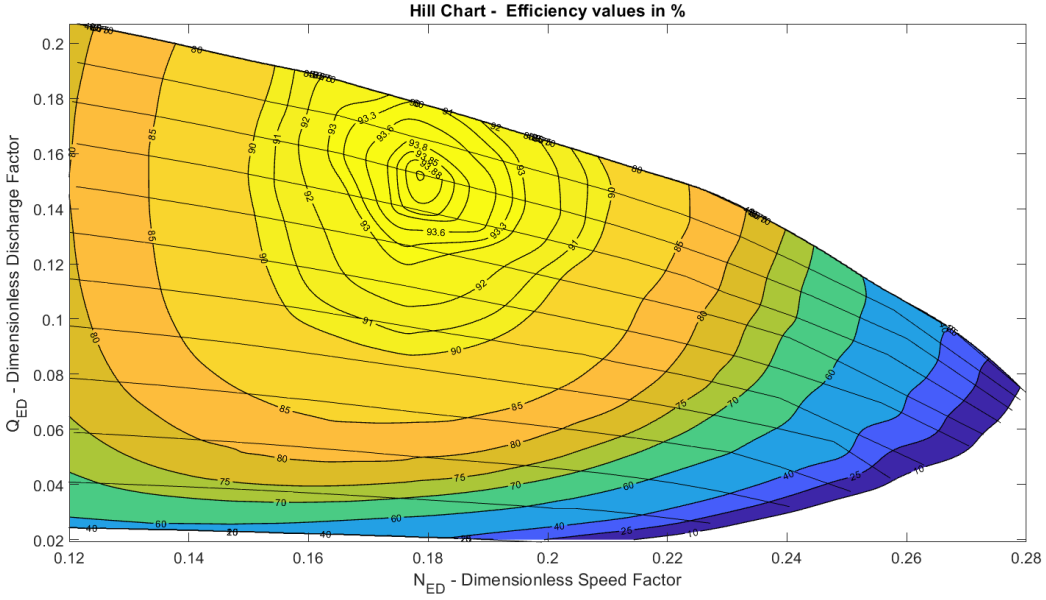

Figure 4.1: Hill chart with efficiency-lines. X-axis N_{ED} from 0.12 to 0.28. Y-axis Q_{ED} from 0.02 to 0.205.Shows hydraulic efficiency at different operating points.

4.1. Pressure pulsation diagrams

The pressure pulsation amplitudes at BEP for the pressure sensors placed at GV4, GV5 and GV6 was 1,6313 KPa, 1,8297 KPa and 1.6660 KPa. The pressure pulsations diagrams presented shows the pressure amplitude values relative to the pressure amplitude values found at BEP.

The three pressure diagrams show varying consternation of pressure pulsation amplitudes at different operating conditions. While all three sensors record high pressure pulsations when approaching speed-no-load, the scenario between 0.12 and 0.22 N_{ED} is hugely variable.

4.1.1. GV4

GV4 has generally low amplitude pressure pulsations from N_{ED} 0.12 to 0.19 below 6 degrees' guide vane opening. As well as a high amplitude at low speed at 8 and 9 degrees' guide vane opening.

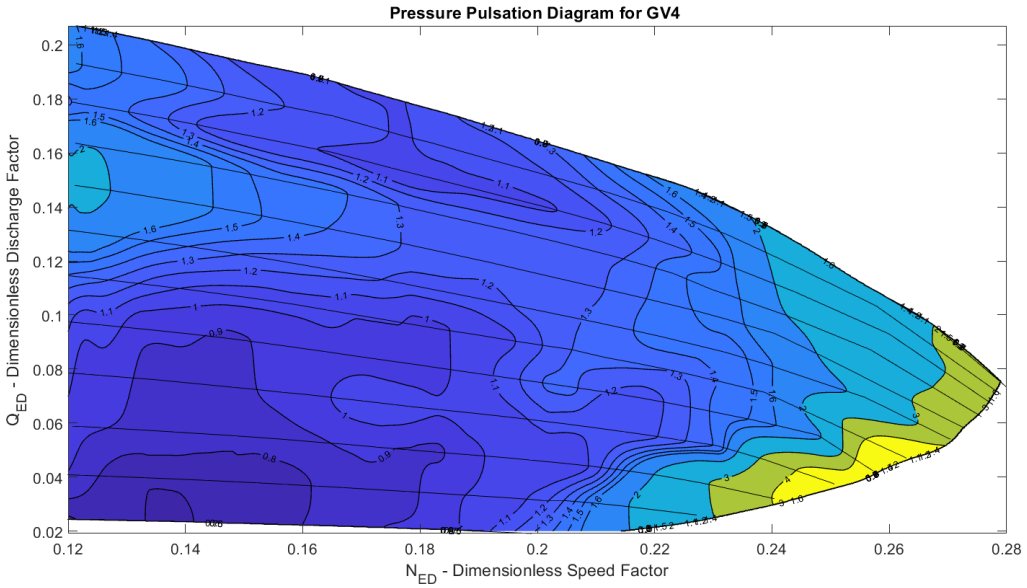

Figure 4.2: Pressure pulsation diagram for GV4. X-axis Dimensionless Speed Factor N_{ED}. Y-axis Dimensionless Discharge Factor Q_{ED}. Shows relative pressure amplitudes compared to pressure amplitudes at BEP.

4.1.2. GV5

The pressure pulsation amplitudes for GV5 appears to be more dependent on runner speed than guide vane opening, except at very low turbine speed where the pressure pulsation rise rapidly from 1 degree to 3 degrees' guide vane opening. GV5 has generally low pressure pulsations around synchronous speed and along low guide vane angles.

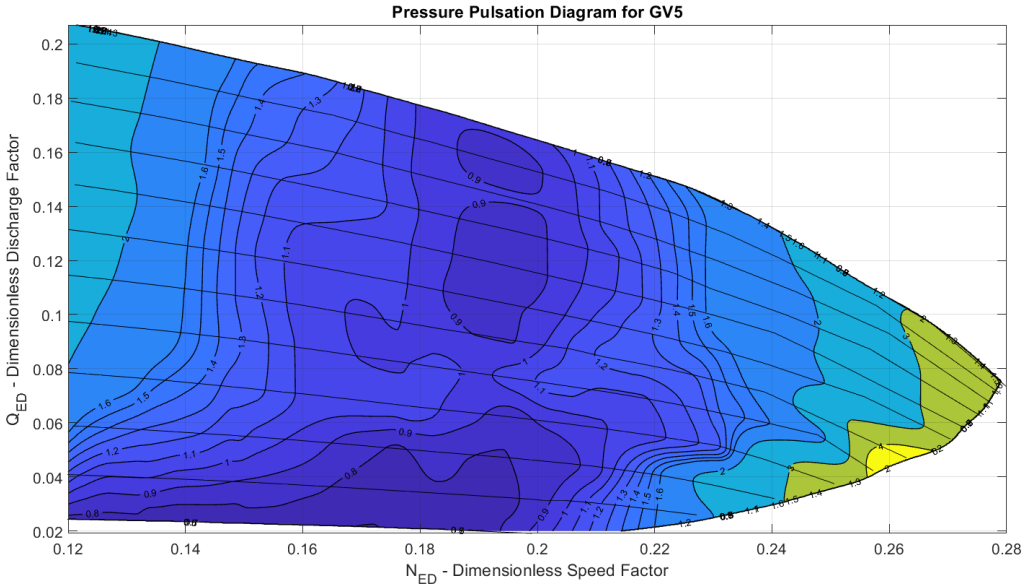

Figure 4.3: Pressure pulsation diagram for GV5. X-axis Dimensionless Speed Factor N_{ED}. Y-axis Dimensionless Discharge Factor Q_{ED}. Shows relative pressure amplitudes compared to pressure amplitudes at BEP.

4.1.3. GV6

GV6 has low pressure pulsation amplitudes between 0.14 and 0.16 N_{ED} up until guide vane angle at 8 degrees. Rather high pressure pulsation amplitudes above 0.21 N_{ED} and below 0.13 N_{ED}.

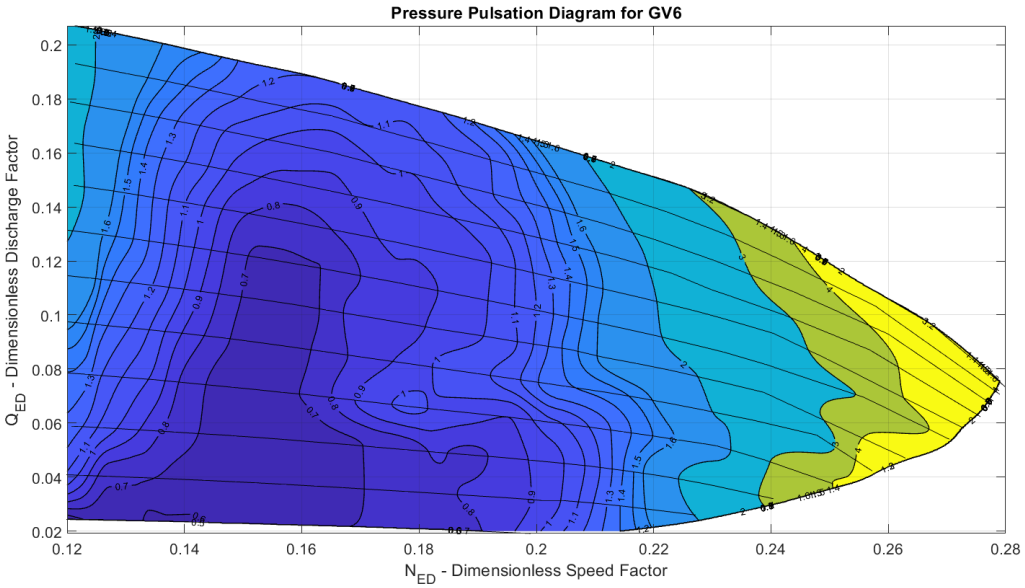

Figure 4.4: Pressure pulsation diagram for GV6. X-axis NED. Y-axis QED. Show relative pressure amplitudes compared to pressure amplitudes at BEP.

4.2. Pressure pulsations along constant guide vane angles

Pressure pulsation amplitudes at 2 degrees' guide vane openings is generally low up until 380 RPM, when pressure pulsation for all three sensors starts rising rapidly. Very similar pressure pulsations for all sensors in the vaneless space at this guide vane angle.

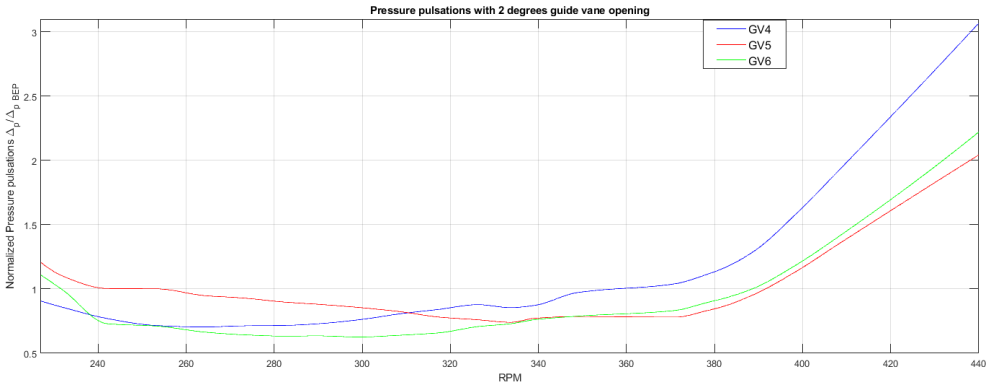

Figure 4.5: Relative pressure pulsations to BEP along constant guide vane at 2 degrees. From 228 to 440 RPM.

At 6 degree's guide vane opening there are a lot more difference in pressure pulsations recorded by the sensors. GV4 never goes above 1.6 in normalized pressure pulsations, and rises up only a bit when the RPM is very low or high. GV5 is very sensitive to low speed, going up to 2.2 at 228 RPM. Relatively low from 300 to 380 RPM and then rising slightly as the RPM increases to 450. GV6 also experiences high pressure pulsations at really low speeds, but goes down very fast until 280 RPM. Has a very low zone between 280 and 300 RPM before a gradual upwards incline to 370 RPM. After 370 RPM, the pressure pulsations for GV6 rises quite fast from 1.1 in normalized frequency up to 2.3.

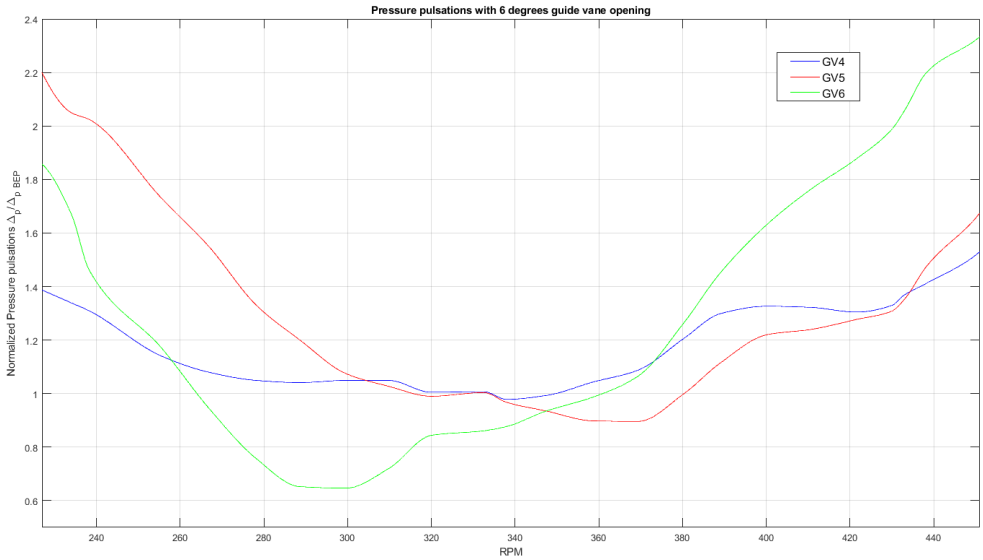

Figure 4.6: Relative pressure pulsations to BEP along constant guide vane at 6 degrees. From 228 to 450 RPM.

Tables showing the results along the constant guide vane angles are presented below. The pressure pulsations amplitudes at synchronous speed ± 10%, 20% and 30% were compared to the pressure pulsations at synchronous speed. This was done for all three sensors as and for their average values combined. The largest reduction is presented as well, compared to the pressure pulsation at synchronous speed and the actual pressure pulsations at BEP.

Pressure pulsations at 1 degree guide vane opening									
Sensor	Pressure pulsation amplitudes from 30% reduced speed to 30% increased speed [KPa]							Largest reduction as to [%]	
	237.2 RPM	271.2 RPM	305.0 RPM	**338,9 RPM**	372.8 RPM	406.7 RPM	440.6 RPM	BEP	338,9 RPM
GV4	1,193	1,148	1,308	**1,504**	1,950	Beyond Runaway	Beyond Runaway	29,63	23,69
GV5	1,394	1,291	1,308	**1,300**	1,529	Beyond Runaway	Beyond Runaway	29,03	0,68
GV6	1,040	0,985	1,103	**1,241**	1,482	Beyond Runaway	Beyond Runaway	40,87	20,64
Combined	3,627	3,424	3,719	**4,046**	4,961	Beyond Runaway	Beyond Runaway	33,08	15,36

Table 4.1: Pressure pulsation at 1 degree guide vane opening.

Pressure pulsations at 2 degrees guide vane opening									
Sensor	Pressure pulsation amplitudes from 30% reduced speed to 30% increased speed [KPa]							Largest reduction as to [%]	
	237.2 RPM	271.2 RPM	305.0 RPM	**338,9 RPM**	372.8 RPM	406.7 RPM	440.6 RPM	BEP	338,9 RPM
GV4	1,317	1,163	1,287	**1,421**	1,719	3,040	Beyond Runaway	28,71	18,17
GV5	1,877	1,695	1,524	**1,403**	1,431	2,391	Beyond Runaway	22,88	-1,95
GV6	1,373	1,074	1,055	**1,266**	1,406	2,281	Beyond Runaway	36,69	16,69
Combined	4,568	3,932	3,865	**4,091**	4,555	7,712	Beyond Runaway	24,47	5,52

Table 4.2: Pressure pulsation at 2 degrees' guide vane opening.

Pressure pulsations at 3 degrees guide vane opening									
Sensor	Pressure pulsation amplitudes from 30% reduced speed to 30% increased speed [KPa]							Largest reduction as to [%]	
	237.2 RPM	271.2 RPM	305.0 RPM	**338,9 RPM**	372.8 RPM	406.7 RPM	440.6 RPM	BEP	338,9 RPM
GV4	1,478	1,391	1,435	**1,462**	1,662	2,360	5,246	14,72	4,85
GV5	2,634	2,162	1,741	**1,465**	1,477	2,088	4,307	19,50	-0,85
GV6	1,838	1,142	1,061	**1,260**	1,427	2,257	4,271	36,31	15,78
Combined	5,950	4,695	4,237	**4,187**	5,322	6,705	13,825	18,18	-1,20

Table 4.3: Pressure pulsation at 3 degrees' guide vane opening.

Pressure pulsations at 4 degrees guide vane opening									
Sensor	Pressure pulsation amplitudes from 30% reduced speed to 30% increased speed [KPa]							Largest reduction as to [%]	
	237.2 RPM	271.2 RPM	305.0 RPM	**338,9 RPM**	372.8 RPM	406.7 RPM	440.6 RPM	BEP	338,9 RPM
GV4	1,560	1,413	1,555	**1,699**	1,762	1,861	2,525	13,38	16,82
GV5	3,264	2,496	1,947	**1,927**	1,577	1,859	2,518	13,35	18,16
GV6	2,036	1,166	1,183	**1,696**	1,531	2,244	3,114	30,03	31,26
Combined	6,861	5,075	4,684	**5,322**	4,869	5,963	8,157	8,46	11,98

Table 4.4: Pressure pulsation at 4 degrees' guide vane opening.

Pressure pulsations at 5 degrees guide vane opening									
Sensor	Pressure pulsation amplitudes from 30% reduced speed to 30% increased speed [KPa]							Largest reduction as to [%]	
	237.2 RPM	271.2 RPM	305.0 RPM	**338,9 RPM**	372.8 RPM	406.7 RPM	440.6 RPM	BEP	338,9 RPM
GV4	1,720	1,463	1,534	**1,556**	1,951	1,921	2,390	10,30	5,94
GV5	3,575	2,640	1,933	**1,827**	1,909	1,984	2,609	-0,41	-4,49
GV6	2,252	1,306	1,158	**1,574**	1,979	2,465	3,449	30,49	26,41
Combined	7,547	5,409	4,625	**4,956**	5,839	5,839	6,370	9,62	6,69

Table 4.5: Pressure pulsation at 5 degrees' guide vane opening.

Pressure pulsations at 6 degrees guide vane opening									
Sensor	Pressure pulsation amplitudes from 30% reduced speed to 30% increased speed [KPa]							Largest reduction as to [%]	
	237.2 RPM	271.2 RPM	305.0 RPM	**338,9 RPM**	372.8 RPM	406.7 RPM	440.6 RPM	BEP	338,9 RPM
GV4	2,148	1,733	1,712	**1,596**	1,823	2,161	2,334	2,14	-7,22
GV5	3,695	2,627	1,905	**1,753**	1,661	2,243	2,757	8,73	5,24
GV6	2,497	1,414	1,122	**1,468**	1,858	2,857	3,718	32,65	23,57
Combined	8,340	5,774	4,738	**4,817**	5,342	7,261	8,809	7,40	1,63

Table 4.6: Pressure pulsation at 6 degrees' guide vane opening.

Pressure pulsations at 7 degrees guide vane opening									
Sensor	Pressure pulsation amplitudes from 30% reduced speed to 30% increased speed [KPa]							Largest reduction as to [%]	
	237.2 RPM	271.2 RPM	305.0 RPM	**338,9 RPM**	372.8 RPM	406.7 RPM	440.6 RPM	BEP	338,9 RPM
GV4	2,821	2,208	2,026	**1,867**	1,986	2,256	2,382	-14,44	-6,37
GV5	3,860	2,646	1,888	**1,754**	1,630	2,213	2,909	10,41	7,04
GV6	2,722	1,514	1,158	**1,469**	1,885	2,948	3,990	30,48	21,15
Combined	9,403	6,367	5,073	**5,090**	5,501	7,416	9,280	0,86	0,33

Table 4.7: Pressure pulsation at 7 degrees' guide vane opening.

Pressure pulsations at 8 degrees guide vane opening									
Sensor	Pressure pulsation amplitudes from 30% reduced speed to 30% increased speed [KPa]							Largest reduction as to [%]	
	237.2 RPM	271.2 RPM	305.0 RPM	**338,9 RPM**	372.8 RPM	406.7 RPM	440.6 RPM	BEP	338,9 RPM
GV4	3,465	2,649	2,313	**2,073**	2,068	2,216	2,536	-26,75	0,24
GV5	4,053	2,811	1,999	**1,785**	1,545	2,082	3,216	15,07	13,42
GV6	3,145	1,687	1,261	**1,526**	1,905	2,942	4,402	24,28	17,36
Combined	10,663	7,147	5,574	**5,384**	5,518	7,239	10,154	-5,22	-2,48

Table 4.8: Pressure pulsation at 8 degrees' guide vane opening.

Pressure pulsations at 9 degrees guide vane opening									
Sensor	Pressure pulsation amplitudes from 30% reduced speed to 30% increased speed [KPa]							Largest reduction as to [%]	
	237.2 RPM	271.2 RPM	305.0 RPM	**338,9 RPM**	372.8 RPM	406.7 RPM	440.6 RPM	BEP	338,9 RPM
GV4	3,235	2,636	2,327	**2,083**	2,052	2,159	2,596	-25,80	1,50
GV5	4,096	2,902	2,136	**1,827**	1,556	2,113	3,324	14,51	14,86
GV6	3,076	1,865	1,453	**1,618**	2,027	3,101	4,580	12,80	10,19
Combined	10,407	7,403	5,916	**5,528**	5,634	7,373	10,500	-8,03	-1,92

Table 4.9: Pressure pulsation at 9 degrees' guide vane opening.

Pressure pulsations at 10 degrees guide vane opening									
Sensor	Pressure pulsation amplitudes from 30% reduced speed to 30% increased speed [KPa]							Largest reduction as to [%]	
	237.2 RPM	271.2 RPM	305.0 RPM	**338,9 RPM**	372.8 RPM	406.7 RPM	440.6 RPM	BEP	338,9 RPM
GV4	2,364	1,922	1,800	**1,631**	1,775	2,021	2,687	0,00	-8,82
GV5	4,166	2,956	2,296	**1,820**	1,648	2,164	3,142	9,46	9,46
GV6	3,212	1,971	1,572	**1,666**	2,122	3,250	4,817	5,63	5,63
Combined	9,742	6,849	5,669	**5,117**	5,545	7,435	10,645	0,00	-8,36

Table 4.10: Pressure pulsation at 10 degrees' guide vane opening.

Pressure pulsations at 11 degrees guide vane opening									
Sensor	Pressure pulsation amplitudes from 30% reduced speed to 30% increased speed [KPa]							Largest reduction as to [%]	
	237.2 RPM	271.2 RPM	305.0 RPM	**338,9 RPM**	372.8 RPM	406.7 RPM	440.6 RPM	BEP	338,9 RPM
GV4	2,525	2,225	1,948	**1,764**	1,887	2,194	2,718	-6,982	-8,12
GV5	4,311	3,099	2,383	**1,872**	1,555	2,149	3,148	16,919	14,55
GV6	3,284	2,239	1,816	**1,778**	2,172	3,453	4,951	-2,102	-6,74
Combined	10,120	7,563	6,147	**5,414**	5,614	7,797	10,817	-5,80	-3,71

Table 4.11: Pressure pulsation at 11 degrees' guide vane opening.

Pressure pulsations at 12 degrees guide vane opening									
Sensor	Pressure pulsation amplitudes from 30% reduced speed to 30% increased speed [KPa]							Largest reduction as to [%]	
	237.2 RPM	271.2 RPM	305.0 RPM	**338,9 RPM**	372.8 RPM	406.7 RPM	440.6 RPM	BEP	338,9 RPM
GV4	2,514	2,073	1,846	**1,787**	2,031	2,474	3,088	-3,34	-9,52
GV5	4,361	3,295	2,572	**1,905**	1,722	2,269	3,193	9,59	5,38
GV6	3,318	2,507	2,010	**1,921**	2,494	3,874	5,416	-4,62	-15,32
Combined	10,193	7,875	6,428	**5,612**	6,247	8,617	11,697	-9,68	-11,31

Table 4.12: Pressure pulsation at 12 degrees' guide vane opening.

4.3. Frequencies in different operating regimes

Observing which frequencies that impacts the different pressure gives valuable information about what are the sources of the pressure pulsations. In the figures below frequency analysis of different signals are shown with normalized frequency $\frac{f}{f_n} = \frac{f}{\frac{n}{60}}$

The size of the amplitudes is shown as pressure in KPa, it should be noted that these values does not represent the amplitudes of the actual pressure pulsations occurring.

4.3.1. BEP

Noticeable normalized frequencies are the Rheingans Frequency at around 0.3, the splitter blade passing frequency at 15 and the blade passing frequency at 30.

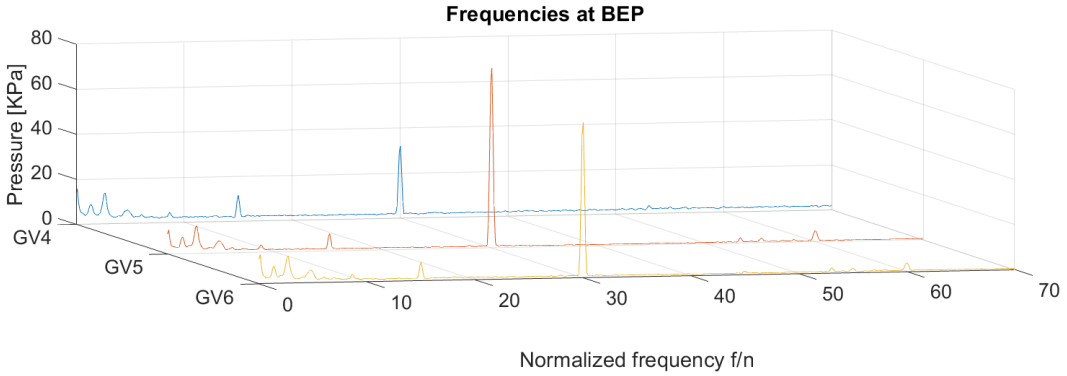

Figure 4.7: Frequencies observed at BEP. Showing values for GV4, GV5 and GV6 for normalized frequencies from 0 to 70.

4.3.2. 2 degrees' guide vane opening

Noticeable normalized frequencies are Rheingans, splitter blade passing and blade passing frequency. The main difference between the three sensors is the magnitude of the blade passing frequency. The amplitudes seen at 60 are likely harmonics of the blade passing frequency. There are also small inclines at around 3 and 11.

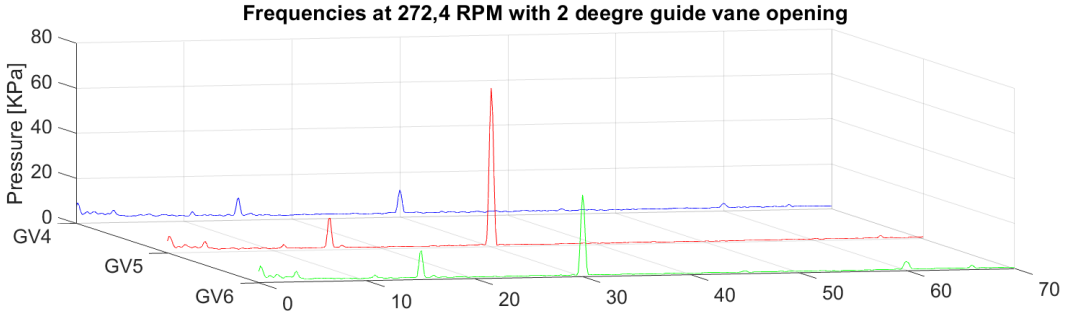

Figure 4.8: Frequencies observed at 2 degrees guide vane opening and 272,4 RPM. Showing values for GV4, GV5 and GV6 for normalized frequencies from 0 to 70.

As the runner speed increase the blade passing frequency grows more significant for GV4. Alongside Rheingans, blade passing and the splitter blade passing frequency there is also a small incline around 3 for all sensors.

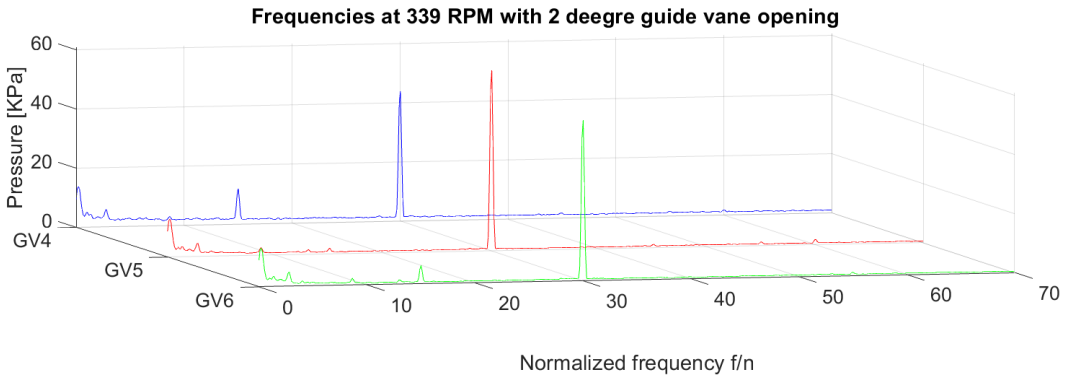

Figure 4.9: Frequencies observed at 2 degrees guide vane opening and 339 RPM.. Showing values for GV4, GV5 and GV6 for normalized frequencies from 0 to 70.

More stochastic pulsation showing along the frequencies as the runner is nearing speed-no-load. Rheingans, blade passing and splitter blade passing frequency still clearly most significant.

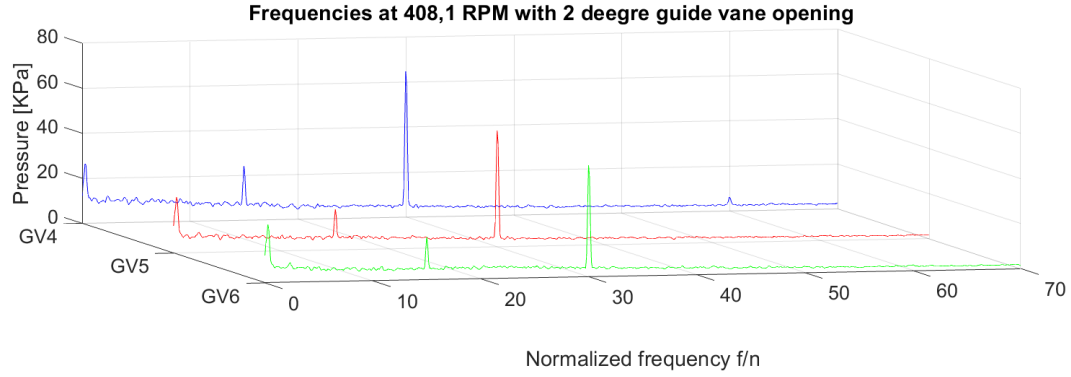

Figure 4.10: Frequencies observed at 2 degrees guide vane opening and 408,1 RPM.. Showing values for GV4, GV5 and GV6 for normalized frequencies from 0 to 70.

4.3.3. 5 degrees' guide vane opening

Blade passing frequency dominating for GV5. Far smaller for GV4 and GV6. Splitter blade passing frequency can also be clearly seen for all sensors. The very low frequencies are too distorted to determine frequencies. Harmonics of the blade passing frequency is observed at 60, as well as another unknown frequency at 65.

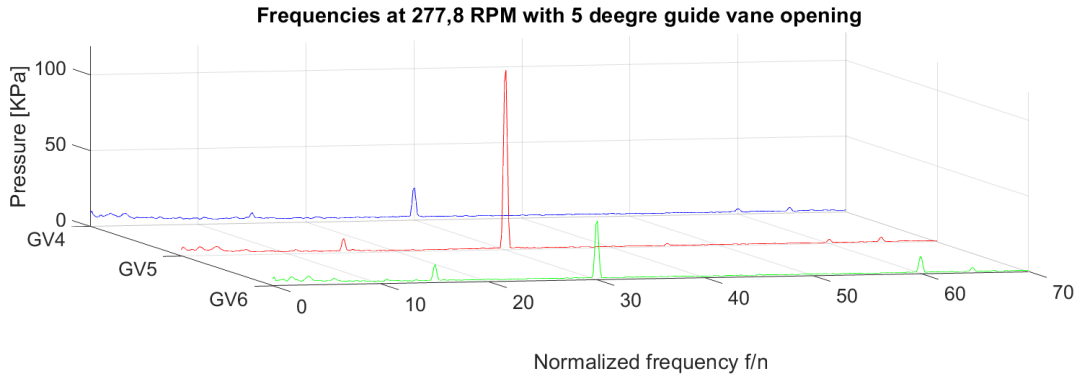

Figure 4.11: Frequencies observed at 5 degrees guide vane opening and 277,8 RPM. Showing values for GV4, GV5 and GV6 for normalized frequencies from 0 to 70.

At 337,8 Rpm the Rheingans frequency is much more noticeable. Blade passing frequency is still dominating and the splitter blade passing frequency is also easy to spot. Harmonics of the blade passing frequency can be seen for GV5 and GV6. There also appears to be an unidentified frequency at 53.

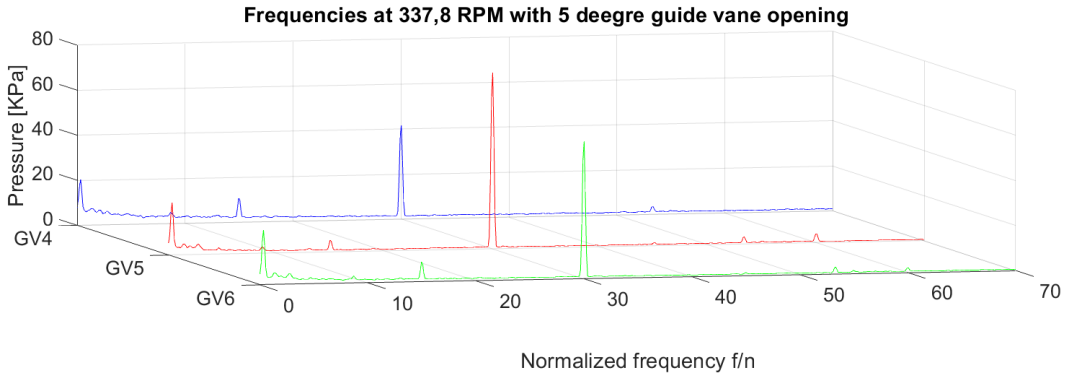

Figure 4.12: Frequencies observed at 5 degrees guide vane opening and 377,8 RPM.. Showing values for GV4, GV5 and GV6 for normalized frequencies from 0 to 70.

4.3.4. 7 degrees' guide vane opening

At 337,6 RPM the blade passing frequency and the splitter blade passing frequency are noticeable for all sensors, with the amplitude of the blade passing frequency being far the largest. Rheingans frequency can also be seen, as well as some other low frequencies, which are hard to pinpoint on exact frequencies due to spectral leakage. For GV5 and GV6 harmonics of the blade passing frequency can also be observed at 60 RPM, as well as a small unknown frequency at 54 for GV5.

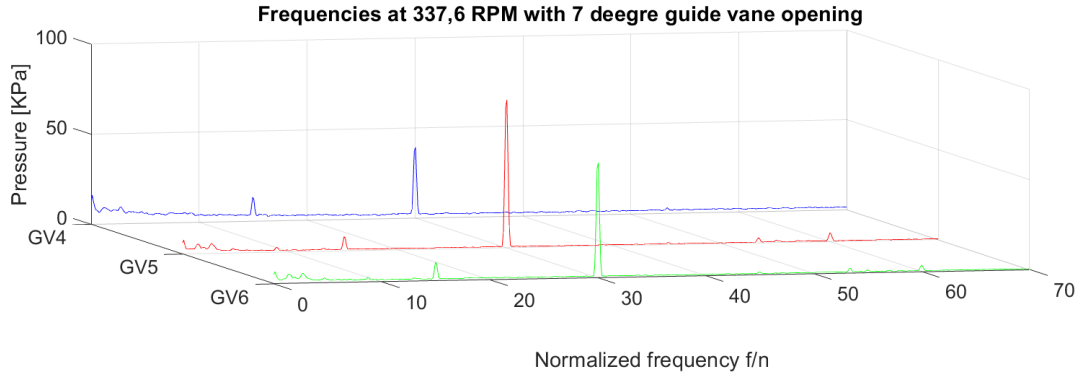

Figure 4.13: Frequencies observed at 7 degrees guide vane opening and 337,6 RPM.. Showing values for GV4, GV5 and GV6 for normalized frequencies from 0 to 70.

At 374,2 RPM the amplitude of splitter blade passing frequency have grown considerably. Rheingans and the blade passing frequency are also significant. Harmonics of the blade passing frequency can be seen at all sensors at 60, as well as two small unknown amplitudes at around 45 for GV5 and 58 for all sensors.

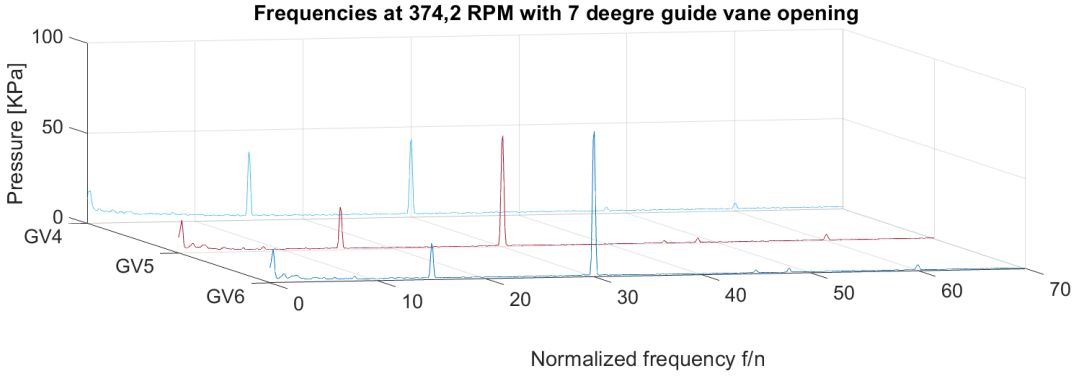

Figure 4.14: Frequencies observed at 7 degrees guide vane opening and 337,6 RPM.. Showing values for GV4, GV5 and GV6 for normalized frequencies from 0 to 70.

4.4. Speed-no-load

When running at speed-no-load, the pressure pulsations are relatively low when the speed is low. The pressure pulsation regime is very similar for all three sensors.

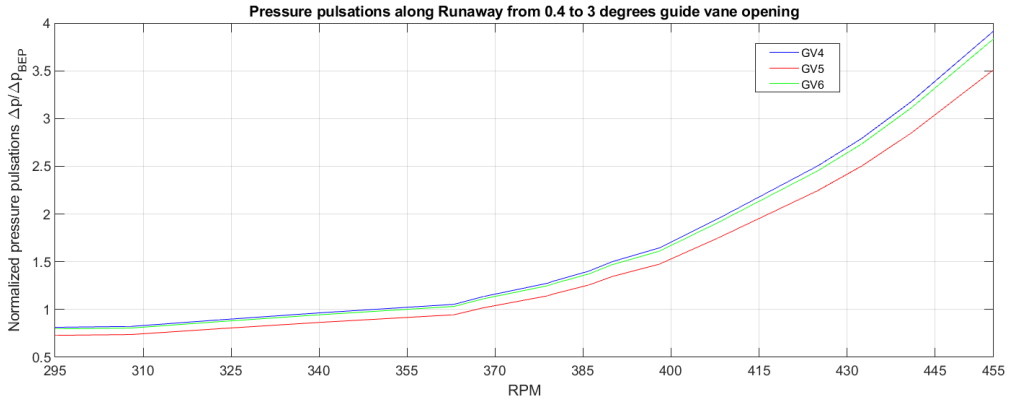

Figure 4.15: Relative pressure pulsation amplitudes at speed-no-load. Pressure pulsations amplitudes at speed-no-load compared to BEP at the y-axis. RPM along the x-axis.

Frequency analysis at speed-no load.

At 295 RPM Rheingans, splitter blade passing and blade passing frequencies are significant, with the blade passing frequency at 30 dominating in magnitude.
The spectral leakage is quite low compared to other signal measurements at speed no load and there are smaller noticeable frequencies at 3 and 60 for all sensors.

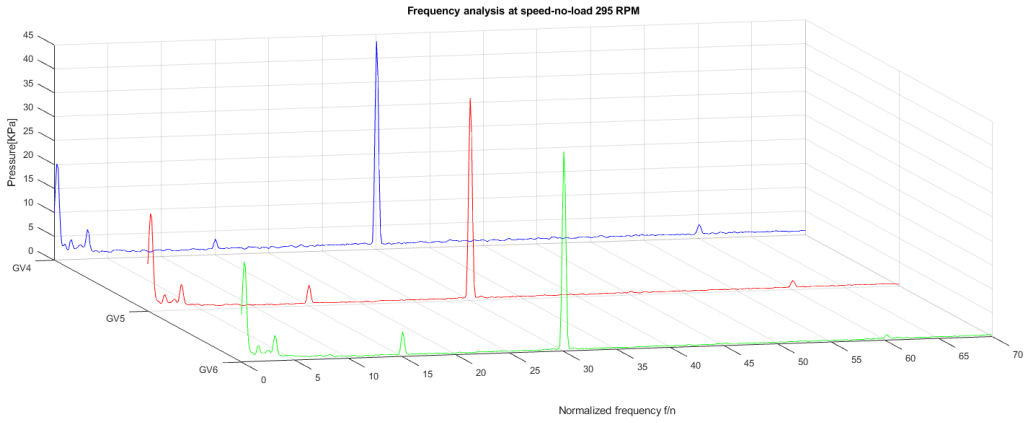

Figure 4.16: Frequencies observed at speed-no-load 295 RPM. Showing values for GV4, GV5 and GV6 for normalized frequencies from 0 to 70.

At 340 RPM the blade passing frequency have similar amplitudes while Rheingans frequency have increased a bit for all. The splitter blade passing frequency has also increased quite a bit for GV4. Harmonics at 60 can only be observed for GV4.

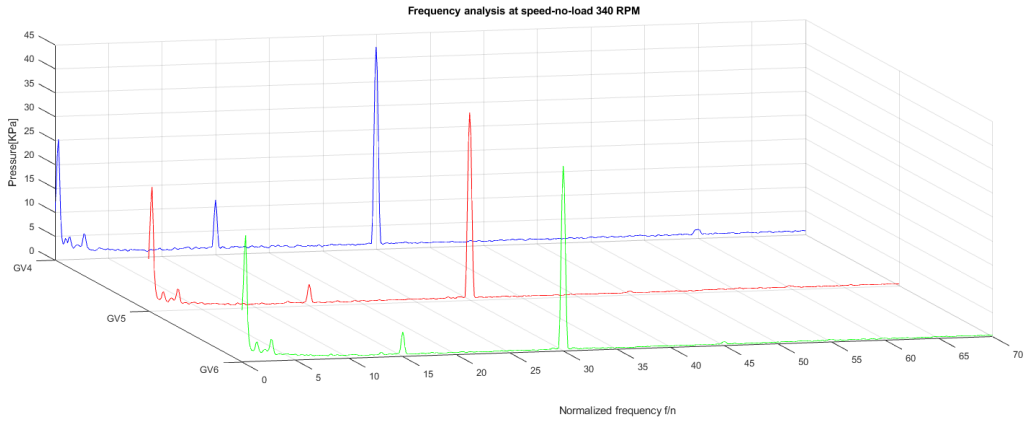

Figure 4.17: Frequencies observed at speed-no-load 340 RPM.. Showing values for GV4, GV5 and GV6 for normalized frequencies from 0 to 70.

At 386 RPM the blade passing frequency has increased in amplitude. The stochastic fluctuations have grown considerably, making the previously noticeable frequency at around 3 disappear. Splitter blade passing frequency and Rheingans frequency are large enough to still be clearly visible.

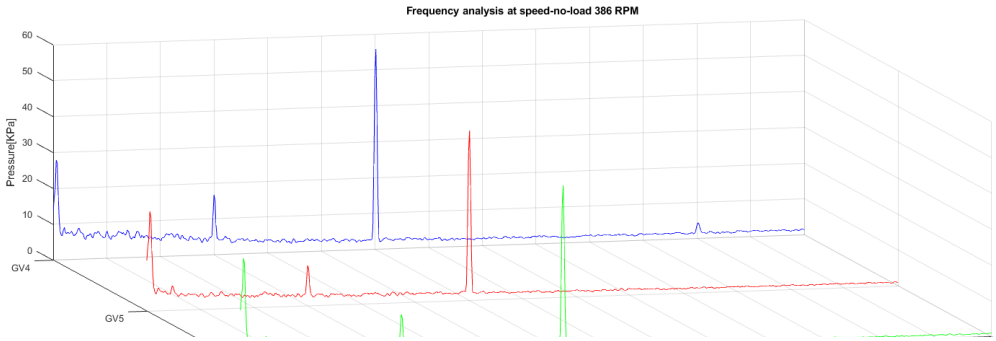

Figure 4.18: Frequencies observed at speed-no-load 386 RPM.. Showing values for GV4, GV5 and GV6 for normalized frequencies from 0 to 70.

At 441 RPM the distortion can be seen over the whole frequency spectrum. Rheingans, splitter blade passing and blade passing frequencies are still noticeable. The blade passing frequency amplitude having increased for GV4 and declined for GV5 and GV6 compared to Figure 4.18.

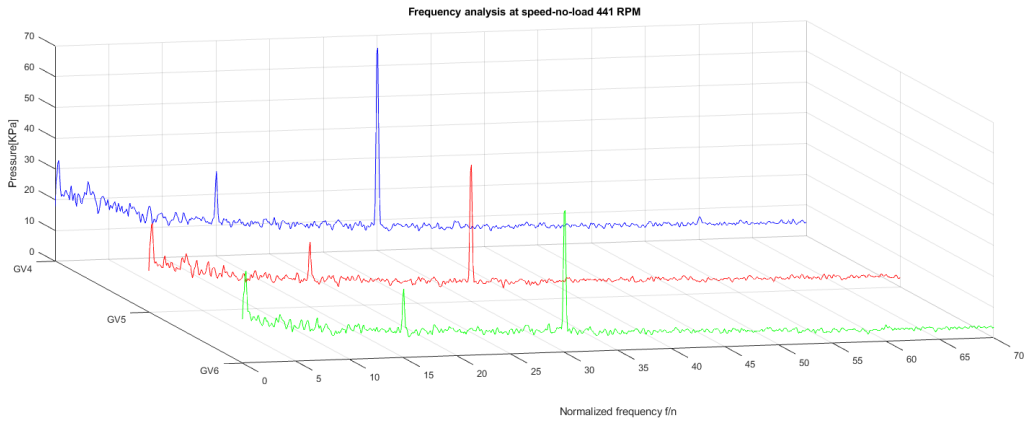

Figure 4.19: Frequencies observed at speed-no-load 441 RPM.. Showing values for GV4, GV5 and GV6 for normalized frequencies from 0 to 70.

4.5. Stress levels

To assess how much flexible speed turbines can reduce the damage contributors to the runner blades, the correlation between the measured pressure pulsations in the vaneless space and the fatigue on the runner blade has to be evaluated.

The relationship between pressure changes in the vaneless space has been mapped together with the von-Mises equivalent stress on the runner blade. This was done with a combination of CFD-analysis, FSI-analysis and experimental measurement on the Francis turbine in the Waterpower Laboratory at NTNU by Valkvæ in 2016. [27] A drop of 10,5 KPa in the vaneless space correlated with a decrease in the maximum equivalent von Mises stress on the runner blade of 3,4 MPa. This maximum stress occurs along the trailing edge at the tip towards the shroud. This provides a factor for stress to pressure $P_\sigma = 328{,}8$
If this is a linear relation, then: $\sigma_{VM} = P_{GV} * P_\sigma + c$ (Pa) [19]

Where σ_{VM} is the maximum equivalent von Mises stress on the runner blade and P_{GV} is the pressure in the vaneless space.

From the measurements conducted in this thesis the minimum mean pressure while operating was 136 KPa, which if with an assumed linear relationship factor of 328,8 would mean a

stress of 44,72 MPa, which is obviously far high. If we deduct the atmospheric pressure of 98,5 KPa, it would still be 12 MPa.

From the measurements Valkvæ analyzed, the drop in pressure was from 68,5 KPa to 58 KPa and the drop in Maximum equivalent von Mises Stress on the runner blade was from 8,4 MPa to 5 MPa. Which mean that if a linear relationship over the whole pressure range is assumed, then the lowest measurement from this thesis would still be far more than what Valkvæ found. So assuming a linear relationship stress to pressure factor of 328,8 is not a valid assumption.

Since a linear relationship doesn't fit, a Polynomial function of the second degree was made based on the data gathered in Valkvæ's thesis. An assumption of close to zero stress when only experiencing atmospheric pressure was made.

$$\sigma_{VM} = {P_{GV}}^2 * P_{\sigma,1} + P_{GV} * P_{\sigma,2} + c \qquad \text{(Pa)} \qquad [20]$$

Where $P_{\sigma,1} = 0{,}0015546$, $P_{\sigma,2} = 8{,}644$ and $c = 66846$

This relationship between pressure in the vaneless space and maximum equivalent von Mises stress is used to calculate the stress mean stresses that occurs on the runner blade.
For the smaller pressure amplitudes occurring because of pressure pulsations, the stress to pressure factor of $P_\sigma = 328{,}8$ will still be used. This assumption is made because that is the factor Valkvæ got for the actual pressure change during measurement, and should based on that correlate fairly well with small pressure changes.

This assumption makes it possible to estimate the amount of equivalent von Mises stress for the whole operating range. Because Valkvæ doesn't make it clear which sensors in the vaneless space was used to measure the pressure in 2016, an average of the values from GV4, GV5 and GV6 is used.

Valkvæ found that maximum Equivalent von Mises stress occurs at the tip of the trailing edge of the runner blade towards the shroud. That will be the part of the runner blade that fatigue analysis will look into.

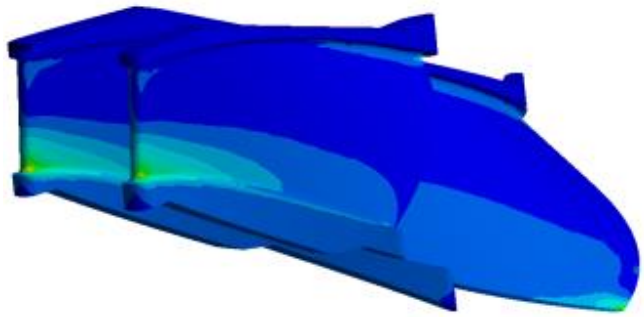

Figure 4:20: Stress distribution on the runner blade. Valkvæ 2016[27]

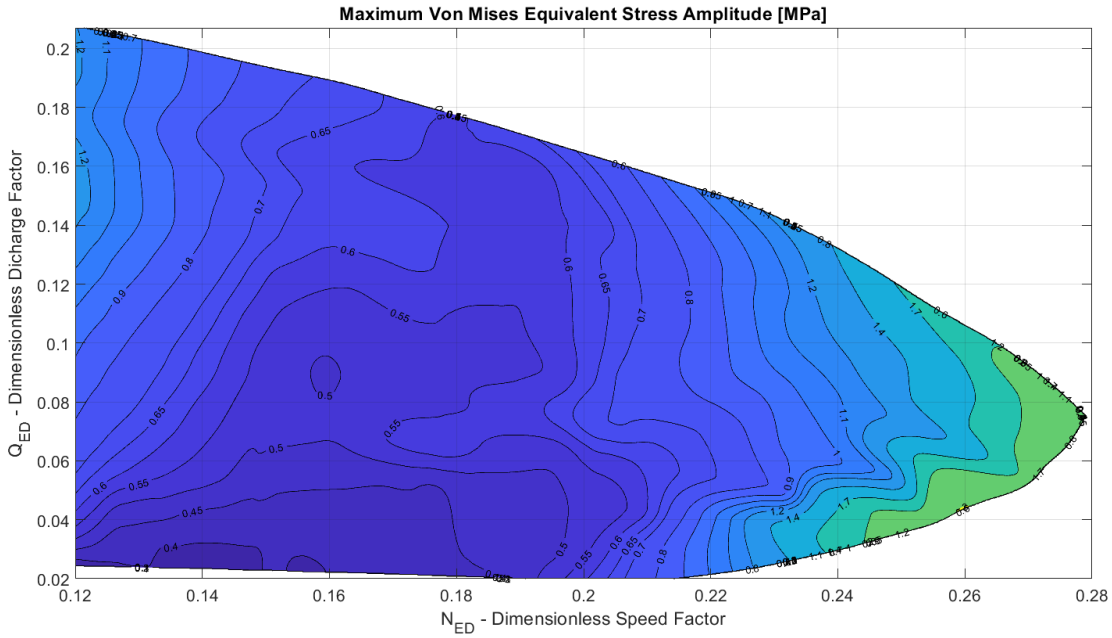

Figure 4.21: Maximum von Mises equivalent stress amplitude diagram. X-axis Dimensionless Speed Factor N_{ED}. Y-axis Dimensionless Discharge Factor Q_{ED}.

The Maximum equivalent von Mises stress amplitudes in the runner blade has low stress amplitudes at low speed and low load. The stress amplitudes have the same ratio between different operating points as the pressure pulsations described in 4.2 and 4.3.

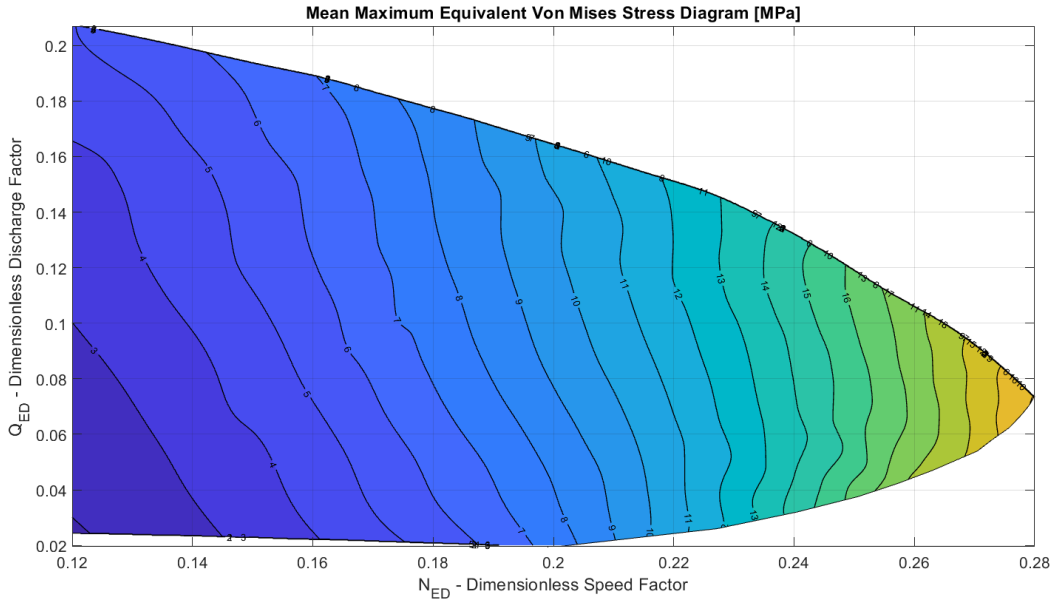

Figure 4.22: Mean maximum equivalent von Mises stress diagram. X-axis Dimensionless Speed Factor N_{ED}. Y-axis Dimensionless Discharge Factor Q_{ED}.

The mean maximum equivalent von Mises stress diagram shows that speed is the most dominating factor for the mean stresses at the runner blade

4.5.1. Stress levels at Speed-no-Load

At speed-no-load the stress amplitudes are relatively similar to those at very low part load. With a slow increase from 300 RPM to 365 RPM before increasing rapidly after that.

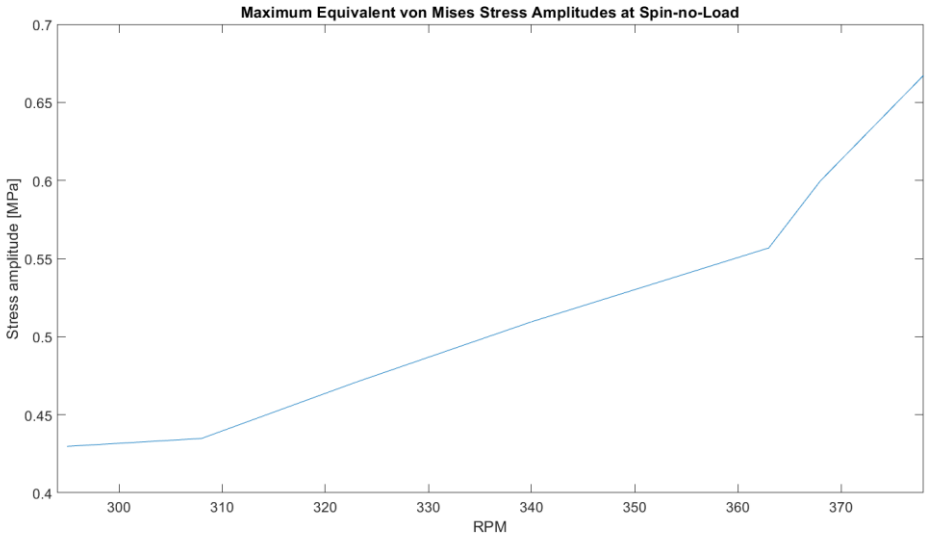

Figure 4.23: Maximum equivalent von Mises stress amplitudes at speed-no-load graph. X-axis RPM. Y-axis stress in MPa. .

The mean stresses at speed-no-load are generally quite a bit higher than those found at lower part load. At synchronous speed it is 8,7 MPa, which is 64% higher than the mean stresses found at synchronous speed at very low part load.

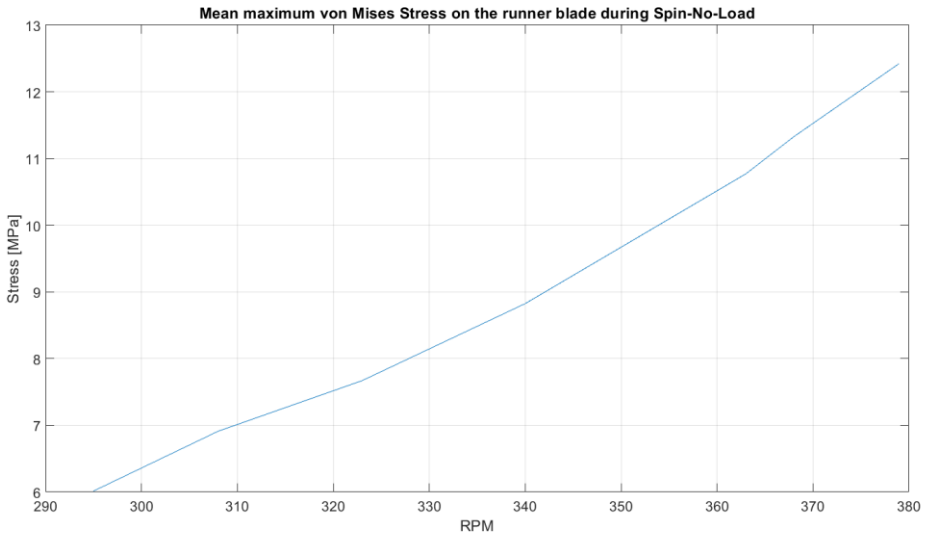

Figure 4.24: Mean maximum equivalent von Mises stress at speed-no-load graph. X-axis RPM. Y-axis stress in MPa.

4.6. Fatigue

The Goodman method is used to obtain the effective stress. Each operating point has two stress amplitudes and two mean stresses. Where one represents the stresses induced by operating at that point and the other represents the stresses induced by starting the turbine, moving to that operating point and then stopping.

The material used to investigate fatigue is a 17Cr-4Ni cast stainless steel, which Hans-Jörg Huth looked into in Fatigue Design of Hydraulic Turbine Runners in 2005. [34]
The material has an ultimate tensile strength of 910 MPa and a yield strength of 661 MPa and a stress concentration factor of 1.36. It should be noted that this yield limit is a bit higher than what the S-N curves from ISO 19902 is based upon.

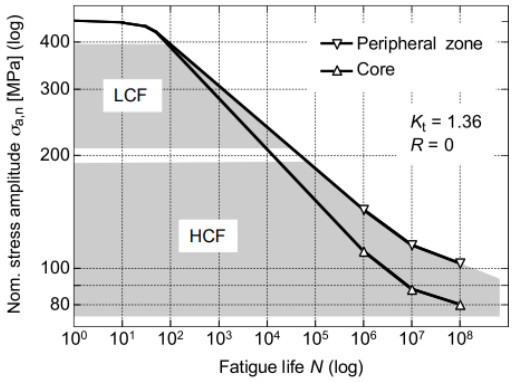

Figure 4.25: S-N curve of 17Cr-4Ni cast stainless steel. From Fatigue Design of Hydraulic Turbine Runners[34]

By using the calculated effective stresses from the Goodman method together with the S-N curve from ISO 19902 the cycles to failure for each operating point is calculated.

$$log_{10}N = log_{10}K_1 - m * log_{10}S \qquad \text{(Cycles)} \qquad [21]$$

$$N = 10^{log_{10}K_1 - m log_{10}S} \qquad \text{(Cycles)} \qquad [22]$$

The constant amplitude stress range can be described as

$$S = 2 * \sigma_a * K_t \qquad \text{[MPa]} \qquad [23]$$

Since the maximum stress occurs close at the edge of the trailing edge right by the connection the material parameters for the S-N curve must reflect that. This fatigue analysis assuming that the blade is welded to the shroud.

From ISO 19902[15], weld metal in load-carrying joints, gives the following K_1 and m values.

	For N>10^7	For N<10^7
K_1	$10^{13,62}$	$10^{10,97}$
m	5	3

Table 4.13: Constants for S-N curve.

For this thesis the values for N>10^7 will be used for High Cycle Fatigue and the values for N<10^7 for Low Cycle Fatigue.

4.6.1. High Cycle Fatigue

The stress amplitudes for the range of operating conditions have been used to calculate the number of cycles to failure when operating at that condition. The cycles to failure are high at low load and low speed, and rapidly decreases when the speed reaches above 0.2 N_{ED} for all levels of load.

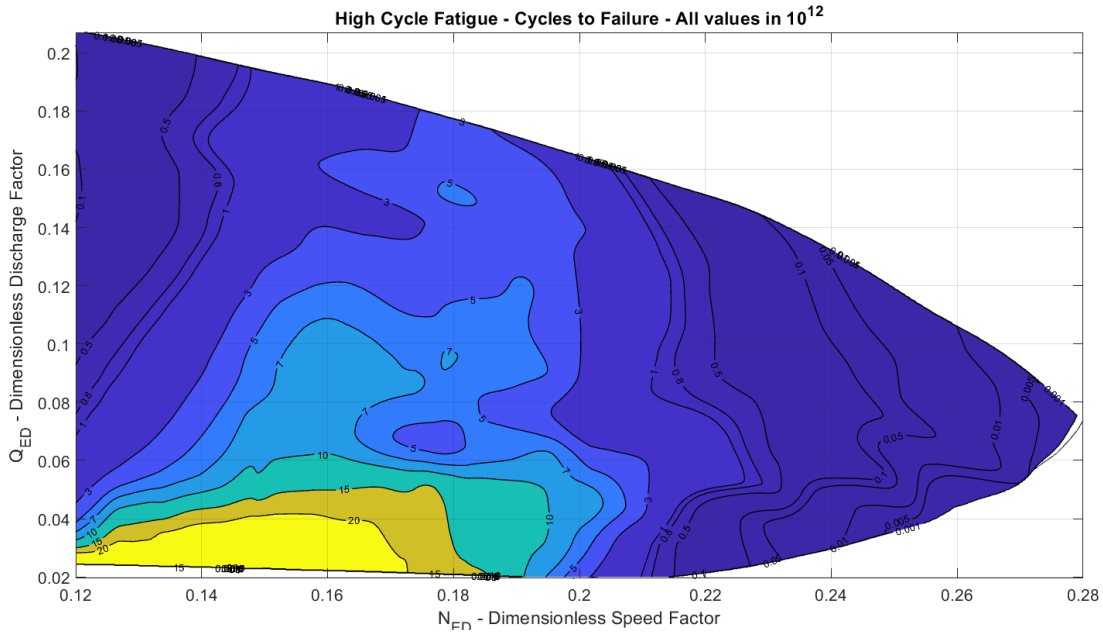

Figure 4.26: High Cycle Fatigue. X-axis Dimensionless Speed Factor N_{ED}. Y-axis Dimensionless Discharge Factor Q_{ED}.

Daniel Sannes conducted pressure measurements in 2018 and found that the dominating pressure amplitude on-board the runner is the guide vane frequency. [7] For this thesis we will assume that the stress amplitudes occurring during operation occurs with that frequency. This is used to calculate the number of cycles per hour of operation.

$$n_h = F_{gv} * 3600 = Z_{gv} * F_n * 3600 = 28 * \frac{n}{60} * 3600 = 1680 * n \qquad (-) \qquad [24]$$

Where n_h is the number of cycles per hour and n is the number of runner revolutions per minute. Miner's rule has been used to calculate damage per hour of operating for all operating conditions.

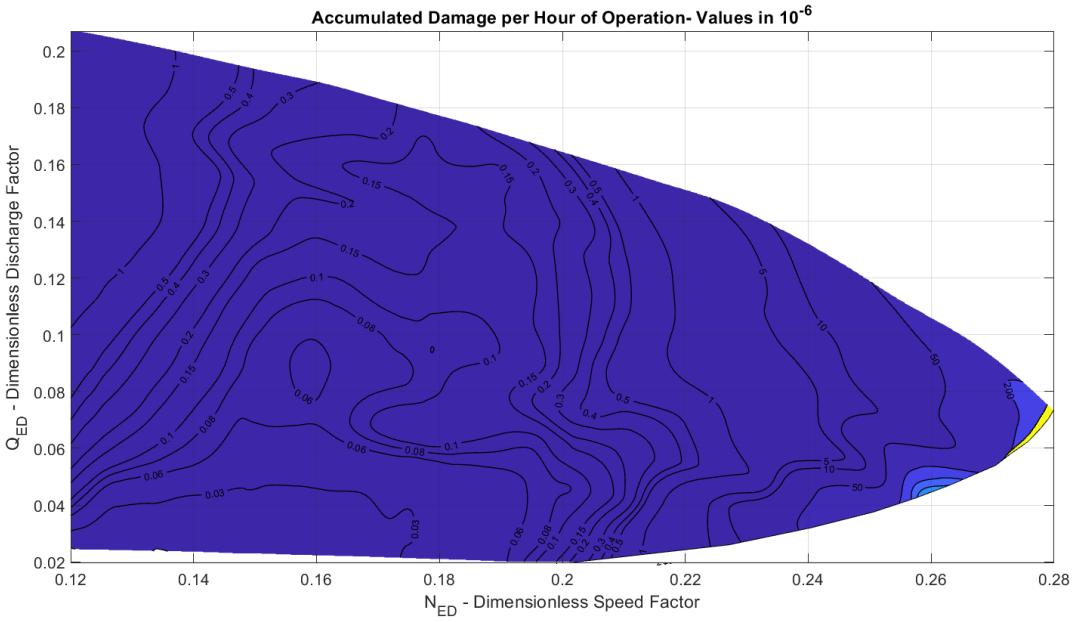

Figure 4.27: Accumulated Damage per Hour of Operation. X-axis Dimensionless Speed Factor N_{ED}. Y-axis Dimensionless Discharge Factor Q_{ED}.

4.6.2. Low Cycle Fatigue

Start-stop cycles have been looked at for LCF. Where each cycle represents going from stationary position to an operating condition and then returning to a stationary position. Due to having only conducted pressure measurements in the vaneless space, another assumption has to be made in regards to calculating fatigue induced by start-stop cycles. The assumption that each start-stop cycle only consists of only one pressure amplitude, namely the difference in effective stress from stationary to the operating point, calculated by using the Goodman method with the stress levels found in 4.5.

The diagram for start-stop cycles to failure shows that going to a reduction in speed reduces the damage done per start-stop cycle significantly.

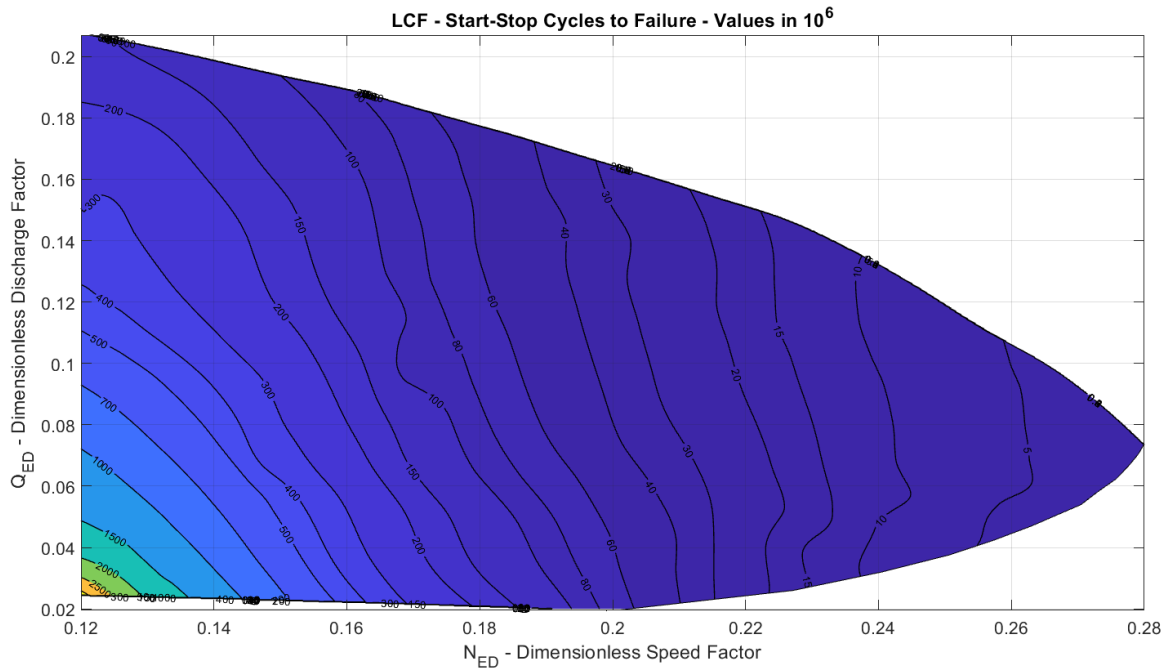

Figure: 4.28: Start-Stop Cycles to Failure. X-axis Dimensionless Speed Factor N_{ED}. Y-axis Dimensionless Discharge Factor Q_{ED}.

5. Discussion

5.1. Reducing pressure pulsations with variable speed turbine

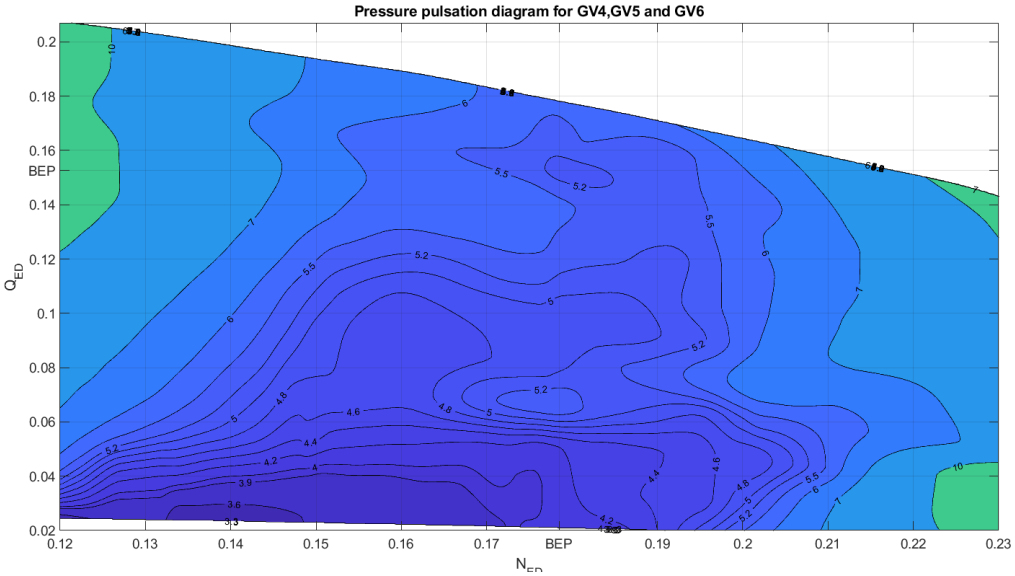

Figure 5.1: Pressure pulsation diagram with values from GV4, GV5 and GV6 added together. With the Dimensionless Speed Factor N_{ED} along the x-axis and the dimensionless discharge factor along the y-axis.

While the pressure pulsations for the individual sensors can be reduced quite drastically by changing the runner speed within a 30 percent range of the synchronous speed, the reduction for all three sensors combined is quite modest for most of the operating range. The exception being low loads, where the reduction for the sensors combined can reach up to 15,36 percent at 1 degree' guide vane opening. At 4 degrees' guide vane opening there is also a reduction of 11,98 percent. Above 6 degrees' guide vane opening the maximum reduction for the combined sensors is only 0,33 percent, achieved by reducing the runner speed 10 percent at 7 degrees' guide vane opening. The largest reduction in an individual sensor above 6 degrees is on the other hand 21,67 percent.

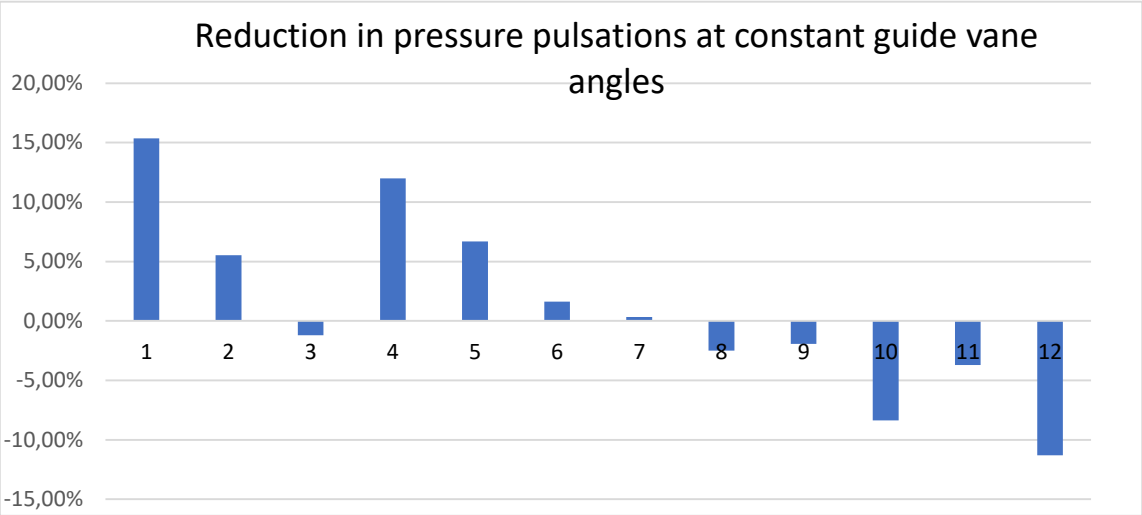

Figure 5.2: Maximum reduction in pressure pulsation along constant guide vane angles. Guide vane angles along the x-axis and percentage decrease along the y-axis. Negative percentage mean that the pressure pulsations could not be reduced and is showing the lowest increase from $N_{ED\text{-}BEP}$ prto 10, 20 or 30 % reduced or increased runner speed.

A slightly larger reduction can be found at speed-no-load. Where a decrease from 340 RPM to 295 RPM decreased the combined pressure pulsation by 15,66 percent. However, while there is a decrease in the pressure pulsation amplitudes, the frequency analysis of the two operating points shows us that the high-amplitude blade passing frequency increases slightly. The decrease is caused by a lower Rheingans and splitter blade passing amplitude. So from a fatigue perspective, where each of those frequencies contributes to fatigue in the runner blade. There might instead be an increase in sum of those fatigue load contributors despite the reduction in pressure pulsations and the increase in the not-normalized frequencies.

Sensors	Lowest pressure pulsation with constant RPM up to 12 degree's		Lowest constant RPM up to 10 degree's		Lowest pressure pulsation with flexible RPM values up to 12 degrees	Lowest pressure pulsation with flexible RPM values up to 10 degrees
	RPM	Sum of pressure pulsations(one measurement for each whole guide vane angle)	RPM	Sum of pressure pulsations		
GV4	338,9	20,443	338,9	16,893	19,343	15,793
GV5	372,8	19,240	372,8	15,963	18,880	15,603
GV6	305,0	15,952	305,0	12,126	15,691	11,991
Combined	338,9	59,563	305,0	48,099	57,651	46,625

Table 5.2: Showing lowest summed values for guide vane openings.

For the combined sensors, the difference in pressure pulsations for their combined results is quite modest.

5.2. Frequency analysis

Frequency analysis on the measured shows that the blade passing frequency is by far the most dominating factor for pressure pulsations over most operating point.

Only in 42 out of 762 measurement series recorded along the constant guide vane angles of 1 to 12 are other frequencies more dominant. 13 of these normalized frequencies are very low, while 28 are of the is the splitter blade passing frequency at 15. The vast majority of these are from GV4, with 27 measurement series with 15 in normalized frequency and 8 with below 1 in normalized frequency. As well as one anomaly with 19.9 in normalized frequency, happening at 224,4 RPM at 2 degrees' guide vane opening. The very low frequency results are not valid for measuring the size of the pressure amplitudes because they appear a very limited amount of times during each window segment when using the welch method, resulting in distorted amplitude peaks.

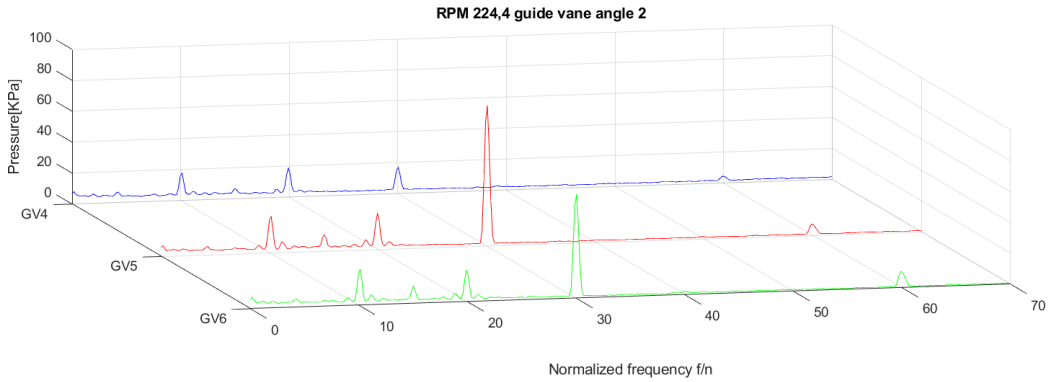

Figure 5.3: Figure 4.18: Frequencies observed at 224,4 RPM with 2 degree's guide vane opening. Showing values for GV4, GV5 and GV6 for normalized frequencies from 0 to 70.

As shown in the 3D-plot, there is a noticeable normalized frequency at 10, 20 and 30. With 20 actually being the largest for GV4. Harmonics of the blade passing frequency can also be seen at 60. This could be a result of the generator changing the torque slightly during the measurement series.

5.3. Strain gauges

Strain gauges can be an effective tool to measure stresses occurring in the runner, but needs to be calibrated properly to provide accurate strain values during the experiments.
In 3.3.2 a calibration of a strain gauge on a runner blade was conducted. But the calibration lacked several key factors to give accurate enough calibration for the operating conditions inside a turbine runner. A calibration procedure should instead be done with the strain gauge submerged and subjected to known pressure and pressure pulsations.

5.4. Fatigue assessment.

Because the pressures used to calculate the stress amplitudes and mean stresses were based on pressure measurements on a scaled model turbine used in the Waterpower Laboratory the damage per hour of operation is very low for almost all operating conditions measured. While operating at BEP it would take 9.16*10^6 hours before failure occurs, which equals 1046 years of constant operation. The main reason for this is that the material used for analyzing fatigue. With an Ultimate tensile strength of 910 MPa both the effective stress amplitudes and the effective mean stresses are very low in comparison.

The results of the fatigue analysis are therefore only useful to show the relative damage contribution.

5.4.1. High Cycle Fatigue

For operation at high load or around BEP, a change in runner speed will increase the damage contribution. Lowering the flow rate generally reduces the damage contribution from operation over the whole operating range. The relevant exception from this is when operating at synchronous speed at part load, where a draft tube vortex creates pressure pulsations that contributes to fatigue load. At part load around Q_{ED} at 0.07, reducing the runner speed 11 percent can decrease the effect of this vortex and thereby decrease the damage contribution from operation. This can result in a decrease of more than 50 percent.

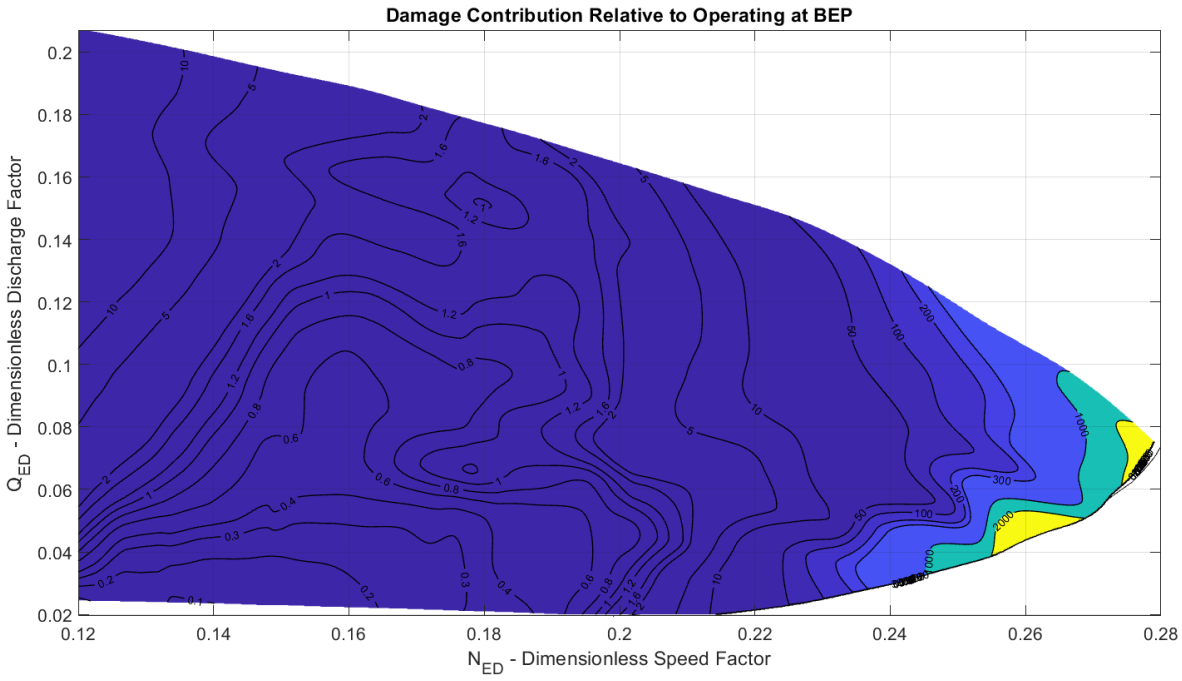

Figure 5.6: Damage contribution relative to steady state operating at BEP. X-axis Dimensionless Speed Factor N_{ED}. Y-axis Dimensionless Discharge Factor Q_{ED}.

By comparing the fatigue load at synchronous speed for various flow rates with the fatigue load with a reduction in runner speed the effectiveness of speed reduction becomes apparent.

Q_{ED}	0,175	0,16	$Q_{ED\text{-}BEP}$ 0,1526	0,14	0,12	0,10	0,08	0,06	0,04
N_{ED} reduced	-	0,1775	-	-	0,160	0,160	0,160	0,1568	0,1487
Reduction in damage [%]	0	2,15	0	0	24,27	24,27	36,49	49,80	38,25

Table 5.2: Reduction in damage by reducing the Dimensionless Speed Factor while holding the Dimensionless Discharge Factor constant. For steady-state operation.

As Table 5.2 demonstrates, reducing the speed at higher loads does not decrease the damage factor of operating at that load. For lower loads the effect of reducing speed is large, especially around 0,06 Dimensionless Discharge factor where a vortex ropes occur when operating at synchronous speed.

5.4.2. Low Cycle Fatigue

For Francis Turbines Low Cycle Fatigue is mostly a result of starting and stopping the turbine, which results in large changes in stresses on the runner blades. Large changes in stresses resulting in Low Cycle Fatigue can also occur as a result of changing the operating conditions, but this thesis focuses on start-stop cycles.

The results show that the damage from a start-stop cycle can be significantly reduced by operating at lower runner speed. For a start-stop cycle to BEP, the number of cycles to failure is 6,06*10^7. Applying Miner's rule and scaling damage relative to a start-stop cycle to BEP reveals the damage contribution per start-stop cycle relative to a start-stop cycle to BEP.

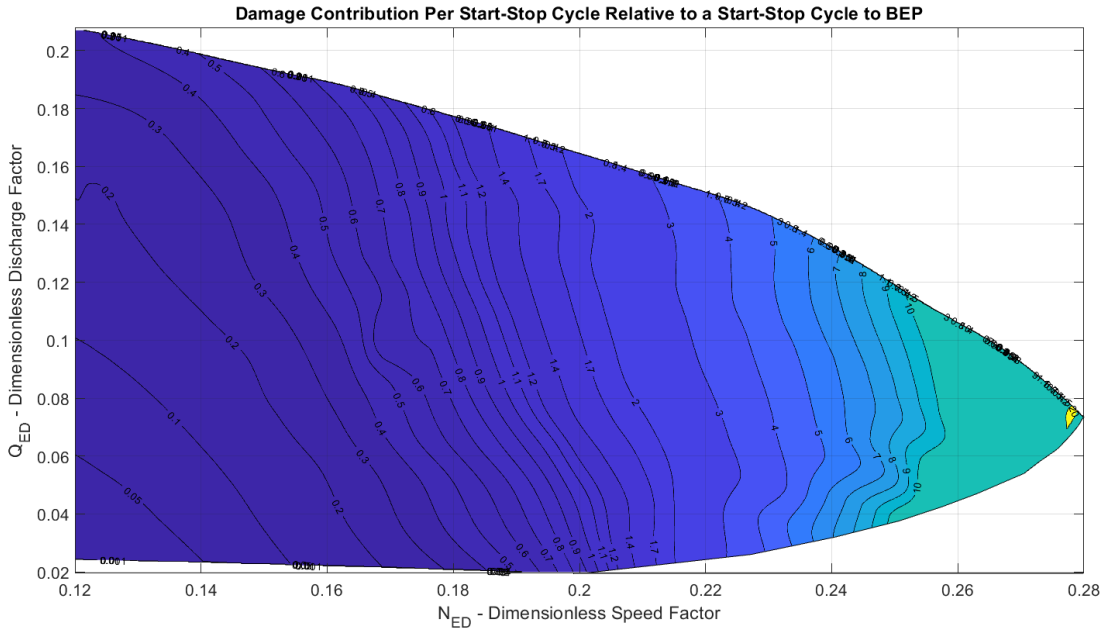

Figure 5.7: Damage contribution relative to start-stop cycle to BEP. X-axis Dimensionless Speed Factor N_{ED}. Y-axis Dimensionless Discharge Factor Q_{ED}.

The diagram shows that reducing the speed of the runner significantly reduces the damage per start-stop cycle. Reducing the flow through the runner also reduces the damage per cycle,

except when being close to Speed-No-Load at high speeds. By reducing the Dimensionless Speed Factor from N_{ED} at synchronous speed to 0,14, the following reductions are made if the Dimensionless Discharge Factor is held constant.

Q_{ED}	0,175	0,16	$Q_{ED\text{-}BEP}$ 0,1526	0,14	0,12	0,10	0,08	0,06	0,04
Reduction in damage [%]	67,71	69,73	70,96	73,15	74,24	78,03	80,67	82,89	83,52

Table 5.3: Reduction in damage by reducing the Dimensionless Speed Factor while holder the Dimensionless Discharge Factor constant. For start-stop cycles.

Which demonstrates clearly that fatigue loads from start-stop cycles can be significantly reduced by reducing the operating speed. While reducing the speed is most efficient at lower loads, it's also very effective at higher loads, as a reduction by 67,71 percent damage for start stop cycles at 0,175 Q_{ED} demonstrates.

5.4.3. Combining start-stop cycles and operating hours.

To compare the damage contributions of both HCF and LCF on the runner blade the number of operating hours it takes to do the same damage as one start-stop cycle to the same operating point has been calculated with Miner's rule.

$\frac{h*n_h}{N_O} = \frac{1}{N_S}\ and\ n_h = 1680 * n \rightarrow h = \frac{N_O}{1680*n*N_S}$ Where n_h is cycles per hour, h is hours, N_O is cycles to failure for steady-state operation at the operating point, N_S is the cycles to failure for start-stop cycles to that operating point and n is runner revolutions per minute.

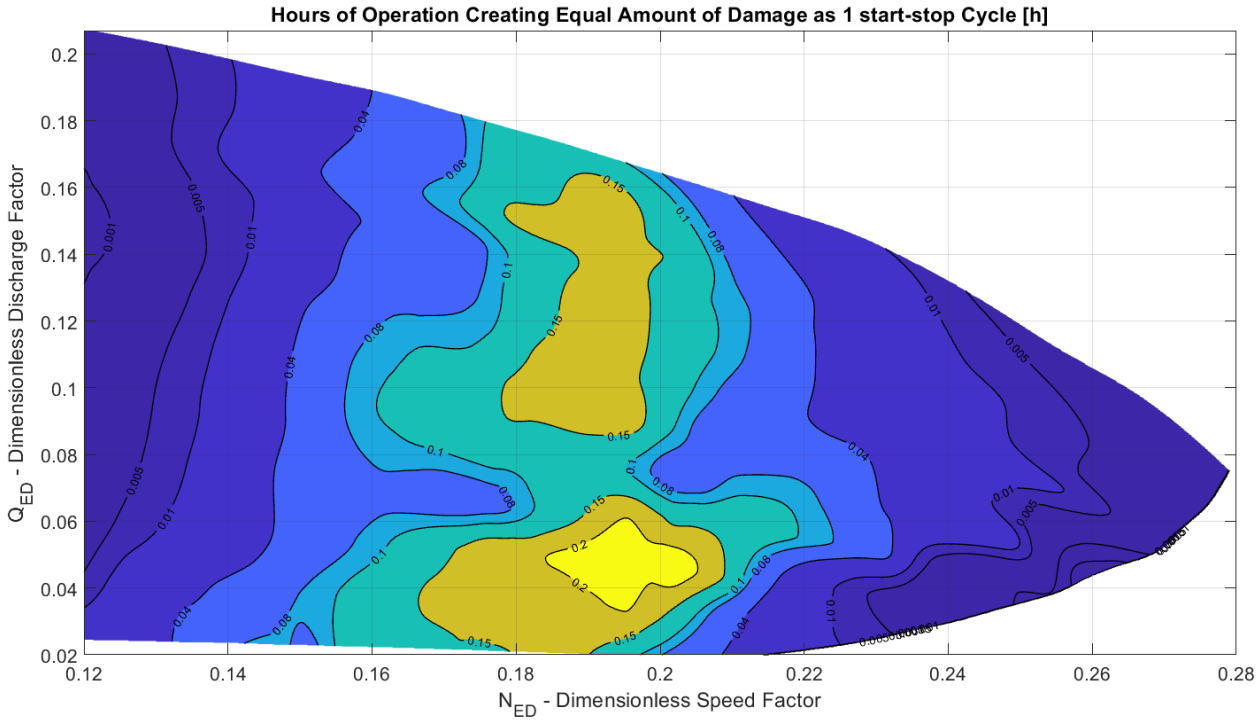

Figure 5.8: Hours of operation at steady state to equal the amount of damage from 1 start-stop cycle. X-axis Dimensionless Speed Factor N_{ED}. Y-axis Dimensionless Discharge Factor Q_{ED}

The results first and foremost shows that something is wrong with the assumptions made to calculate fatigue. Even while operating inside of the zones with relatively low pressure pulsations the fatigue from the pressure pulsations will in a matter of minutes accumulate more damage than a start-stop cycle to the same operation point. That is most likely the result of a start-stop cycle only being counted as one cycle, instead of several thousands.

The figure 5.8 does make a recommendation for what operation conditions should be chosen to minimize damage based how long planned operation is. However, due to the invalid calculation of the relation of the damage from pressure pulsations during steady-state operation and start-stop cycles, it only serves to show the relative difference between operating inside and outside of the low-pressure pulsation zones.

5.4.4. Impact of variable speed turbines

As shown in the previous sections of this chapter, a variable speed turbine can significantly reduce the damage accumulated for the runner blades and increase the lifespan of the turbine. Especially the damage from start-stop cycles can be reduced significantly by reducing the speed. As table 5.3 demonstrates, with over 60 percent reduction in fatigue load for start-stop cycles by reducing N_{ED} from synchronous speed to 0.14. The damage accumulated during continuous operation can mostly be reduced at lower loads.

This fatigue calculated does not factor in the reduced time, and therefore reduced number of stress amplitudes, start-up would take with a variable speed turbine, as it calculates only one amplitude per start-stop. Changing the model to account for the actual start-stop process would likely change the results drastically.

5.4.5. Scaling to a larger turbine

In a larger turbine, the stresses would be much higher and damage accumulated would be significantly increased compared to the numbers presented here. While the stresses used to calculate fatigue in this thesis was derived from experiments done on a smaller scaled model turbine at the Waterpower Laboratory, the material used for analyzing fatigue loads had material properties similar to those used in larger turbines.

5.5. Known errors and assumptions made.

5.5.1. Stress levels

The main assumption that the results presented here is based upon is the correlation between Equivalent von Mises Stress on the runner blade and the pressure in the vaneless space. While there is a correlation between the pressure pulsations in the vaneless space and the stresses occurring in the runner blades, the factors determining this correlation is based upon only one pressure drop and its corresponding Equivalent von Mises stress reduction analyzed by Valkvæ in 2016. [27] Analyzing the results using the linear ratio between the stress and pressure drop was attempted at first, but it became clear that a linear relationship between them could not be assumed for the whole pressure range. A second degree polynomial function based on that pressure drop and the assumed slope to a zero value for both stress and pressure was used instead.

The only way to validate these results was to compare them to previous stress analysis done one the runner blades of the scaled model turbine at the Waterpower Laboratory. Andreas Nilssen Skorpen found the following Maximum mean equivalent Von Mises Stresses for the runner blades in Impact from flexible operation on High head Francis turbines in 2018 [20]: 17.62, 14.92, 14.65 and 16.50 MPa for low part load, part load, BEP and High load respectively, while the values used in this thesis for similar operating points was 5.9, 7.3, 8,0

and 8,34 MPa respectively. Which would imply that the factors used to calculate stresses in this thesis is far too low.

However, comparing them to the stresses Daniel Sannes found stresses when conducting measurements and simulations in 2018 paints another picture. [7] His results for mean maximum equivalent von Mises stresses was 7,575 MPa for BEP, 5,138 for part load and 2,301 for minimum load. Which are similar to the values used in this thesis for part load and BEP, while a lot lower for minimum load.

5.5.2. Stress frequencies

Another assumption is that all the pressure pulsation amplitudes originates from the Guide vane passing frequency, which is not the case in reality. While the guide vane passing frequency is the dominating frequency for the runner blades, as demonstrated in Daniel Sannes's thesis from 2018[7], stochastic pressure pulsations, harmonics and some lower frequency pressure pulsations also occur. What is in fact several different pressure amplitudes occurring with different frequencies are all counted as one larger amplitude, distorting the calculated damage. As this increases the amplitude of the highest significant frequency, and thereby increases the accumulated damage from steady-state operation. This in fact introduces a safety factor to the calculations.

By applying a rainflow counting algorithm on the signal one could calculate the fatigue load from the pressure pulsations correctly. But since this thesis only has signals from the pressure pulsations in the vaneless space this was not possible.

5.5.3. Start-stop cycles.

With regards to start-stop cycles two assumptions were made, both significant.
First that a start-stop cycle only consists of one effective stress amplitude, which led to some bizarre results as can be seen in figure 5.8. A study by Gagnon, Tahan, Bocher and Thibault in 2010 [31], shows that a startup consists of thousands of effective stress amplitudes of varying magnitude. So even though the effective amplitude stress used for start-stop cycles in this study is comparable with stresses found by Daniel Sannes in 2018[7], the lifetime assessment based upon them get is of by a factor of over 1000.

The other assumption made in regard to start-stop cycles is that the effective amplitude stress is simply a function of mean von Mises stress and the stress amplitude created by the pressure pulsations at steady state operation. Both found with the assumption discussed in 5.5.1. While the study from Gagnon et al [31] shows that there are a lot of different stress amplitudes occurring during the cycle, with a large portion of them being high frequency amplitudes occurring at speed-no-load before connecting the generator. This Thesis completely neglects the reduction in fatigue loads that could be made by not having to subject the runner to the stresses occurring at speed-no-load for large portion of the startup duration.

6. Conclusion

Pressure measurements has been conducted on a model turbine at the Waterpower Laboratory at the Norwegian University of Science and Technology. The results of these measurements show that pressure pulsations in the vaneless space can be significantly reduced by operating with a flexible speed turbine. The largest reductions can be found when operating at part loads.

A correlation between pressure pulsations in the vaneless space and stresses on the runner blade found in a previous measurement at the Waterpower Laboratory was used to analyze the Fatigue on the runner blades. [27] The fatigue analysis focused on how accumulated damage to the runner blades could be reduced by operating with a flexible speed turbine.

The results of the fatigue analysis show that damage to the runner blades can be significantly reduced by reducing the speed of the runner. A slight reduction in runner speed at part load gave above 80 percent reduction in fatigue load for start-stop cycles, and can also significantly be reduced at all other load levels, while damage accumulated during steady-state operation could mostly be reduced at lower loads.

In order to do this fatigue analysis based only on pressure measurements from the vaneless space between the guide vanes and the runner blades several key assumptions had to be made, and the value of the results presented here can only be treated as indicative. The way fatigue load from start-stop cycles were calculated was especially questionable, as no measurements from actual start-stop scenarios were done.

7. Further Work

To properly calculate the impact of flexible speed turbines, the stresses occurring in the runner blades has to be accurately measured during both steady-state and transient operation. And then compared to the stresses occurring when operating the turbine as if it were not a variable speed turbine, only using the generator when synchronous speed is reached and stable enough.
This could be done with strain gages directly on the turbine at the Waterpower Laboratory. The strain gages would have to be calibrated beforehand and checked for drift during the experiments. With accurate results from strain gages the stresses and the frequencies they occur at can be calculated accurately. Rainflow counting can then be used on the measured stresses to calculate the fatigue over the whole operating range.

Because of the increased demand for Hydropower to act as a battery to balance out the grid, start-stop cycles are the most important phase to reduce fatigue at in the future. Therefore, the focus of the experiments should be the stresses occurring while going from a completely stationary turbine to various operating conditions and then shutting it down. Doing such an experiment and combining it with rainflow counting would make it possible to predict the damage reductions from operating at runner speeds outside of the speed at the Best Efficiency Point without having to make as many assumptions that invalidates the end-result.

8. Bibliography

[1] Bjørndal, Halvard & Reynaud, Andre & L. Holo, Anders. 2011. Mechanical robustness of Francis runners, requirements to reduce the risk of cracks in blades.

[2] Huang, Oram, Sick. 2014. Static and Dynamic stress analyses of the prototype high head Francis runner based on site measurement doi:10.1088/1755-1315/22/3/032052

[3] Huang, Chamberland-Lauzon, Oram, Klopfer, Runchonnet. 2014. Fatigue analyses of the prototype Francis runners based on site measurements and simulations. Doi:10.1088/1755-1315/22/1/012014

[4] Iliev, Trivedi, Agnalt, Dahlhaug. 2018. Variable-speed operation and pressure pulsations in a Francis turbine and a pump-turbine.

[5] Tovsild. 2013. Trykkpulsasjoner i Francisturbiner - sammenligning av modell og prototypmålinger. Norwegian University of Science and Technology.

[6] Haugan.2007. Trykkpulsasjoner i Francisturbiner. Norwegian University of Science and Technology.

[7] Sannes.2018. Pressure Pulsation and Stresses in a Francis Turbine Operating at Variable Speed. Norwegian University of Science and Technology.

[8] Dörfler, Sick, Coutu, 2013, Flow-Induced Pulsation and Vibration in Hydroelectric Machinery. Springer London

[9] Ruchonnet N, Nicolet C, Avellan F. One-dimensional modeling of rotor stator interaction in Francis pump-turbine. Proceedings of the 23rd IAHR Symposium on Hydraulic Machinery and Systems 2006.

[10] Haga. 2014. Dynamic load on High Head Francis turbines during start/stop. Norwegian University of Science and Technology.

[11] Seidel, Mende, Hubner, Weber, Otto. 2014. Dynamic loads in Francis runners and their impact on fatigue life. doi:10.1088/1755-1315/22/3/032054

[12] 2014. Guideline DKD-R 6-1, Calibration of Pressure Gauges. German Calibration Service.

[13] Agnalt. 2016. Pressure measurements inside a Francis turbine runner. Norwegian University of Science and Technology.

[14] R. A. Gujar, S. V. Bhaskar.2013. Shaft Design under Fatigue Loading By Using Modified Goodman Method. International Journal of Engineering Research and Applications.

[15] ISO 19902:2007 Petroleum and natural gas industries - Fixed steel offshore structures

[16] IEC60193 Hydraulic turbines, storage pumps and pump-turbines - Model acceptance tests

[17] IEC 60041 Field acceptance tests to determine the hydraulic performance of hydraulic turbines, storage pumps and pump-turbines

[18] https://www.ntnu.edu/nvks/francis-99

[19] IEC 17025 General requirements for the competence of testing and calibration laboratories.

[20] Andreas Nilssen Skorpen. 2018. Impact from flexible operation on High head Francis turbines. Norwegian University of Science and Technology.

[21] Scott Woodward.2009. MAE 334 – Introduction to computers and instrumentation. Signal Characteristics. University at Buffalo.

[22] https://se.mathworks.com/help/matlab/ref/fft.html(timestamp 14.14 14.12.2018)

[23] Datasheet for NI-cDAQ 9178 http://www.ni.com/pdf/manuals/374046a.pdf (timestamp 11.12 5.12.2018)

[24] Datasheet for NI 9237 http://www.ni.com/pdf/manuals/374186a_02.pdf (timestamp 11.17 5.12.2018)

[25] Einar Agnalt. 2018. Measurement report 2018. HiFrancis WP 1.3***

[26] Arne Kjølle.2006. Hydropower in Norway, Mechanical Equipment.

[27] Valkvæ, I. 2016. Dynamic loads on Francis turbines. Norwegian University of Science and Technology.

[28] Shannon.1949. Communication in the Presence of Noise*

[29] https://se.mathworks.com/help/signal/ref/hann.html (timestamp 10.50 06.01 2019)

[30] Welch. 1967. The Use of Fast Fourier Transform for the Estimation of Power Spectra. A Method Based on Time Averaging Over Short, Modified Periodograms. IEEE Trans. Audio and Electrocoust.

[31] Gagnon, Tahan, Bocher, Thibault. 2010. Impact of startup scheme on Francis runner life expectancy. IOP Conf. Series: Earth and Environmental Science. doi:10.1088/1755-1315/12/1/012107

[32] Michael Bak. 2016. Mean Stress Corrections in Fatigue. https://caeai.com/blog/mean-stress-corrections-fatigue (timestamp 13.50 07.01 2019)

[33] DeLuca. Understanding Fatigue. https://files.asme.org/igti/knowledge/articles/13048.pdf (timestamp 14.21 07.01 2019)

[34] Hans-Jorg Huth.2005. Fatigue Design of Hydraulic Turbine Runners. Norwegian University of Science and Technology.

Appendix A – Risk Assesment

NTNU		Utarbeidet av	Nummer	Dato
		HMS-avd.	HMSRV2601	22.03.2011
	Kartlegging av risikofylt aktivitet	Godkjent av		Erstatter
HMS		Rektor		01.12.2006

Enhet: Institutt for Maskinteknikk og Produksjon **Dato:** 18.10.2018

Linjeleder:

Deltakere ved kartleggingen (m/ funksjon)**:** Roy Johnsen, veileder. Ole Gunnar Dahlhaug, veileder. Eirik Lødemel, student.
(Ansv. veileder, student, evt. medveiledere, evt. andre m. kompetanse)

Kort beskrivelse av hovedaktivitet/hovedprosess: Analyse av utmattingslaster i et høytrykks Francis løpehjul

Er oppgaven rent teoretisk? (JA/NEI)**:** NEI *«JA» betyr at veileder innestår for at oppgaven ikke inneholder noen aktiviteter som krever risikovurdering. Dersom «JA»: Beskriv kort aktiviteten i kartleggingsskjemaet under. Risikovurdering trenger ikke å fylles ut.*

Signaturer: *Ansvarlig veileder: Roy Johnsen* *Veileder: Ole Gunnar Dahlhaug* *Student: Eirik Lødemel*

ID nr.	Aktivitet/prosess	Ansvarlig	Eksisterende dokumentasjon	Eksisterende sikringstiltak	Lov, forskrift o.l.	Kommentar
1	Bruk av laboratoriet på vannkraftlaboratoriet	EL		Brannslukkningsapparat, brannalarm, førstehjelp, vernesko, vernebriller.		

NTNU	Kartlegging av risikofylt aktivitet	Utarbeidet av	Nummer	Dato	
		HMS-avd.	HMSRV2601	22.03.2011	
		Godkjent av		Erstatter	
HMS		Rektor		01.12.2006	

1a	Operasjon av Francis-riggen	EL	Prosedyrer for operasjon av riggen.	Nødstopp, vernebriller.		
1b	Bruk av lim(og andre sammenføyningsmidler)	EL	Sikkerhetsdatablad og produktets brukermanual.	Sikkerhetsdatablad, vernebriller.		
1c	Bruk av vekter(opp til 140 kg)	EL		Vernesko		

NTNU	Kartlegging av risikofylt aktivitet	Utarbeidet av	Nummer	Dato	
		HMS-avd.	HMSRV2601	22.03.2011	
		Godkjent av		Erstatter	
HMS		Rektor		01.12.2006	

Enhet: Institutt for Maskinteknikk og Produksjon **Dato:** 18.10.2018

Linjeleder:

Deltakere ved kartleggingen (m/ funksjon): Roy Johnsen, veileder. Ole Gunnar Dahlhaug, veileder. Eirik Lødemel, student.
(Ansv. Veileder, student, evt. medveiledere, evt. andre m. kompetanse)

Risikovurderingen gjelder hovedaktivitet: Analyse av utmattingslaster i et høytrykks Francis løpehjul

Signaturer: *Ansvarlig veileder: Roy Johnsen* *Veileder: Ole Gunnar Dahlhaug* *Student: Eirik Lødemel*

ID nr	Aktivitet fra kartleggings-skjemaet	Mulig uønsket hendelse/ belastning	Vurdering av sannsyn-lighet	Vurdering av konsekvens:				Risiko-Verdi (menn-eske)	Kommentarer/status Forslag til tiltak
			(1-5)	Menneske (A-E)	Ytre miljø (A-E)	Øk/ materiell (A-E)	Om-dømme (A-E)		
1	Bruk av laboratoriet på vannkraftlaboratoriet								

NTNU	Kartlegging av risikofylt aktivitet	Utarbeidet av	Nummer	Dato	
		HMS-avd.	HMSRV2601	22.03.2011	
		Godkjent av		Erstatter	
HMS		Rektor		01.12.2006	

1a-1	Operasjon av Francis-riggen	Skade turbinen	2	A	A	C	A	2A	Opplæring i operasjon av Francisriggen
1a-2		Falle ned bratt trapp ved Turbinen	1	C	A	A	A	1C	Gå sakte, alltid en hånd på gelenderet.
1a-3		Skade på utstyr ved oppstart av riggen	3	A	A	B	A	3A	Gå igjennom prosedyrene for oppstart
1a-4		Skade på utstyr ved nedstenging av riggen	3	A	A	B	A	3A	Gå igjennom prosedyrene for nedstenging av riggen
1b-1	Bruk av lim(og andre sammenføyingsmidler)	Eksponering øye	2	B	A	A	A	2B	Vernebriller.
1b-2		Eksponering hud	3	A	A	A	A	3A	Sikkerhetsdatablad tilgjengelig

NTNU	Kartlegging av risikofylt aktivitet	Utarbeidet av	Nummer	Dato	
		HMS-avd.	HMSRV2601	22.03.2011	
		Godkjent av		Erstatter	
HMS		Rektor		01.12.2006	

1b-3		Eksponering åndedrett	3	A	A	A	A	3A	Sikkerhetsdatablad tilgjengelig. Arbeide i godt ventilert område.
1c-1	Bruk av vekter(opp til 140 kg)	Kroppsskade av fallende vekter	2	C	A	A	A	2C	Vernesko, sjekke at vektskålen er godt festet.
1c-2		Belastningsskade	3	A	A	A	A	2A	Løfte vektene en og en, løfte med god positur, strekke før og etter økt med løft.

NTNU	Kartlegging av risikofylt aktivitet	Utarbeidet av	Nummer	Dato	
		HMS-avd.	HMSRV2601	22.03.2011	
		Godkjent av		Erstatter	
HMS		Rektor		01.12.2006	

Sannsynlighet vurderes etter følgende kriterier:

Svært liten 1	Liten 2	Middels 3	Stor 4	Svært stor 5
1 gang pr 50 år eller sjeldnere	1 gang pr 10 år eller sjeldnere	1 gang pr år eller sjeldnere	1 gang pr måned eller sjeldnere	Skjer ukentlig

Konsekvens vurderes etter følgende kriterier:

Gradering	Menneske	Ytre miljø Vann, jord og luft	Øk/materiell	Omdømme
E Svært Alvorlig	Død	Svært langvarig og ikke reversibel skade	Drifts- eller aktivitetsstans >1 år.	Troverdighet og respekt betydelig og varig svekket
D Alvorlig	Alvorlig personskade. Mulig uførhet.	Langvarig skade. Lang restitusjonstid	Driftsstans > ½ år Aktivitetsstans i opp til 1 år	Troverdighet og respekt betydelig svekket
C Moderat	Alvorlig personskade.	Mindre skade og lang restitusjonstid	Drifts- eller aktivitetsstans < 1 mnd	Troverdighet og respekt svekket
B Liten	Skade som krever medisinsk behandling	Mindre skade og kort restitusjonstid	Drifts- eller aktivitetsstans < 1uke	Negativ påvirkning på troverdighet og respekt

NTNU	Kartlegging av risikofylt aktivitet	Utarbeidet av	Nummer	Dato	
		HMS-avd.	HMSRV2601	22.03.2011	
		Godkjent av		Erstatter	
HMS		Rektor		01.12.2006	

A **Svært liten**	Skade som krever førstehjelp	Ubetydelig skade og kort restitusjonstid	Drifts- eller aktivitetsstans < 1dag	Liten påvirkning på troverdighet og respekt

Risikoverdi = Sannsynlighet x Konsekvens
Beregn risikoverdi for Menneske. Enheten vurderer selv om de i tillegg vil beregne risikoverdi for Ytre miljø, Økonomi/materiell og Omdømme. I så fall beregnes disse hver for seg.

Til kolonnen "Kommentarer/status, forslag til forebyggende og korrigerende tiltak":
Tiltak kan påvirke både sannsynlighet og konsekvens. Prioriter tiltak som kan forhindre at hendelsen inntreffer, dvs. sannsynlighetsreduserende tiltak foran skjerpet beredskap, dvs. konsekvensreduserende tiltak.

NTNU	Kartlegging av risikofylt aktivitet	Utarbeidet av	Nummer	Dato	
		HMS-avd.	HMSRV2601	22.03.2011	
		Godkjent av		Erstatter	
HMS		Rektor		01.12.2006	

MATRISE FOR RISIKOVURDERINGER ved NTNU

KONSEKVENS						
	Svært alvorlig	E1	E2	E3	E4	E5
	Alvorlig	D1	D2	D3	D4	D5
	Moderat	C1	C2	C3	C4	C5
	Liten	B1	B2	B3	B4	B5
	Svært liten	A1	A2	A3	A4	A5
		Svært liten	Liten	Middels	Stor	Svært stor

NTNU	Kartlegging av risikofylt aktivitet	Utarbeidet av	Nummer	Dato	
		HMS-avd.	HMSRV2601	22.03.2011	
		Godkjent av		Erstatter	
HMS		Rektor		01.12.2006	

		SANNSYNLIGHET

Prinsipp over akseptkriterium. Forklaring av fargene som er brukt i risikomatrisen.

Farge	Beskrivelse
Rød	Uakseptabel risiko. Tiltak skal gjennomføres for å redusere risikoen.
Gul	Vurderingsområde. Tiltak skal vurderes.
Grønn	Akseptabel risiko. Tiltak kan vurderes ut fra andre hensyn.

Appendix B – Matlab scripts

Because of limited time the Matlab scripts have not been properly organized and might be hard to understand. Matlab version R2018a has been used. All functions that aren't part of the standard Matlab functions are mentioned.

Hill chart and pressure diagrams

```
%script to extract values from excel and tdms files to create hill charts
and pressure data

%Trykkhilling is an excelfile containing operating parameters

[num,txt,raw]=xlsread('trykkhilling');
i=1;
for i=3:14798
hill{1,i-2}=raw{i,21};
hill{2,i-2}=raw{i,22};
hill{3,i-2}=raw{i,23};
hill{4,i-2}=raw{i,41};
hill{5,i-2}=raw{i,9};
end
i=1;
for i=10001:14798
hill2{1,i-10000}=raw{i,21};
hill2{2,i-10000}=raw{i,22};
hill2{3,i-10000}=raw{i,23};
hill2{4,i-10000}=raw{i,41};
hill2{5,i-10000}=raw{i,9};
end

i=1;

for i=1:14796
hill{1,i}=str2num(hill{1,i});
hill{2,i}=str2num(hill{2,i});
hill{3,i}=str2num(hill{3,i});
hill{4,i}=str2num(hill{4,i});
hill{5,i}=str2num(hill{5,i});
end
for i=1:length(hill)
if hill{1,i} > 2
hill{1,i}=hill{1,i};
elseif hill{1,i} ==0;
hill{1,i}=0;
hill{2,i}=0;
hill{3,i}=0;
hill{4,i}=0;
hill{5,i}=0;
else
hill{1,i}=0;
hill{2,i}=0;
hill{3,i}=0;
hill{4,i}=0;
```

```
hill{5,i}=0;
end
end

HILL=zeros(7,258);
a=0;
b=0;
n=1;
i=1;
Eff=0;
Ned=0;
Qed=0;
GV=0;
RPM=0;
NumOfMeasurements=0;
for n=1:255
    Eff=0;
    Ned=0;
    Qed=0;
    GV=0;
    a=0;
    NumOfMeasurements=0;
    RPM=0;
    extra=0;
    if n==255;
        extra=15;
    end




for i=1:70-extra
    b=b+1;
       if hill{1,b} >0.1
           %Skip point 127
           if b==127
               b=128;
           end


        Eff=Eff+hill{1,b};
        Ned=Ned+hill{2,b};
        Qed=Qed+hill{3,b};
        GV=GV+hill{4,b};
        RPM=RPM+hill{5,b};
        NumOfMeasurements=NumOfMeasurements+1;
       else
           a=i;
           b=b+1;
           break;
       end



end

if extra==15;
    a=i+1;
```

```
end
    HILL(1,n)=Eff/(a-1);
    HILL(2,n)=Ned/(a-1);
    HILL(3,n)=Qed/(a-1);
    HILL(4,n)=GV/(a-1);
    HILL(5,n)=RPM/(a-1);
    HILL(6,n)=NumOfMeasurements;
    HILL(7,n)=(a-1);



end
%Skip point 233
for n=1:232
HILLTO(:,n)=HILL(:,n);
end
for n=233:254
    HILLTO(:,(n))=HILL(:,n+1);
end

HILL=zeros(7,254);
HILL=HILLTO;
%Should only be used if some sequences are missplaced, ignore if
%the data is fine.
%Sortering=zeros(5,5);
%i=0;
%for i=1:5
 %   Sortering(:,i)=HILL(:,i+62);
%end

%HILL(:,63)=Sortering(:,3);
%HILL(:,64)=Sortering(:,4);
%HILL(:,65)=Sortering(:,5);
%HILL(:,66)=Sortering(:,1);
%HILL(:,67)=Sortering(:,2);

i=0;
for i=1:254
RPM(1,i)=HILL(5,i);
Qed(1,i)=HILL(3,i);
Ned(1,i)=HILL(2,i);
Eff(1,i)=HILL(1,i);
end

clearvars raw HILLTO extra a b n i NumOfMeasurements num hill txt

%TDMS_readTDMSFile is a function written by Jim Hokanson
%trykkfredag and trykksenfredag are files containing sensor output from
%pressure measurements
tolvtilni =
TDMS_readTDMSFile('C:\Users\eirilo\Documents\MATLAB\trykkfredag.tdms');
attetilen=TDMS_readTDMSFile('C:\Users\eirilo\Documents\MATLAB\trykksenfreda
g.tdms');

for i=3:length(tolvtilni.data)
    Trykk{1,i}=tolvtilni.data{1,i};
    b=i;
end
for i=3:length(attetilen.data)
    Trykk{1,b+i-1}=attetilen.data{1,i};
```

```
end
%constants for for the sensors to match the atmospheric pressure
Off1=16,44964607;
Off2=7,014733975;
Off3=-4,140070341;
a1=attetilen.propValues{1,3}{1,11};
a2=attetilen.propValues{1,4}{1,11};
a3=attetilen.propValues{1,5}{1,11};

i=0;
j=0;
l=1;
k=0;

%Extracting pressure amplitudes and mean values

for k=3:length(Trykk)


    T=Trykk{1,k};
PressFreq=Trykk{1,k};

[N,e] = histcounts(T,1000);
Me = mean(T);
NumberOfPoints = sum(N);
temp=0;
conf=0.97;
for i=1:length(N)
    temp=temp +N(i); value=temp/NumberOfPoints;
    if value >=(1-conf)/2
         lower=e(i);
         break
    end
end



for j=1:length(N)
temp=temp +N(j); value=temp/NumberOfPoints;
if value >=conf+(1-conf)/2
upper=e(j);
break
end
end



VoltAmp=(upper-lower)/2;

if l == 1
    m = (k/4)+0.25;
    if NumberOfPoints > 198000
    GV4Volts{1,m}=VoltAmp;
    GV4Stress(1,m)=Me*a1+Off1;
    FrekA{1,m}=PressFreq;
    end
l=10;
end
if l == 2
```

```
    m = (k/4);
    if NumberOfPoints > 198000
    LabVolts{1,m}=VoltAmp;
    GV5Stress(1,m)=Me*a2+Off2;
    FrekA{2,m}=PressFreq;
    end
    l=11;
end
if l == 3
    m = (k/4)-0.25;
    if NumberOfPoints > 198000
    GV6Volts{1,m}=VoltAmp;
    GV6Stress(1,m)=Me*a3+Off3;
    FrekA{3,m}=PressFreq;
    end
    l=12;
end

if l == 4
    l=13;
end

l=l-8;

if l == 5
    l=1;
end



end
i=0;
b=0;
for i=1:length(GV4Volts);
if GV4Volts{1,i} >0
    b=b+1;
    CGV4{1,b}=GV4Volts{1,i};
    FrekAC{1,b}=FrekA{1,i};
    CGV4Stress(1,b)=GV4Stress(1,i);
end
end
i=0;
b=0;
for i=1:length(LabVolts);
if GV6Volts{1,i} >0
    b=b+1;
    CGV6{1,b}=GV6Volts{1,i};
    FrekAC{3,b}=FrekA{3,i};
    CGV5Stress(1,b)=GV5Stress(1,i);
end
end
i=0;
b=0;
for i=1:length(LabVolts);
if LabVolts{1,i} >0
    b=b+1;
    CLab{1,b}=LabVolts{1,i};
    FrekAC{2,b}=FrekA{2,i};
    CGV6Stress(1,b)=GV6Stress(1,i);
end
end
```

```
G4=cell2mat(CGV4);
G6=cell2mat(CGV6);
GLab=cell2mat(CLab);
for i=1:118
    G4A(1,i)=G4(1,i);
    G6A(1,i)=G6(1,i);
    GLA(1,i)=GLab(1,i);
    G4ST(1,i)=CGV4Stress(1,i);
    G5ST(1,i)=CGV5Stress(1,i);
    G6ST(1,i)=CGV6Stress(1,i);
    FrequencyRaw{1,i}=FrekAC{1,i};
    FrequencyRaw{2,i}=FrekAC{2,i};
    FrequencyRaw{3,i}=FrekAC{3,i};
end
for i=119:167
    G4A(1,i)=G4(1,i+1);
    G6A(1,i)=G6(1,i+1);
    GLA(1,i)=GLab(1,i+1);
    G4ST(1,i)=CGV4Stress(1,i+1);
    G5ST(1,i)=CGV5Stress(1,i+1);
    G6ST(1,i)=CGV6Stress(1,i+1);
    FrequencyRaw{1,i}=FrekAC{1,i+1};
    FrequencyRaw{2,i}=FrekAC{2,i+1};
    FrequencyRaw{3,i}=FrekAC{3,i+1};
end
for i=168:232
    G4A(1,i)=G4(1,i+2);
    G6A(1,i)=G6(1,i+2);
    GLA(1,i)=GLab(1,i+2);
    G4ST(1,i)=CGV4Stress(1,i+2);
    G5ST(1,i)=CGV5Stress(1,i+2);
    G6ST(1,i)=CGV6Stress(1,i+2);
    FrequencyRaw{1,i}=FrekAC{1,i+2};
    FrequencyRaw{2,i}=FrekAC{2,i+2};
    FrequencyRaw{3,i}=FrekAC{3,i+2};
end
for i=233:254
    G4A(1,i)=G4(1,i+3);
    G6A(1,i)=G6(1,i+3);
    GLA(1,i)=GLab(1,i+3);
    G4ST(1,i)=CGV4Stress(1,i+3);
    G5ST(1,i)=CGV5Stress(1,i+3);
    G6ST(1,i)=CGV6Stress(1,i+3);
    FrequencyRaw{1,i}=FrekAC{1,i+3};
    FrequencyRaw{2,i}=FrekAC{2,i+3};
    FrequencyRaw{3,i}=FrekAC{3,i+3};
end

numb=1000;
x=linspace(0.120,0.28,numb);
Speed=linspace(227,530,numb);
%1-17 18-34 35-50 51-69 70-90 91-109 110-134 135-160 161-189 190-217
%218-239 240-254
%Create new interpolated Q_ed based on Ned
q(:,12)=interp1(Ned(1:17),Qed(1:17),x,'PCHIP','extrap');
q(:,11)=interp1(Ned(18:34),Qed(18:34),x,'PCHIP','extrap');
q(:,10)=interp1(Ned(35:50),Qed(35:50),x,'PCHIP','extrap');
q(:,9)=interp1(Ned(51:69),Qed(51:69),x,'PCHIP','extrap');
q(:,8)=interp1(Ned(70:90),Qed(70:90),x,'PCHIP','extrap');
q(:,7)=interp1(Ned(91:109),Qed(91:109),x,'PCHIP','extrap');
```

```
q(:,6)=interp1(Ned(110:134),Qed(110:134),x,'PCHIP','extrap');
q(:,5)=interp1(Ned(135:160),Qed(135:160),x,'PCHIP','extrap');
q(:,4)=interp1(Ned(161:189),Qed(161:189),x,'PCHIP','extrap');
q(:,3)=interp1(Ned(190:217),Qed(190:217),x,'PCHIP','extrap');
q(:,2)=interp1(Ned(218:239),Qed(218:239),x,'PCHIP','extrap');
q(:,1)=interp1(Ned(240:254),Qed(240:254),x,'PCHIP','extrap');

%Create new interpolated Q_ed based on RPM
qS(:,12)=interp1(RPM(1:17),Qed(1:17),Speed,'PCHIP','extrap');
qS(:,11)=interp1(RPM(18:34),Qed(18:34),Speed,'PCHIP','extrap');
qS(:,10)=interp1(RPM(35:50),Qed(35:50),Speed,'PCHIP','extrap');
qS(:,9)=interp1(RPM(51:69),Qed(51:69),Speed,'PCHIP','extrap');
qS(:,8)=interp1(RPM(70:90),Qed(70:90),Speed,'PCHIP','extrap');
qS(:,7)=interp1(RPM(91:109),Qed(91:109),Speed,'PCHIP','extrap');
qS(:,6)=interp1(RPM(110:134),Qed(110:134),Speed,'PCHIP','extrap');
qS(:,5)=interp1(RPM(135:160),Qed(135:160),Speed,'PCHIP','extrap');
qS(:,4)=interp1(RPM(161:189),Qed(161:189),Speed,'PCHIP','extrap');
qS(:,3)=interp1(RPM(190:217),Qed(190:217),Speed,'PCHIP','extrap');
qS(:,2)=interp1(RPM(218:239),Qed(218:239),Speed,'PCHIP','extrap');
qS(:,1)=interp1(RPM(240:254),Qed(240:254),Speed,'PCHIP','extrap');

%Create new interpolated Eff based on NED
ef(:,12)=interp1(Ned(1:17),Eff(1:17),x,'PCHIP','extrap');
ef(:,11)=interp1(Ned(18:34),Eff(18:34),x,'PCHIP','extrap');
ef(:,10)=interp1(Ned(35:50),Eff(35:50),x,'PCHIP','extrap');
ef(:,9)=interp1(Ned(51:69),Eff(51:69),x,'PCHIP','extrap');
ef(:,8)=interp1(Ned(70:90),Eff(70:90),x,'PCHIP','extrap');
ef(:,7)=interp1(Ned(91:109),Eff(91:109),x,'PCHIP','extrap');
ef(:,6)=interp1(Ned(110:134),Eff(110:134),x,'PCHIP','extrap');
ef(:,5)=interp1(Ned(135:160),Eff(135:160),x,'PCHIP','extrap');
ef(:,4)=interp1(Ned(161:189),Eff(161:189),x,'PCHIP','extrap');
ef(:,3)=interp1(Ned(190:217),Eff(190:217),x,'PCHIP','extrap');
ef(:,2)=interp1(Ned(218:239),Eff(218:239),x,'PCHIP','extrap');
ef(:,1)=interp1(Ned(240:254),Eff(240:254),x,'PCHIP','extrap');

%Create new interpolated RPM based on NED
r(:,12)=interp1(Ned(1:17),RPM(1:17),x,'PCHIP','extrap');
r(:,11)=interp1(Ned(18:34),RPM(18:34),x,'PCHIP','extrap');
r(:,10)=interp1(Ned(35:50),RPM(35:50),x,'PCHIP','extrap');
r(:,9)=interp1(Ned(51:69),RPM(51:69),x,'PCHIP','extrap');
r(:,8)=interp1(Ned(70:90),RPM(70:90),x,'PCHIP','extrap');
r(:,7)=interp1(Ned(91:109),RPM(91:109),x,'PCHIP','extrap');
r(:,6)=interp1(Ned(110:134),RPM(110:134),x,'PCHIP','extrap');
r(:,5)=interp1(Ned(135:160),RPM(135:160),x,'PCHIP','extrap');
r(:,4)=interp1(Ned(161:189),RPM(161:189),x,'PCHIP','extrap');
r(:,3)=interp1(Ned(190:217),RPM(190:217),x,'PCHIP','extrap');
r(:,2)=interp1(Ned(218:239),RPM(218:239),x,'PCHIP','extrap');
r(:,1)=interp1(Ned(240:254),RPM(240:254),x,'PCHIP','extrap');


%Create new interpolated Pressure amplitude values based on Ned
GV4(:,12)=interp1(Ned(1:17),G4A(1:17),x,'PCHIP');
GV4(:,11)=interp1(Ned(18:34),G4A(18:34),x,'PCHIP');
GV4(:,10)=interp1(Ned(35:50),G4A(35:50),x,'PCHIP');
GV4(:,9)=interp1(Ned(51:69),G4A(51:69),x,'PCHIP');
GV4(:,8)=interp1(Ned(70:90),G4A(70:90),x,'PCHIP');
GV4(:,7)=interp1(Ned(91:109),G4A(91:109),x,'PCHIP');
GV4(:,6)=interp1(Ned(110:134),G4A(110:134),x,'PCHIP');
GV4(:,5)=interp1(Ned(135:160),G4A(135:160),x,'PCHIP');
GV4(:,4)=interp1(Ned(161:189),G4A(161:189),x,'PCHIP');
```

```
GV4(:,3)=interp1(Ned(190:217),G4A(190:217),x,'PCHIP');
GV4(:,2)=interp1(Ned(218:239),G4A(218:239),x,'PCHIP');
GV4(:,1)=interp1(Ned(240:254),G4A(240:254),x,'PCHIP');

%Create new interpolated mean Pressure values based on Ned
GV4STR(:,12)=interp1(Ned(1:17),G4ST(1:17),x,'PCHIP');
GV4STR(:,11)=interp1(Ned(18:34),G4ST(18:34),x,'PCHIP');
GV4STR(:,10)=interp1(Ned(35:50),G4ST(35:50),x,'PCHIP');
GV4STR(:,9)=interp1(Ned(51:69),G4ST(51:69),x,'PCHIP');
GV4STR(:,8)=interp1(Ned(70:90),G4ST(70:90),x,'PCHIP');
GV4STR(:,7)=interp1(Ned(91:109),G4ST(91:109),x,'PCHIP');
GV4STR(:,6)=interp1(Ned(110:134),G4ST(110:134),x,'PCHIP');
GV4STR(:,5)=interp1(Ned(135:160),G4ST(135:160),x,'PCHIP');
GV4STR(:,4)=interp1(Ned(161:189),G4ST(161:189),x,'PCHIP');
GV4STR(:,3)=interp1(Ned(190:217),G4ST(190:217),x,'PCHIP');
GV4STR(:,2)=interp1(Ned(218:239),G4ST(218:239),x,'PCHIP');
GV4STR(:,1)=interp1(Ned(240:254),G4ST(240:254),x,'PCHIP');

%Create new interpolated Pressure amplitude values based on Ned
GV6(:,12)=interp1(Ned(1:17),G6A(1:17),x,'PCHIP','extrap');
GV6(:,11)=interp1(Ned(18:34),G6A(18:34),x,'PCHIP','extrap');
GV6(:,10)=interp1(Ned(35:50),G6A(35:50),x,'PCHIP','extrap');
GV6(:,9)=interp1(Ned(51:69),G6A(51:69),x,'PCHIP','extrap');
GV6(:,8)=interp1(Ned(70:90),G6A(70:90),x,'PCHIP','extrap');
GV6(:,7)=interp1(Ned(91:109),G6A(91:109),x,'PCHIP','extrap');
GV6(:,6)=interp1(Ned(110:134),G6A(110:134),x,'PCHIP','extrap');
GV6(:,5)=interp1(Ned(135:160),G6A(135:160),x,'PCHIP','extrap');
GV6(:,4)=interp1(Ned(161:189),G6A(161:189),x,'PCHIP','extrap');
GV6(:,3)=interp1(Ned(190:217),G6A(190:217),x,'PCHIP','extrap');
GV6(:,2)=interp1(Ned(218:239),G6A(218:239),x,'PCHIP','extrap');
GV6(:,1)=interp1(Ned(240:254),G6A(240:254),x,'PCHIP','extrap');

%Create new interpolated mean Pressure values based on Ned
GV6STR(:,12)=interp1(Ned(1:17),G6ST(1:17),x,'PCHIP');
GV6STR(:,11)=interp1(Ned(18:34),G6ST(18:34),x,'PCHIP');
GV6STR(:,10)=interp1(Ned(35:50),G6ST(35:50),x,'PCHIP');
GV6STR(:,9)=interp1(Ned(51:69),G6ST(51:69),x,'PCHIP');
GV6STR(:,8)=interp1(Ned(70:90),G6ST(70:90),x,'PCHIP');
GV6STR(:,7)=interp1(Ned(91:109),G6ST(91:109),x,'PCHIP');
GV6STR(:,6)=interp1(Ned(110:134),G6ST(110:134),x,'PCHIP');
GV6STR(:,5)=interp1(Ned(135:160),G6ST(135:160),x,'PCHIP');
GV6STR(:,4)=interp1(Ned(161:189),G6ST(161:189),x,'PCHIP');
GV6STR(:,3)=interp1(Ned(190:217),G6ST(190:217),x,'PCHIP');
GV6STR(:,2)=interp1(Ned(218:239),G6ST(218:239),x,'PCHIP');
GV6STR(:,1)=interp1(Ned(240:254),G6ST(240:254),x,'PCHIP');

%Create new interpolated Pressure amplitude values based on Ned
GV5(:,12)=interp1(Ned(1:17),GLA(1:17),x,'PCHIP','extrap');
GV5(:,11)=interp1(Ned(18:34),GLA(18:34),x,'PCHIP','extrap');
GV5(:,10)=interp1(Ned(35:50),GLA(35:50),x,'PCHIP','extrap');
GV5(:,9)=interp1(Ned(51:69),GLA(51:69),x,'PCHIP','extrap');
GV5(:,8)=interp1(Ned(70:90),GLA(70:90),x,'PCHIP','extrap');
GV5(:,7)=interp1(Ned(91:109),GLA(91:109),x,'PCHIP','extrap');
GV5(:,6)=interp1(Ned(110:134),GLA(110:134),x,'PCHIP','extrap');
GV5(:,5)=interp1(Ned(135:160),GLA(135:160),x,'PCHIP','extrap');
GV5(:,4)=interp1(Ned(161:189),GLA(161:189),x,'PCHIP','extrap');
GV5(:,3)=interp1(Ned(190:217),GLA(190:217),x,'PCHIP','extrap');
GV5(:,2)=interp1(Ned(218:239),GLA(218:239),x,'PCHIP','extrap');
GV5(:,1)=interp1(Ned(240:254),GLA(240:254),x,'PCHIP','extrap');
```

```
%Create new interpolated mean Pressure values based on Ned
GV5STR(:,12)=interp1(Ned(1:17),G5ST(1:17),x,'PCHIP');
GV5STR(:,11)=interp1(Ned(18:34),G5ST(18:34),x,'PCHIP');
GV5STR(:,10)=interp1(Ned(35:50),G5ST(35:50),x,'PCHIP');
GV5STR(:,9)=interp1(Ned(51:69),G5ST(51:69),x,'PCHIP');
GV5STR(:,8)=interp1(Ned(70:90),G5ST(70:90),x,'PCHIP');
GV5STR(:,7)=interp1(Ned(91:109),G5ST(91:109),x,'PCHIP');
GV5STR(:,6)=interp1(Ned(110:134),G5ST(110:134),x,'PCHIP');
GV5STR(:,5)=interp1(Ned(135:160),G5ST(135:160),x,'PCHIP');
GV5STR(:,4)=interp1(Ned(161:189),G5ST(161:189),x,'PCHIP');
GV5STR(:,3)=interp1(Ned(190:217),G5ST(190:217),x,'PCHIP');
GV5STR(:,2)=interp1(Ned(218:239),G5ST(218:239),x,'PCHIP');
GV5STR(:,1)=interp1(Ned(240:254),G5ST(240:254),x,'PCHIP');

%Create new interpolated Pressure amplitude values based on RPM
GV4S(:,12)=interp1(RPM(1:17),G4A(1:17),Speed,'PCHIP');
GV4S(:,11)=interp1(RPM(18:34),G4A(18:34),Speed,'PCHIP');
GV4S(:,10)=interp1(RPM(35:50),G4A(35:50),Speed,'PCHIP');
GV4S(:,9)=interp1(RPM(51:69),G4A(51:69),Speed,'PCHIP');
GV4S(:,8)=interp1(RPM(70:90),G4A(70:90),Speed,'PCHIP');
GV4S(:,7)=interp1(RPM(91:109),G4A(91:109),Speed,'PCHIP');
GV4S(:,6)=interp1(RPM(110:134),G4A(110:134),Speed,'PCHIP');
GV4S(:,5)=interp1(RPM(135:160),G4A(135:160),Speed,'PCHIP');
GV4S(:,4)=interp1(RPM(161:189),G4A(161:189),Speed,'PCHIP');
GV4S(:,3)=interp1(RPM(190:217),G4A(190:217),Speed,'PCHIP');
GV4S(:,2)=interp1(RPM(218:239),G4A(218:239),Speed,'PCHIP');
GV4S(:,1)=interp1(RPM(240:254),G4A(240:254),Speed,'PCHIP');

%Create new interpolated Pressure amplitude values based on RPM
GV5S(:,12)=interp1(RPM(1:17),GLA(1:17),Speed,'PCHIP');
GV5S(:,11)=interp1(RPM(18:34),GLA(18:34),Speed,'PCHIP');
GV5S(:,10)=interp1(RPM(35:50),GLA(35:50),Speed,'PCHIP');
GV5S(:,9)=interp1(RPM(51:69),GLA(51:69),Speed,'PCHIP');
GV5S(:,8)=interp1(RPM(70:90),GLA(70:90),Speed,'PCHIP');
GV5S(:,7)=interp1(RPM(91:109),GLA(91:109),Speed,'PCHIP');
GV5S(:,6)=interp1(RPM(110:134),GLA(110:134),Speed,'PCHIP');
GV5S(:,5)=interp1(RPM(135:160),GLA(135:160),Speed,'PCHIP');
GV5S(:,4)=interp1(RPM(161:189),GLA(161:189),Speed,'PCHIP');
GV5S(:,3)=interp1(RPM(190:217),GLA(190:217),Speed,'PCHIP');
GV5S(:,2)=interp1(RPM(218:239),GLA(218:239),Speed,'PCHIP');
GV5S(:,1)=interp1(RPM(240:254),GLA(240:254),Speed,'PCHIP');

%Create new interpolated Pressure amplitude values based on RPM
GV6S(:,12)=interp1(RPM(1:17),G6A(1:17),Speed,'PCHIP');
GV6S(:,11)=interp1(RPM(18:34),G6A(18:34),Speed,'PCHIP');
GV6S(:,10)=interp1(RPM(35:50),G6A(35:50),Speed,'PCHIP');
GV6S(:,9)=interp1(RPM(51:69),G6A(51:69),Speed,'PCHIP');
GV6S(:,8)=interp1(RPM(70:90),G6A(70:90),Speed,'PCHIP');
GV6S(:,7)=interp1(RPM(91:109),G6A(91:109),Speed,'PCHIP');
GV6S(:,6)=interp1(RPM(110:134),G6A(110:134),Speed,'PCHIP');
GV6S(:,5)=interp1(RPM(135:160),G6A(135:160),Speed,'PCHIP');
GV6S(:,4)=interp1(RPM(161:189),G6A(161:189),Speed,'PCHIP');
GV6S(:,3)=interp1(RPM(190:217),G6A(190:217),Speed,'PCHIP');
GV6S(:,2)=interp1(RPM(218:239),G6A(218:239),Speed,'PCHIP');
GV6S(:,1)=interp1(RPM(240:254),G6A(240:254),Speed,'PCHIP');

%Include the calibration constant to convert voltage change to pressure
change in kpa
RGV4=GV4*a1;
RGV5=GV5*a2;
RGV6=GV6*a3;
```

```
RGV4S=GV4S*a1;
RGV5S=GV5S*a2;
RGV6S=GV6S*a3;


%For BEP=GV10 0,1785NED
GALL=RGV4+RGV5+RGV6;
GV4=GV4/G4A(1,42);
GV5=GV5/GLA(1,42);
GV6=GV6/G6A(1,42);
GALLS=GV4S+GV5S+GV6S;
GV4S=GV4S/G4A(1,42);
GV5S=GV5S/GLA(1,42);
GV6S=GV6S/G6A(1,42);


BEPGV4=G4A(1,42)*a1;
BEPGV5=GLA(1,42)*a2;
BEPGV6=G6A(1,42)*a3;

%Interpolate values for plotting based on NED and QED
N=zeros(numb,numb);
Q=N;
E=N;
for t=1:numb
N(:,t)=x;
Q(t,:)=linspace(0.207,0.02,numb);
end
for t=1:numb
EFF(t,:)=interp1(q(t,:),ef(t,:),Q(t,:),'PCHIP',0);
RRPM(t,:)=interp1(q(t,:),r(t,:),Q(t,:),'PCHIP',0);
GALLP(t,:)=interp1(q(t,:),GALL(t,:),Q(t,:),'PCHIP',0);
GV4P(t,:)=interp1(q(t,:),GV4(t,:),Q(t,:),'PCHIP',0);
GV5P(t,:)=interp1(q(t,:),GV5(t,:),Q(t,:),'PCHIP',0);
GV6P(t,:)=interp1(q(t,:),GV6(t,:),Q(t,:),'PCHIP',0);
Stress4(t,:)=interp1(q(t,:),GV4STR(t,:),Q(t,:),'PCHIP',0);
Stress5(t,:)=interp1(q(t,:),GV5STR(t,:),Q(t,:),'PCHIP',0);
Stress6(t,:)=interp1(q(t,:),GV6STR(t,:),Q(t,:),'PCHIP',0);
RGV4P(t,:)=interp1(q(t,:),RGV4(t,:),Q(t,:),'PCHIP',0);
RGV5P(t,:)=interp1(q(t,:),RGV5(t,:),Q(t,:),'PCHIP',0);
RGV6P(t,:)=interp1(q(t,:),RGV6(t,:),Q(t,:),'PCHIP',0);
end

%Interpolate values for plotting based on RPM and QED

NS=zeros(numb,numb);
QS=NS;
ES=NS;

for t=1:numb
NS(:,t)=Speed;
QS(t,:)=linspace(0.207,0.02,numb);
end
for t=1:numb
GV4PS(t,:)=interp1(qS(t,:),GV4S(t,:),QS(t,:),'PCHIP',0);
GV5PS(t,:)=interp1(qS(t,:),GV5S(t,:),QS(t,:),'PCHIP',0);
GV6PS(t,:)=interp1(qS(t,:),GV6S(t,:),QS(t,:),'PCHIP',0);
RGV4PS(t,:)=interp1(qS(t,:),RGV4S(t,:),QS(t,:),'PCHIP',0);
RGV5PS(t,:)=interp1(qS(t,:),RGV5S(t,:),QS(t,:),'PCHIP',0);
RGV6PS(t,:)=interp1(qS(t,:),RGV6S(t,:),QS(t,:),'PCHIP',0);
```

```
end

for i=1:1000
    for k=1:1000
        if EFF(i,k)< 10
            GV4P(i,k)=0;
            GV5P(i,k)=0;
            GV6P(i,k)=0;
            RGV4P(i,k)=0;
            RGV5P(i,k)=0;
            RGV6P(i,k)=0;
        end
    end
end

%Beyond this point there is only code to create different plots

%Decide value of lines in the hill chart
%Efflines=[10 25 40 60 70 75 80 85 90 91 92 93 93.3 93.6 93.8 93.85 93.88
93.903 93.95 94 95];
%Speedlines=[210 220 230 240 250 260 270 280 290 300 310 320 330 340 350
360 370 380 390 400 410 420 430 450 470 490 510 530 550 570 600];
%Pressurelines=[0.1 0.4 0.7 0.8 0.9 1 1.1 1.2 1.3 1.4 1.5 1.7 1.9  2.2 2.4
2.6 2.8 3 3.3 4 5 5.6 6 8 10 20];
%SmallPL=[0.5 0.6 0.7 0.8 0.9 1 1.1 1.2 1.3 1.4 1.5 1.6 2 3 4];
%PressAllLines=[3 3.3  3.6  3.9 4 4.2 4.4 4.6 4.8 5 5.2 5.5 6 7 10 15];
%StressLines=[120 125 130 135 140 145 150 155 160 165 170 175 180 185 190
195 200 205 210];
%Plotting hill chart
%contourf(N,Q,EFF,Efflines)
%Plotting wierd speed chart
% contourf(N,Q,RRPM,Speedlines)

%Plotting pressure diagrams
%contourf(N,Q,GV4P,Pressurelines)
%contourf(N,Q,GV5P,Pressurelines)
%contourf(N,Q,GV6P,Pressurelines)
%contourf(N,Q,GV4P,SmallPL)
%contourf(N,Q,GV5P,SmallPL)
%contourf(N,Q,GV6P,SmallPL)
%1:17 18:34 35:50 51:69 70:90 91:109 110:134 135:160 161:189 190:217
%218:239 239:254
%Plotting guide vane angles
hold on;
plot(Ned(1:17),Qed(1:17),'-k');
plot(Ned(18:34),Qed(18:34),'-k');
plot(Ned(35:50),Qed(35:50),'-k');
plot(Ned(51:69),Qed(51:69),'-k');
plot(Ned(70:90),Qed(70:90),'-k');
plot(Ned(91:109),Qed(91:109),'-k');
plot(Ned(110:134),Qed(110:134),'-k');
plot(Ned(135:160),Qed(135:160),'-k');
plot(Ned(161:189),Qed(161:189),'-k');
plot(Ned(190:217),Qed(190:217),'-k');
plot(Ned(218:239),Qed(218:239),'-k');
plot(Ned(240:254),Qed(240:254),'-k');

%Plotting guide vane angles(RPM)
%hold on;
%plot(RPM(1:17),Qed(1:17),'-k');
%plot(RPM(18:34),Qed(18:34),'-k');
```

```
%plot(RPM(35:50),Qed(35:50),'-k');
%plot(RPM(51:69),Qed(51:69),'-k');
%plot(RPM(70:90),Qed(70:90),'-k');
%plot(RPM(91:109),Qed(91:109),'-k');
%plot(RPM(110:134),Qed(110:134),'-k');
%plot(RPM(135:160),Qed(135:160),'-k');
%plot(RPM(161:189),Qed(161:189),'-k');
%plot(RPM(190:217),Qed(190:217),'-k');
%plot(RPM(218:239),Qed(218:239),'-k');
%plot(RPM(240:254),Qed(240:254),'-k');

xlim([0.12 0.28]);
ylim([0.02 0.207])
% Create ylabel
ylabel('Q_E_D');

% Create xlabel
xlabel('N_E_D');

% Create title
%title({'Pressure Pulsation Diagram for GV6'});


RunNed(1)=Ned(17);
RunNed(2)=Ned(34);
RunNed(3)=Ned(50);
RunNed(4)=Ned(69);
RunNed(5)=Ned(90);
RunNed(6)=Ned(109);
RunNed(7)=Ned(134);
RunNed(8)=Ned(160);
RunNed(9)=Ned(189);
RunNed(10)=Ned(217);
RunNed(11)=Ned(239);
RunNed(12)=Ned(254);

RunQed(1)=Qed(17);
RunQed(2)=Qed(34);
RunQed(3)=Qed(50);
RunQed(4)=Qed(69);
RunQed(5)=Qed(90);
RunQed(6)=Qed(109);
RunQed(7)=Qed(134);
RunQed(8)=Qed(160);
RunQed(9)=Qed(189);
RunQed(10)=Qed(217);
RunQed(11)=Qed(239);
RunQed(12)=Qed(254);
%Plotting runaway line
plot(RunNed(1:12),RunQed(1:12),'-k');

%Plotting pressure pulsations based on RPM and guide vane opening
%for i=1:12
%hold on
%plot3(i.*ones(1,1000),Speed/3.389,GV4S(:,i));
%end
```

Stress levels

```
%run exceltilhill.m first


Kof=323.8095238;
%1000 to convert from KPa to MPa
Mises4M=Stress4*Kof/1000;
Mises4A=RGV4P*Kof/1000;
Mises5M=Stress5*Kof/1000;
Mises5A=RGV5P*Kof/1000;
Mises6M=Stress6*Kof/1000;
Mises6A=RGV6P*Kof/1000;
ATM=98.5*Kof/1000;

MisesAVG=(Mises4A+Mises5A+Mises6A)/3;

MisesAVGMean=(Mises4M+Mises5M+Mises6M)/3;

MisesAmp=[0.1 0.2 0.3 0.4 0.45 0.5 0.55 0.6 0.65 0.7 0.8 0.9 1 1.1 1.2  1.4
1.7 2 3];
MisesMean=[35 40 42 44 46 48 50 52 54 56 58 60 62 64 67 70 75 80];
%contourf(N,Q,MisesAVG,MisesAmp);
%contourf(N,Q,MisesAVGMean,MisesMean);
UTS=910;
KT=1.36; %strain intensity factor

for i=1:1000
    for k=1:1000
StressEff4(i,k)=Mises4A(i,k)*((UTS)/((UTS)-Mises4M(i,k)));
StressEff5(i,k)=Mises5A(i,k)*((UTS)/((UTS)-Mises5M(i,k)));
StressEff6(i,k)=Mises6A(i,k)*((UTS)/((UTS)-Mises6M(i,k)));
StressEffAVG(i,k)=MisesAVG(i,k)*((UTS)/((UTS)-MisesAVGMean(i,k)));
    end
end

for i=1:1000
    for k=1:1000
        if Mises4M(i,k)==0;
            ATME=0;
        else
            ATME=ATM;
        end
StressEff4LCF(i,k)=(Mises4M(i,k)+Mises4A(i,k)-ATME)*((UTS)/((UTS)-ATM));
if Mises5M(i,k)==0;
            ATME=0;
        else
            ATME=ATM;
        end
StressEff5LCF(i,k)=(Mises5M(i,k)+Mises5A(i,k)-ATME)*((UTS)/((UTS)-ATM));
if Mises6M(i,k)==0;
            ATME=0;
        else
            ATME=ATM;
        end
StressEff6LCF(i,k)=(Mises6M(i,k)+Mises6M(i,k)-ATME)*((UTS)/((UTS)-ATM));
if MisesAVGMean(i,k)==0;
            ATME=0;
        else
```

```
            ATME=ATM;
        end
StressEffAVGLCF(i,k)=(MisesAVGMean(i,k)+MisesAVG(i,k)-ATME)*((UTS)/((UTS)-
ATM));
    end
end

SLevels=[0.2 0.4 0.6 0.7 0.8 0.9 1 1.1 1.2 1.3 1.4 1.5 1.6 1.8 2];
%contourf(N,Q,StressEff4,SLevels)

k1HCF=13.62;
m1HCF=5;
for i=1:1000;
    for k=1:1000;
CF4HCF(i,k)=10^(k1HCF-m1HCF*log10(2*KT*StressEff4(i,k)));
CF5HCF(i,k)=10^(k1HCF-m1HCF*log10(2*KT*StressEff5(i,k)));
CF6HCF(i,k)=10^(k1HCF-m1HCF*log10(2*KT*StressEff6(i,k)));
CFAVGHCF(i,k)=10^(k1HCF-m1HCF*log10(2*KT*StressEffAVG(i,k)));
if CF4HCF(i,k)>10^50
    CF4HCF(i,k)=0;
end
if CF5HCF(i,k)>10^50
    CF5HCF(i,k)=0;
end
if CF6HCF(i,k)>10^50
    CF6HCF(i,k)=0;
end
if CFAVGHCF(i,k)>10^50
    CFAVGHCF(i,k)=0;
end
    end
end

k1LCF=10.97;
m1LCF=3;
for i=1:1000;
    for k=1:1000;
CF4LCF(i,k)=10^(k1LCF-m1LCF*log10(KT*StressEff4LCF(i,k)));
CF5LCF(i,k)=10^(k1LCF-m1LCF*log10(KT*StressEff5LCF(i,k)));
CF6LCF(i,k)=10^(k1LCF-m1LCF*log10(KT*StressEff6LCF(i,k)));
CFAVGLCF(i,k)=10^(k1LCF-m1LCF*log10(KT*StressEffAVGLCF(i,k)));

if CFAVGLCF(i,k)>10^50
    CFAVGLCF(i,k)=0;
end

LCFDPC(i,k)=1/CFAVGLCF(i,k);
    end
end
CyclesToFailure=[10 10^2 10^3 5*10^3 10^4 5*10^4 10^5 2*10^5 3*10^5 4*10^5
5*10^5 6*10^12 10^6 5*10^6 10^7 10^8]*10^7;
ScaledCyclesToFailure=[0.1 1 5 10 50 100 500 1000 2000 3000 4000 5000 6000
8000 10^4 10^5 2*10^5 5*10^5];
LCFCyclesToFailure=[1 5 10 20 30 40 50 60 70 80 90 10^2  120 140 160 180
200 250 300 350 10^3]*10^5;

%contourf(N,Q,CF4HCF,CyclesToFailure)
%contourf(N,Q,CF5HCF,CyclesToFailure)
%contourf(N,Q,CF6HCF,CyclesToFailure)
%contourf(N,Q,CF4LCF,LCFCyclesToFailure)
```

```
%contourf(N,Q,CF5LCF,LCFCyclesToFailure)
%contourf(N,Q,CF6LCF,LCFCyclesToFailure)
%contourf(N,Q,CFAVGHCF/(10^9),ScaledCyclesToFailure)
%contourf(N,Q,CFAVGHCF/(10^3),ScaledCyclesToFailure)

CF4LCFScaled=CF4LCF/(10^6);
CF5LCFScaled=CF5LCF/(10^6);
CF6LCFScaled=CF6LCF/(10^6);
CFAVGLCFScaled=CFAVGLCF/(10^6);


ScaledLCFCyclesToFailure=[0.2 0.4 0.6 0.8 1 1.2 1.4 2 3 4 5 6 7 8 9 10 11
12 13 14 20 30 40 50 60 70 80 90 10^2  120 140 160 180 200 ];
%contourf(N,Q,CF4LCFScaled,ScaledLCFCyclesToFailure)
%contourf(N,Q,CF5LCFScaled,ScaledLCFCyclesToFailure)
%contourf(N,Q,CF6LCFSclaed,ScaledLCFCyclesToFailure)
%contourf(N,Q,CFAVGLCFScaled,ScaledLCFCyclesToFailure)

RelLCFDamage=[0.001 0.01 0.05 0.1 0.2 0.3 0.4 0.5 0.6 0.7 0.8 0.9 1 1.1 1.2
1.4 1.7 2 3 4 5 6 7 8 9 10 20 30 40 50];
%contourf(N,Q,LCFDPC,RelLCFDamage*10^-7)
%contourf(N,Q,LCFDPC/(3.487*10^-7),RelLCFDamage)
for i=1:1000;
    for k=1:1000;
DPH(i,k)=1680*RRPM(i,k)/CFAVGHCF(i,k);

    end
end

for i=1:1000;
    for k=1:1000;
        if isinf(DPH(i,k))==1
            DPH(i,k)=0;
        end
        if isinf(LCFDPC(i,k))==1
            LCFDPC(i,k)=0;
        end

    end
end


DPHScaled=DPH*10^6;
DamageNumber=[0.01 0.06 0.08 0.1 0.2 0.3 0.4 0.5 1 5 10 50 200 400 600 800
2000];
%contourf(N,Q,DPHScaled/0.142,DamageNumber)
RelDamage=[0.01 0.05 0.1 0.2 0.3 0.4 0.6 0.8 1 1.2 1.6 2 5 10 50 100 200
300 1000 2000 10000];
set(axes,'BoxStyle','full','FontSize',16,'Layer','top','XGrid','on','YGrid'
,'on');
hold on;
contourf(N,Q,DPHScaled/0.142,RelDamage)

xlabel('N_E_D - Dimensionless Speed Factor')
ylabel('Q_E_D - Dimensionless Discharge Factor')

for i=1:1000;
    for k=1:1000;
HoursToOneStartStop(i,k)=CFAVGHCF(i,k)/(RRPM(i,k)*1680*CFAVGLCF(i,k));
```

```
if isinf(HoursToOneStartStop(i,k))==1
    HoursToOneStartStop(i,k)=0;
end
    end
end

Hours=[0.001 0.01 0.05 0.1 0.2 0.4 0.6 0.8 1 1.2 1.4 1.6 1.8 2 2.2 2.5 2.8
3 3.5 4 5 6 7 8 9 10];
%contourf(N,Q,HoursToOneStartStop,Hours)

for i=1:1000
    for k=1:1000

DamagePerSession(i,k)=DPH(i,k)*2.456+(1/CFAVGLCF(i,k));

    end
end

DPSScaled=DamagePerSession*10^6;
Dscaled=[0.001 0.01 0.05 0.1 0.2 0.3 0.4 0.5 0.6 0.7 0.8 0.9 1 1.4 1.7 3 5
8 10 50 100 500 1000 2000 3000];
DscaledLow=[0.001 0.01 0.05 0.10 0.15 0.2 0.25 0.3 0.35 0.4 0.45 0.5 0.6
0.7 0.8 0.9 1 1.4 1.7 3 5];
%contourf(N,Q,DPSScaled,Dscaled)
hold on;
plot(RunNed(1:12),RunQed(1:12),'-k');
plot(Ned(1:17),Qed(1:17),'-k');
plot(Ned(18:34),Qed(18:34),'-k');
plot(Ned(35:50),Qed(35:50),'-k');
plot(Ned(51:69),Qed(51:69),'-k');
plot(Ned(70:90),Qed(70:90),'-k');
plot(Ned(91:109),Qed(91:109),'-k');
plot(Ned(110:134),Qed(110:134),'-k');
plot(Ned(135:160),Qed(135:160),'-k');
plot(Ned(161:189),Qed(161:189),'-k');
plot(Ned(190:217),Qed(190:217),'-k');
plot(Ned(218:239),Qed(218:239),'-k');
plot(Ned(240:254),Qed(240:254),'-k');
```

Frequencies

```
i=0;
k=0;
for i=1:length(Trykk)
    if length(Trykk{1,i})>190000
        k=k+1;
        Pressure{1,k}=Trykk{1,i};
    end
end

i=0;
k=0;
for k=1:3
    for i=1:length(Pressure)/3;
    P{k,i}=Pressure{1,(3*i)-3+k};
```

```
    end
end


i=0;
for i=1:145
    PC{1,i}=P{1,i};
    PC{2,i}=P{2,i};
    PC{3,i}=P{3,i};
    PC{4,i}=HILL(5,i);
end
for i=146:168
    PC{1,i}=P{1,i+1};
    PC{2,i}=P{2,i+1};
    PC{3,i}=P{3,i+1};
    PC{4,i}=HILL(5,i);
end
for i=169:254
    PC{1,i}=P{1,i+2};
    PC{2,i}=P{2,i+2};
    PC{3,i}=P{3,i+2};
    PC{4,i}=HILL(5,i);

end

BEPVolt(1,1)=G4A(1,42);
BEPVolt(2,1)=GLA(1,42);
BEPVolt(3,1)=G6A(1,42);

A(1,1)=a1;
A(2,1)=a2;
A(3,1)=a3;


for i=1:3
FA=P{i,82};
[pxx,f]=JKwelch(FA,5000,length(FA)/40,[]);
hold on;
pxx=pxx*A(i,1);
f=60*f/PC{4,82};
plot(f,pxx)
xlim([0 70])
end
```

Welch

This script was made by Johannes Kverno

```
function [ pxx, f ] = JKwelch( Signal, Fs, window, noverlap )
% Welch [pxx, f] = JKwelch(Signal, Fs, window, noverlap)
%   An attempt to create a function to do the spectral analysis of a signal

S1=sum(window);
S2=sum(window.^2);
ENBW=Fs*(S2/(S1^2));
```

```
[pxx,f]=pwelch(detrend(Signal),window,floor(noverlap*length(window)),[],Fs)
; %Signal, Window, noverlap, frequency, Sample rate

pxx=pxx.*ENBW;
pxx=sqrt(pxx)*sqrt(2);
end
```

Runaway

```
%Exceltilhill og FrekvensAnalyse må kjøres først
clearvars Trun TrunA
Runaway=TDMS_readTDMSFile('C:\Users\eirilo\Documents\MATLAB\testmalingerRUN
AWAY.tdms');
b=0;
for i=3:length(Runaway.data)
    if length(Runaway.data{1,i})>140000
        b=b+1;
    TR{1,b}=Runaway.data{1,i};
    end

end
RunPM=[295 308 323 340 363 368 379 380 386 390 398 408 425 432.5 441
457.5];
GVopening=[0.440 0.484 0.572 0.660 0.791 0.879 0.967 1.0111 1.055 1.143
1.231 1.407 1.758 1.9779 2.242 3.0326];
for i=1:7
    Trun{1,i}=TR{1,(3*i)-2};
    Trun{2,i}=TR{1,(3*i)-1};
    Trun{3,i}=TR{1,(3*i)};
    Trun{4,i}=RunPM(1,i);
    Trun{5,i}=GVopening(1,i);
end
%1


Trun{1,8}=PC{1,255};
Trun{2,8}=PC{2,255};
Trun{3,8}=PC{3,255};
Trun{4,8}=RunPM(1,8);
Trun{5,8}=GVopening(1,8);
for i=9:13
    Trun{1,i}=TR{1,(3*(i-1))-2};
    Trun{2,i}=TR{1,(3*(i-1))-1};
    Trun{3,i}=TR{1,(3*(i-1))};
    Trun{4,i}=RunPM(1,i);
    Trun{5,i}=GVopening(1,i);
end

%2
Trun{1,14}=PC{1,240};
Trun{2,14}=PC{2,240};
Trun{3,14}=PC{3,240};
Trun{4,14}=RunPM(1,14);
Trun{5,14}=GVopening(1,14);
%2.2
Trun{1,15}=TR{1,37};
Trun{2,15}=TR{1,38};
```

```
Trun{3,15}=TR{1,39};
Trun{4,15}=RunPM(1,15);
Trun{5,15}=GVopening(1,15);

%3
Trun{1,16}=PC{1,217};
Trun{2,16}=PC{2,217};
Trun{3,16}=PC{3,217};
Trun{4,16}=RunPM(1,16);
Trun{5,16}=GVopening(1,16);

A(1,1)=a1;
A(2,1)=a2;
A(3,1)=a3;


for m=1:3
for k=1:length(Trun)


    T=Trun{1,k};


[N,e] = histcounts(T,1000);
Me = mean(T);
NumberOfPoints = sum(N);
temp=0;
conf=0.97;
SNLTRYKK(m,k)=Me;
for i=1:length(N)
    temp=temp +N(i); value=temp/NumberOfPoints;
    if value >=(1-conf)/2
         lower=e(i);
         break
    end
end



for j=1:length(N)
temp=temp +N(j); value=temp/NumberOfPoints;
if value >=conf+(1-conf)/2
upper=e(j);
break
end
end



VoltAmp=(upper-lower)/2;
SNLAmp(m,k)=VoltAmp;

TrunA(m,k)=VoltAmp*A(m,1);
end
end
for i=1:length(Trun);
TrunA(4,i)=Trun{4,i};
TrunA(5,i)=Trun{5,i};
```

```
end


TrunAR=TrunA;
TrunAR(1,:)=TrunA(1,:)/(G4A(1,42)*A(1,1));
TrunAR(2,:)=TrunA(1,:)/(GLA(1,42)*A(2,1));
TrunAR(3,:)=TrunA(1,:)/(G6A(1,42)*A(3,1));

FA=Trun{1,4};
[pxx,f]=JKwelch(FA,5000,length(FA)/40,50);
f=f*60/Trun{4,4};
hold on;
plot(f,pxx);

for i=1:3
FA=Trun{i,4};
[pxx(:,i),f(:,i)]=JKwelch(FA,5000,length(FA)/40,50);
hold on;
pxx(:,i)=pxx(:,i)*A(i);
f(:,i)=f(:,i)*60/Trun{4,4};
plot3(i.*ones(1,length(pxx)),f(:,i),pxx(:,i));
xlim([0 70])
end


FA=Trun{1,4};
[pxx,f]=JKwelch(FA,5000,length(FA)/20,50);
f=f*60/Trun{4,4};
hold on;
plot(f,pxx);
MaxP=max(pxx)
for i=1:length(pxx)
    if pxx(i,1)==MaxP

        MainFreq=f(i)
    end
end



for i=1:3
FA=Trun{i,1};
[pxx(:,i),f(:,i)]=JKwelch(FA,5000,length(FA)/30,50);
hold on;
pxx(:,i)=pxx(:,i)*A(i);
f(:,i)=f(:,i)*60/Trun{4,1};
plot3(i.*ones(1,length(pxx)),f(:,i),pxx(:,i));
xlim([0 70])
zlim([1 3])
end
```

Appendix C – Calibration reports

Calibration report for GV4 – Meas XP5

CALIBRATION REPORT

CALIBRATION PROPERTIES
Calibrated by: Eirik Lødemel
Type/Producer: Meas XP5
SN: 1
Range: 0-10 bar a
Unit: kPa
test
Meas XP5
0-10 bar a
kPa

CALIBRATION SOURCE PROPERTIES
Type/Producer: GE deadweight tester, P3023-6-P
SN: 66256
Uncertainty [%]: 0,008

POLY FIT EQUATION:
Y= + 31.33166440E+0X^0 + 28.45441519E+3X^1

CALIBRATION SUMARY:
Max Uncertainty : 0.063825 [%]
Max Uncertainty : 0.066300 [kPa]
RSQ : 0.999994
Calibration points : 36

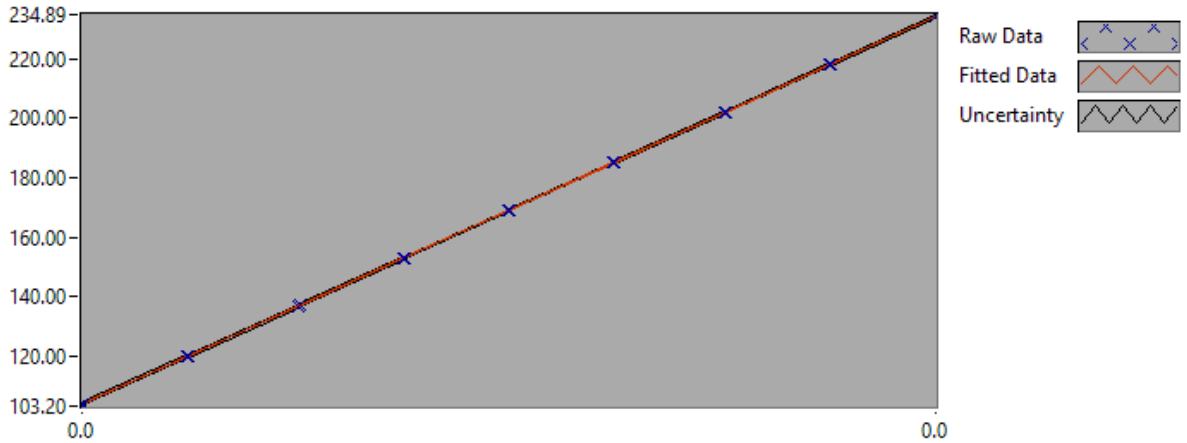

Figure 1 : Calibration chart (The uncertainty band is multiplied by 10)

CALIBRATION VALUES

Value [kPa]	Voltage [V]	Best Poly Fit [kPa]	Deviation [kPa]	Uncertainty [%]	Uncertainty [kPa]
103.946554	0.002560	104.175338	-0.228784	0.063563	0.066072
119.970725	0.003123	120.200364	-0.229639	0.045926	0.055098
136.993407	0.003720	137.178042	-0.184635	0.032923	0.045103
153.017579	0.004283	153.189433	-0.171854	0.025101	0.038409
169.039750	0.004844	169.161712	-0.121962	0.021254	0.035927
185.063921	0.005407	185.183181	-0.119260	0.020776	0.038448
202.087604	0.006004	202.166490	-0.078887	0.022605	0.045681
218.110775	0.006567	218.197337	-0.086562	0.025302	0.055186
234.133946	0.007131	234.228785	-0.094839	0.028272	0.066194
234.128946	0.007128	234.167334	-0.038388	0.028248	0.066137
218.104775	0.006562	218.040535	0.064239	0.025261	0.055095
202.076604	0.005997	201.968698	0.107905	0.022552	0.045573
185.050921	0.005397	184.913758	0.137164	0.020733	0.038367
169.026750	0.004833	168.865249	0.161501	0.021252	0.035922
153.002579	0.004271	152.861690	0.140888	0.025170	0.038510
136.978407	0.003708	136.839688	0.138720	0.033053	0.045275
119.942725	0.003111	119.841545	0.101180	0.046119	0.055316
103.912554	0.002549	103.868932	0.043622	0.063799	0.066295
103.904554	0.002551	103.907901	-0.003347	0.063765	0.066254
119.928725	0.003114	119.930155	-0.001430	0.046078	0.055260
136.952407	0.003712	136.945692	0.006716	0.033020	0.045222
152.976579	0.004275	152.985285	-0.008706	0.025153	0.038478
168.993750	0.004838	168.994423	-0.000672	0.021256	0.035921
185.013921	0.005401	185.026414	-0.012493	0.020754	0.038398
202.039604	0.006000	202.056533	-0.016929	0.022579	0.045619
218.063775	0.006564	218.112321	-0.048546	0.025283	0.055132
234.082946	0.007127	234.127331	-0.044385	0.028243	0.066113
234.088946	0.007127	234.113962	-0.025016	0.028242	0.066111
218.062775	0.006562	218.048715	0.014060	0.025266	0.055096
202.038604	0.005996	201.941098	0.097506	0.022551	0.045562
185.007921	0.005397	184.908500	0.099421	0.020736	0.038364
168.980750	0.004834	168.873672	0.107078	0.021258	0.035922
152.955579	0.004270	152.836628	0.118950	0.025184	0.038521
136.930407	0.003708	136.844992	0.085416	0.033066	0.045278
119.903725	0.003110	119.828231	0.075494	0.046150	0.055335
103.877554	0.002549	103.861083	0.016471	0.063825	0.066300

COMMENTS:

The uncertainty is calculated with 95% confidence. The uncertainty includes the randomness in the calibrated instrument during the calibration, systematic uncertainty in the instrument or property which the instrument under calibration is compared with (dead weight manometer, calibrated weights etc.), and due to regression analysis to fit the calibration points to a linear calibration equation.The calculated uncertainty can be used as the total systematic uncertianty of the calibrated instrument with the given calibration equation.

Calibration report for GV5 – Kulite XTE

CALIBRATION REPORT

CALIBRATION PROPERTIES
Calibrated by: Eirik Lødemel
Type/Producer: Kulite XTE
SN: 1-205
Range: 0-10 bar a
Unit: kPa
The son had a cat
Druck PTX 1830
2867610
0-10 bar a
kPa

CALIBRATION SOURCE PROPERTIES
Type/Producer: Ge Deadweight test, P3023-6-P
SN: 66256
Uncertainty [%]: 0,008

POLY FIT EQUATION:
Y= + 13.82326641E+0X^0 + 34.38755698E+3X^1

CALIBRATION SUMARY:
Max Uncertainty : 0.025194 [%]
Max Uncertainty : 0.026171 [kPa]
RSQ : 0.999999
Calibration points : 36

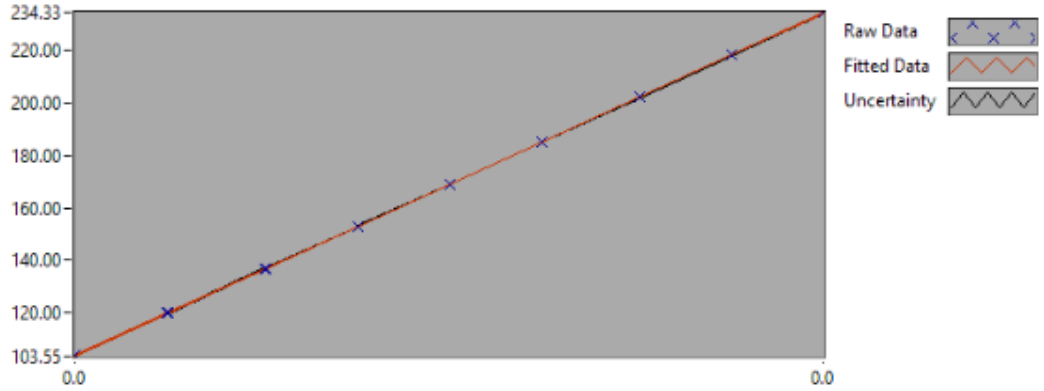

Figure 1 : Calibration chart (The uncertainty band is multiplied by 10)

Eirik Lødemel

CALIBRATION VALUES

Value [kPa]	Voltage [V]	Best Poly Fit [kPa]	Deviation [kPa]	Uncertainty [%]	Uncertainty [kPa]
103.946554	0.002619	103.883821	0.062733	0.025164	0.026157
119.970725	0.003086	119.950094	0.020631	0.018181	0.021812
136.993407	0.003582	137.009920	-0.016512	0.013019	0.017835
153.017579	0.004049	153.053293	-0.035714	0.009923	0.015184
169.039750	0.004515	169.079324	-0.039574	0.008390	0.014183
185.063921	0.004981	185.097064	-0.033143	0.008197	0.015170
202.087604	0.005475	202.102417	-0.014813	0.008915	0.018015
218.110775	0.005940	218.090617	0.020157	0.009969	0.021742
234.133946	0.006405	234.068764	0.065182	0.011135	0.026072
234.128946	0.006405	234.064602	0.064345	0.011139	0.026079
218.104775	0.005940	218.093336	0.011439	0.009972	0.021750
202.076604	0.005475	202.100428	-0.023824	0.008913	0.018011
185.050921	0.004981	185.095319	-0.044398	0.008199	0.015172
169.026750	0.004515	169.074531	-0.047781	0.008395	0.014190
153.002579	0.004049	153.043057	-0.040478	0.009918	0.015175
136.978407	0.003582	136.990048	-0.011641	0.013018	0.017831
119.942725	0.003085	119.925624	0.017102	0.018183	0.021809
103.912554	0.002618	103.854170	0.058384	0.025171	0.026156
103.904554	0.002618	103.847995	0.056559	0.025174	0.026157
119.928725	0.003085	119.910879	0.017847	0.018186	0.021811
136.952407	0.003581	136.966161	-0.013754	0.013031	0.017846
152.976579	0.004048	153.009285	-0.032706	0.009925	0.015183
168.993750	0.004514	169.032312	-0.038562	0.008395	0.014187
185.013921	0.004979	185.054748	-0.040827	0.008198	0.015167
202.039604	0.005474	202.054885	-0.015281	0.008911	0.018004
218.063775	0.005939	218.040655	0.023120	0.009972	0.021746
234.082946	0.006403	234.023757	0.059189	0.011128	0.026050
234.088946	0.006404	234.025518	0.063428	0.011131	0.026056
218.062775	0.005939	218.050127	0.012648	0.009971	0.021742
202.038604	0.005474	202.057371	-0.018767	0.008914	0.018009
185.007921	0.004980	185.056512	-0.048590	0.008196	0.015164
168.980750	0.004513	169.030787	-0.050037	0.008395	0.014185
152.955579	0.004047	152.997475	-0.041896	0.009928	0.015185
136.930407	0.003581	136.950500	-0.020092	0.013039	0.017854
119.903725	0.003084	119.889579	0.014147	0.018200	0.021823
103.877554	0.002617	103.816073	0.061481	0.025194	0.026171

COMMENTS:

Calibration report for GV6 – Kulite XTE

CALIBRATION PROPERTIES
Calibrated by: Eirik Lødemel
Type/Producer: Kulite XTE
SN: 1-204
Range: 0-10 bar a
Unit: kPa
test
Kulite XTE
2867610
0-10 bar a
kPa

CALIBRATION SOURCE PROPERTIES
Type/Producer: GE deadweight tester, P3023-6-P
SN: 66256
Uncertainty [%]: 0,008

POLY FIT EQUATION:
Y= -2.91529341E+0X^0 + 34.61201977E+3X^1

CALIBRATION SUMARY:
Max Uncertainty : 0.022958 [%]
Max Uncertainty : 0.023848 [kPa]
RSQ : 0.999999
Calibration points : 36

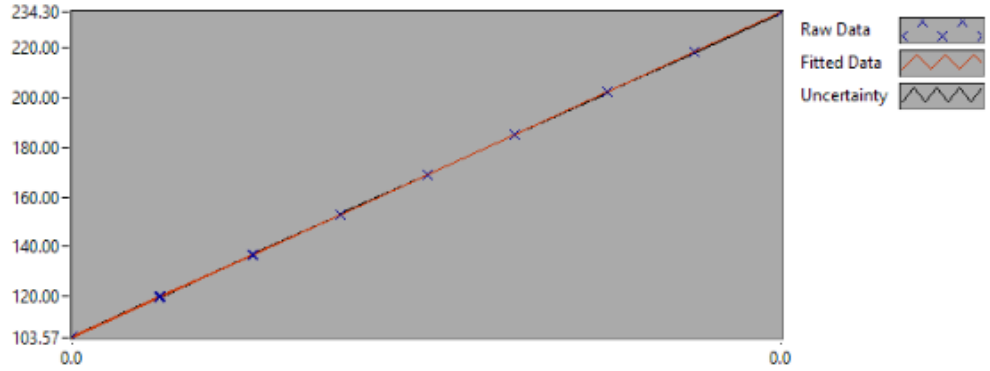

Figure 1 : Calibration chart (The uncertainty band is multiplied by 10)

Eirik Lødemel

CALIBRATION VALUES

Value [kPa]	Voltage [V]	Best Poly Fit [kPa]	Deviation [kPa]	Uncertainty [%]	Uncertainty [kPa]
103.946554	0.003086	103.884208	0.062346	0.022925	0.023829
119.970725	0.003550	119.945213	0.025512	0.016558	0.019864
136.993407	0.004043	137.008695	-0.015287	0.011865	0.016254
153.017579	0.004506	153.050367	-0.032788	0.009038	0.013830
169.039750	0.004969	169.078542	-0.038792	0.007651	0.012933
185.063921	0.005432	185.095367	-0.031446	0.007468	0.013820
202.087604	0.005923	202.098861	-0.011257	0.008123	0.016417
218.110775	0.006385	218.085183	0.025592	0.009083	0.019811
234.133946	0.006847	234.057919	0.076027	0.010147	0.023758
234.128946	0.006847	234.064310	0.064636	0.010151	0.023766
218.104775	0.006385	218.093712	0.011063	0.009086	0.019817
202.076604	0.005923	202.099643	-0.023039	0.008121	0.016411
185.050921	0.005432	185.097105	-0.046184	0.007472	0.013826
169.026750	0.004969	169.077157	-0.050407	0.007646	0.012924
153.002579	0.004506	153.046441	-0.043862	0.009037	0.013827
136.978407	0.004042	136.994505	-0.016098	0.011863	0.016250
119.942725	0.003549	119.927475	0.015250	0.016565	0.019868
103.912554	0.003085	103.852359	0.060195	0.022933	0.023830
103.904554	0.003084	103.841427	0.063127	0.022948	0.023844
119.928725	0.003549	119.905831	0.022895	0.016569	0.019871
136.952407	0.004041	136.966871	-0.014463	0.011879	0.016268
152.976579	0.004505	153.004209	-0.027630	0.009044	0.013836
168.993750	0.004968	169.035206	-0.041456	0.007650	0.012928
185.013921	0.005431	185.055316	-0.041395	0.007472	0.013825
202.039604	0.005922	202.058301	-0.018698	0.008121	0.016408
218.063775	0.006384	218.039832	0.023943	0.009087	0.019815
234.082946	0.006846	234.023502	0.059445	0.010145	0.023747
234.088946	0.006846	234.025659	0.063288	0.010142	0.023742
218.062775	0.006384	218.052711	0.010064	0.009086	0.019813
202.038604	0.005922	202.062493	-0.023890	0.008123	0.016411
185.007921	0.005431	185.061726	-0.053804	0.007470	0.013819
168.980750	0.004968	169.036214	-0.055464	0.007649	0.012926
152.955579	0.004505	153.004888	-0.049310	0.009047	0.013838
136.930407	0.004041	136.952808	-0.022401	0.011885	0.016274
119.903725	0.003548	119.894108	0.009618	0.016584	0.019885
103.877554	0.003084	103.812883	0.064671	0.022958	0.023848

COMMENTS:

Calibration report for Friction Torque – TW T2

CALIBRATION REPORT

CALIBRATION PROPERTIES
Calibrated by: Eirik Lødemel
Type/Producer: WT T2 - Friction torque
SN:
Range:
Unit: Nm

CALIBRATION SOURCE PROPERTIES
Type/Producer: Calibrated weights and gravity
SN:
Uncertainty [%]: 0,01

POLY FIT EQUATION:
Y= -127.31354078E-3X^0 + 2.85964204E+0X^1

CALIBRATION SUMARY:
Max Uncertainty : Inf [%]
Max Uncertainty : 0.091010 [Nm]
RSQ : 0.999813
Calibration points : 27

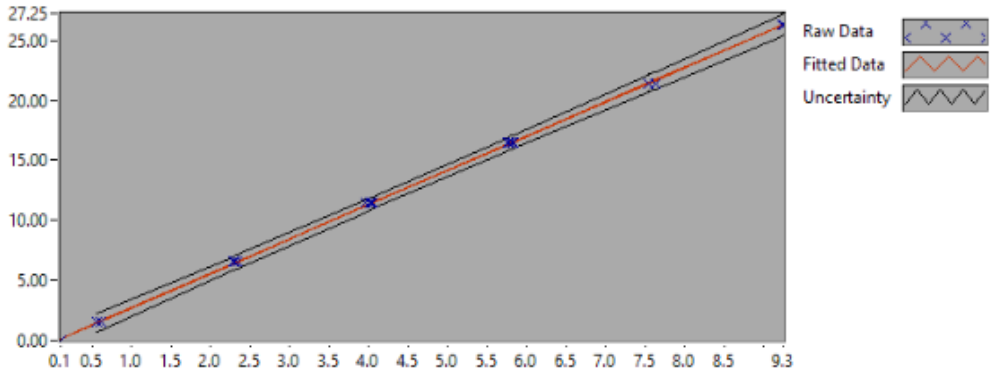

Figure 1 : Calibration chart (The uncertainty band is multiplied by 10)

Eirik Lødemel

CALIBRATION VALUES

Value [Nm]	Voltage [V]	Best Poly Fit [Nm]	Deviation [Nm]	Uncertainty [%]	Uncertainty [Nm]
0.000000	0.100555	0.160239	-0.160239	Inf	NaN
1.605115	0.557612	1.467257	0.137859	4.747814	0.076208
11.495199	4.010249	11.340564	0.154635	0.438709	0.050430
16.438781	5.809084	16.484588	-0.045807	0.335724	0.055189
21.383171	7.628236	21.686712	-0.303541	0.334473	0.071521
26.328058	9.241354	26.299651	0.028407	0.345390	0.090934
26.328058	9.253701	26.334960	-0.006902	0.345676	0.091010
21.383171	7.552203	21.469285	-0.086114	0.330680	0.070710
16.438781	5.777165	16.393312	0.045469	0.334332	0.054960
11.495199	4.037684	11.419018	0.076181	0.438260	0.050379
6.549978	2.303820	6.460786	0.089192	0.896346	0.058710
1.605115	0.611554	1.621513	-0.016397	4.708348	0.075574
0.000000	0.102571	0.166002	-0.166002	Inf	NaN
0.000000	0.100878	0.161162	-0.161162	Inf	NaN
1.605115	0.552161	1.451670	0.153445	4.751950	0.076274
6.549978	2.279956	6.392544	0.157434	0.899149	0.058894
11.495199	3.960116	11.197201	0.297998	0.438870	0.050449
16.438781	5.754518	16.328549	0.110232	0.333563	0.054834
21.383171	7.543938	21.445649	-0.062478	0.330261	0.070620
26.328058	9.231493	26.271452	0.056606	0.344595	0.090725
26.328058	9.247019	26.315852	0.012206	0.345343	0.090922
21.383171	7.538768	21.430864	-0.047693	0.330041	0.070573
16.438781	5.825134	16.530484	-0.091703	0.336239	0.055274
11.495199	4.054565	11.467292	0.027907	0.437295	0.050268
6.549978	2.332469	6.542713	0.007265	0.892852	0.058482
1.605115	0.617318	1.637995	-0.032879	4.704170	0.075507
0.000000	0.105338	0.173916	-0.173916	Inf	NaN

COMMENTS:

Calibration report for Generator Torque – WT T2

CALIBRATION REPORT

CALIBRATION PROPERTIES
Calibrated by: Eirik Lødemel
Type/Producer: WT T1 - Generator Torque
SN:
Range:
Unit: Nm

CALIBRATION SOURCE PROPERTIES
Type/Producer: Calibrated weights and gravity
SN:
Uncertainty [%]: 0,01

POLY FIT EQUATION:
Y= -198.73889174E+0X^0 + 182.01007819E+0X^1

CALIBRATION SUMARY:
Max Uncertainty : 0.248597 [%]
Max Uncertainty : 0.686223 [Nm]
RSQ : 1.000000
Calibration points : 30

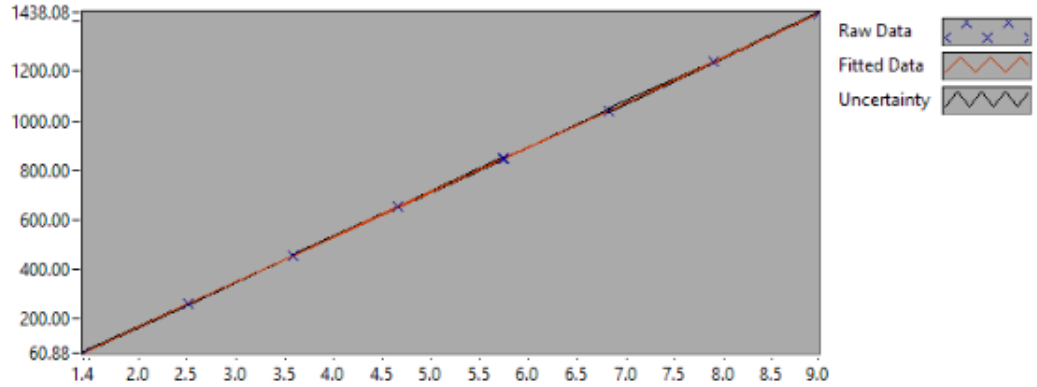

Figure 1 : Calibration chart (The uncertainty band is multiplied by 10)

Eirik Lødemel

CALIBRATION VALUES

Value [Nm]	Voltage [V]	Best Poly Fit [Nm]	Deviation [Nm]	Uncertainty [%]	Uncertainty [Nm]
62.299777	1.436536	62.725153	-0.425376	0.247326	0.154084
258.278254	2.510977	258.284261	-0.006007	0.063245	0.163348
454.274957	3.587841	454.284379	-0.009422	0.027336	0.124181
650.266956	4.665562	650.440360	-0.173404	0.066754	0.434078
846.244943	5.742530	846.459467	-0.214524	0.015059	0.127432
1042.169431	6.818148	1042.232748	-0.063317	0.065846	0.686223
1433.993615	8.971202	1434.110218	-0.116603	0.027694	0.397136
1433.993615	8.971394	1434.145238	-0.151623	0.022992	0.329704
1042.169431	6.817804	1042.170085	-0.000654	0.029635	0.308851
846.244943	5.740037	846.005777	0.239166	0.014829	0.125491
650.266956	4.662948	649.964580	0.302376	0.027760	0.180512
454.274957	3.586583	454.055391	0.219566	0.046379	0.210688
258.278254	2.510004	258.107213	0.171041	0.055110	0.142336
62.299777	1.434688	62.388710	-0.088934	0.241752	0.150611
62.299777	1.435514	62.539201	-0.239424	0.235787	0.146894
258.278254	2.510564	258.209019	0.069235	0.091549	0.236450
454.274957	3.588332	454.373756	-0.098799	0.065913	0.299425
650.266956	4.664561	650.258223	0.008733	0.027205	0.176907
846.244943	5.740998	846.180570	0.064373	0.017809	0.150708
1042.169431	6.817675	1042.146645	0.022785	0.022759	0.237189
1238.089411	7.894274	1238.098462	-0.009051	0.019766	0.244718
1433.993615	8.971877	1434.233076	-0.239461	0.018750	0.268874
1433.993615	8.971220	1434.113516	-0.119901	0.012224	0.175296
1238.089411	7.894853	1238.203900	-0.114489	0.021861	0.270662
1042.169431	6.817536	1042.121289	0.048141	0.024374	0.254023
846.244943	5.739116	845.837986	0.406957	0.057433	0.486023
650.266956	4.660464	649.512459	0.754497	0.051185	0.332842
454.274957	3.587895	454.294071	-0.019115	0.037401	0.169904
258.278254	2.510795	258.251065	0.027189	0.068558	0.177071
62.299777	1.435539	62.543731	-0.243954	0.248597	0.154875

COMMENTS:

Eirik Lødemel

Fatigue loads in a Francis turbine runner

NTNU
Norwegian University of
Science and Technology